Visible light communication control in a platoon vehicle environment

Luis Emmanuel Plascencia Cruz

université PARIS-SACLAY

Contrôle de la communication par lumière visible dans un environnement de véhicule de peloton

Visible light communication control in a platoon vehicle environment

Thèse de doctorat de l'université Paris-Saclay

École doctorale n°580 : sciences et technologies de l'information et de la communication (STIC)
Spécialité de doctorat : Réseaux, information et communications
Graduate School : Sciences de l'ingénierie et des systèmes, Référent : Université de Versailles-Saint-Quentin-en-Yvelines

Thèse préparée dans la unité de recherche **LISV** (Université Paris-Saclay, UVSQ), sous la direction de **Luc CHASSAGNE**, Professeur, le co-encadrement de **Hongyu GUAN**, Ingénieur de recherche, et **Oyunchimeg SHAGDAR**, Chargée de recherche.

Thèse soutenue à Vélizy-Villacoublay, le 30 mai 2022, par

Luis Emmanuel PLASCENCIA CRUZ

Composition du jury

Anne Julien-Vergonjanne Professeure des universités, Université de Limoges	Présidente
Valeria Loscrì Chargée de recherche, FUN team at Inria Lille-Nord Europe	Rapporteur & Examinatrice
Rafael Perez-Jimenez Professeur, Universidad de Las Palmas de Gran Canaria	Rapporteur & Examinateur
Luc Chassagne Professeur, Université Paris-Saclay, UVSQ (LISV)	Directeur de thèse

THESE DE DOCTORAT
NNT : 2022UPAST075

université PARIS-SACLAY

ÉCOLE DOCTORALE
Sciences et technologies de l'information et de la communication (STIC)

Titre : Contrôle de la communication par lumière visible dans un environnement de véhicule de peloton
Mots clés : Reseaux routiers intelligents, télécommunications optiques, vehicules autonomes

Résumé : Les premières études sur la technologie VLC (Visible Light Communication) ont montré que la technologie peut être bien applicable aux communications nécessaires pour maintenir un peloton stable de véhicules. Les études se limitent aux aspects de la couche physique pour le codage et le décodage des informations et la mesure de distance lorsque les véhicules sont strictement en visibilité directe. L'utilisation de VLC pour des applications aussi différentes nécessite d'abord une intégration fluide de la technologie dans la pile de protocoles. La première question est de savoir comment un module d'application peut être conscient qu'un lien VLC est disponible, comment il peut découvrir les voisins et comment il peut trouver l'homologue de communication prévu. Dans les WLAN, par exemple, le balisage de couche MAC et le protocole de découverte de voisin IPv6 (NDP) jouent les rôles clés dans la découverte de voisin / route au niveau des couches MAC et réseau, permettant la transmission de données au voisin prévu. Malheureusement, à notre connaissance, aucun travail n'a été effectué sur la découverte de voisins pour les réseaux VLC et les protocoles WLAN / IPv6 ne peuvent pas être simplement connectés à VLC, principalement en raison des caractéristiques uniques du FOV unidirectionnel et étroit. Plus précisément, afin de rendre VLC opérationnel dans des environnements véhiculaires réels, il est nécessaire de concevoir un protocole de contrôle d'accès moyen (MAC) qui assure un échange d'informations V2V continu avec la présence des problèmes difficiles provenant de la dynamique de la mobilité, des interférences multi-utilisateurs. et le bruit ambiant.

Title : Visible light communication control in a platoon vehicle environment
Keywords : Intelligent road networks, optical telecommunications, autonomous vehicles

Abstract : Early studies Visible Light Communication (VLC) technology have been shown that the technology can be well applicable for communications necessary to maintain a stable platoon of vehicles. The studies are restricted to the Physical layer aspects for information encoding and decoding and distance measurement when vehicles are strictly in light-of-sight positions. Using VLC for such different applications first requires a smooth integration of the technology into the protocol stack. The first question is how an application module can be aware that a VLC link is available, how it can discover the neighbors, and how it can find the intended communication peer. In WLANs for instance, the MAC layer beaconing and the IPv6 neighbor discovery protocol (NDP) play the key roles in neighbor/route discovery at both the MAC and network layers, allowing data transmission to the intended neighbor. Unfortunately, in our knowledge there is no work has been done on neighbor discovery for VLC networks and the WLAN/IPv6 protocols cannot be simply plugged to VLC, mainly because of the unique uni-directional and narrow FOV characteristics. More specifically, in order to make VLC be operational in real vehicular environments, it is necessary to design a Medium Access Control (MAC) protocol which ensure continuous V2V information exchange with the presence of the challenging issues coming from the mobility dynamics, multi-user interference, and environmental noise.

Remerciements

A toutes les personnes qui m'ont soutenu et ont permis la réussite de ce travail, merci !

Je tiens à remercier mon directeur de thèse, Luc Chassagne, pour son aide, sa patience et son dévouement. Je tiens à remercier mon co-directeur de thèse, Hongyu Guan, pour son aide durant mon doctorat ! Je tiens à exprimer ma gratitude à ma co-directrice, Oyunchimeg Shagdar, pour son aide et son soutien inestimables !

Je tiens à remercier Bastien, Carlos et Alex, ainsi que Jérémie, Artiol, Mohamed et toute l'équipe REVECOM pour leurs conseils et leur soutien dans la réalisation de cette thèse ! Merci de m'avoir conseillé sur la façon de m'améliorer en tant que chercheur !

Je tiens à remercier les examinateurs et les membres du jury qui ont accepté d'évaluer cette thèse ! Je me rends compte que c'est une tâche qui prends du temps !

Je tiens à remercier toutes les personnes et tous mes collègues du LISV et de Vedecom !

Je remercie toute ma famille pour leur amour et leurs soins ! Merci à mes parents et mes sœurs, d'avoir été là pour moi même s'ils étaient loin, pour leurs innombrables enseignements et pour tout ce qu'ils ont fait pour moi, je vous aime ! Merci d'être là pour moi et de m'aider dans mes moments les plus difficiles, Angie, Mary, Yajaira, Carlos, Aicha, Alex, Liz, Pao, Lina et le reste de mes amis de la vie et du travail ! Merci de m'avoir aidé à grandir en tant que personne !

«Le développement progressif de l'homme dépend de manière vitale de l'invention.» - ***Nikola Tesla***

Table des matières

Table des figures

Liste des tableaux

Acronymes

ADAS advanced driver assist systems.

AFE Analog Front-End.

AHS Automatic Highway System.

AWGN Additive White Gaussian Noise.

BBB Beagle Bone Black.

BER Bit-Error Rate.

BJT bipolar junction transistors.

C-ITS Cooperative Intelligent Transportation Systems.

C-V2X Cellular Vehicle-to-everything communication.

CACC cooperative adaptative cruise control.

CAN controller-area network.

CSMA/CA Carrier Sense Multiple Access with Collision Avoidance.

DAC Digital to Analog Converter.

EMI Electromagnetic interference.

ESA European Space Agency.

ETSI European Telecommunications Standards Institute.

FET field-effect transistors.

FSO Free Space Optical communication.

GaAs Gallium - Arsenide.

GPS Global Positioning System.

HeNe Helium - Neon.

HMI human machine interface.

IEEE Institute of Electrical and Electronics Engineers.

IM/DD Intensity Modulation with Direct Detection.

IrDA Infrared Data Association.

LED Light Emitter Diode.

LFSR linear feedback shift register.

LiFi Light Fidelity communication.

LOS Line Of Sight.

MAC Medium Access Control.

MATLAB MATrix LABoratory Software.

MLCD Mars Laser Communication Demonstration.

MUI Multi-Users Interference.

NASA National Aeronautics and Space Administration.

NDP Neighbor Discovery Protocol.

NEC Nippon Electric Company.

OBU vehicle on-board unit.

OFDM Orthogonal Frequency Division Multiplexing.

OMEGA Home Gigabit Access Project.

OOK On - Off Keying.

OS Operating System.

OWC Optical Wireless Communication.

PATH California Partners for Advanced Transportation Technology.

PCACC Predicted Cooperative Adaptive Cruise Control.

PD Photodiode.

PDR Packet Delivery Ratio.

PDT packet delivery time.

PER Packet Error Rate.

PHY-I Physical Layer Type I.

PRU programmable real-time units.

PSD power spectral density.

QoS Quality of Service.

RF Radio-Frequency.

RSU Road-Side Unit.

SILEX Semiconductor-Laser Intersatellite Link Experiment.

SINR Signal to Interference Noise Ratio.

TDMA Time Division Multiple Access.

TIA trans-impedance amplifier.

UDP User Datagram Protocol.

USDOT United States Department of Transportation.

V2N Vehicle-to-Network communication.

V2R Vehicle-to-Road side unit communication.

V2V Vehicle-to-Vehicle communication.

V2X Vehicle-to-everything communication.

VANET Vehicular Ad-hoc Network.

VLC Visible Light Communication.

VLCC Visible Light Communication Consortium.

VPPM Variable Pulse Position Modulation.

WAVE Wireless Access in Vehicular Environments.

WLAN Wireless Local Area Networks.

WPAN Wireless Personal Area Network.

Nomenclature

α	LED half angle
β	Poison distribution density (cars/meters/lane)
γ	FET channel noise factor
λ_a	Auto-correlation constraint
λ_c	Cross-correlation constraint
$\phi_{1/2}$	Semi-angle half-power of the LED
ψ_c	FOV
$\sigma(t)$	Additive noise
σ^2_{shot}	Shot noice variance
$\sigma^2_{thermal}$	Thermal noise variance
σ^2_{Tot}	Total noise variance
τ	Channel access probability
$a \star b$	Correlation of code "a" with code "b"
A_r	Active region of the PD
A_{eff}	Effective reception area of the PD
B	Bandwidth of electrical filter
c	Speed of light in a vacuum
C_{pd}	Photodetector fixed capacitance
d_L	Lateral distance between PD and LEDs
d_w	Vehicle width
d_{ir}	Distance between interference Tx and Rx
d_{len}	Vehicle length
d_{Lx}	Longitudinal distance inside the MUI zonefor x lane
d_{MUI}	Maximum communication distance due to LOS condition
d_{tr}	Distance between intended Tx and Rx
$g(\psi)$	Optical gain concentrator

G_{ol} Open-loop voltage gain

gm FET transconductance

$H(\phi, \psi)$ DC gain

$h(t)$ Baseband channel impulse response

i Number of vehicles on an l-kilometer

I_2 Noise-bandwidth factor (0.562)

I_3 Noise-bandwidth factor (0.0868)

I_{bg} Background photocurrent

k Boltzmann constant

L_b Packet size

L_w Lane width

L_{sc} Length of OCDMA code

L_{Tot} Total length of lanes inside the MUI zone

$m(t)$ Modulated signal

M Total number of cars with VLC link to the target vehicle

m_i Lambertian coefficient

n Internal refractive index of the concentrator

N_c Total number of possible spreading codes

n_c Number of code groups

P_i Interference power

P_r Power received

P_t Transmission power

q Electronic charge

R Photodetector responsivity

$R_0(\phi)$ Angular distribution of a Lambertian light source

s Longitudinal distance in the adjacent lane between the Rx and the FOV

T_k Absolute temperature

$T_s(\psi)$ Optical band-pass filter

$T_{interval}$ Message generating interval

T_{tx}	Average packet transmission time
$U(\phi)$	Radiant intensity
w_c	Weight of OCDMA code (non-zero bits)
$x(t)$	Signal captured by the PD
$y(t)$	Photo-current generated by the PD

1 - Introduction

Sommaire

The primary goal of the Cooperative Intelligent Transportation Systems (C-ITS) is to improve road safety and traffic efficiency by enabling vehicles and infrastructure to communicate via Vehicle-to-everything communication (V2X). The key players for V2X are radio communications technologies, notably 802.11p, Cellular Vehicle-to-everything communication (C-V2X), and 4G/5G that provide omni-directional medium to long-distance communications, allowing automobiles and roadside infrastructure to interact directly with each other (Vehicle-to-Vehicle communication (V2V) or Vehicle-to-Road side unit communication (V2R)) or through a network (V2N).

While radio communication technologies are likely the *de-facto* choice for many C-ITS applications, there is a need for complementary technology, particularly for applications that require close to 100% reliability and strong cybersecurity protection. Radio resources are limited and vulnerable to security attacks. Particularly, applications for autonomous driving have highly stringent accuracy and security requirements. Vehicle platooning is one such application with rigorous requirements, in which V2V communication between platoon members is necessary for longitudinal and lateral controls to minimize chain instability. Because the information will be used to operate vehicles, it must be very reliable and secure. Recent research studies recommend Visible Light Communication (VLC) for V2V as a complementary technology to radio communications for applications such as vehicle platooning [2, 3, 4, 5, 6].

1.1 . What is vehicle platooning ?

The automotive platooning principle can be characterized as a group of vehicles that travel in chain formation and are strongly coordinated [7], as seen in Figure

1.1. These vehicles are connected via a headway control mechanism, such as radar-based or magnetic-based systems, with minimal inter-vehicle spacing, as little as a few meters. The first vehicle of the platoon, the leader, keeps the other vehicles, the followers, up to date on the Automatic Highway System (AHS) circumstances and what movements, if any, the platoon make [8]. These vehicles maintain a constant set space between them at all speeds up to motorway speeds. Because the close spacing, roadway capacity is boosted. Since the vehicles are traveling at such a low relative speed, even violent accelerations and deceleration do not significantly influence the vehicles, increasing passenger comfort, and decreasing fuel consumption, especially for trucks platoon ($\approx 20\%$) [9].

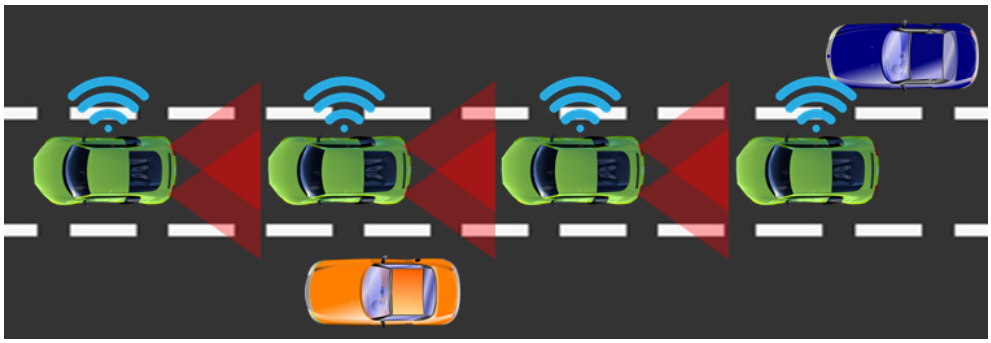

Figure 1.1 – Vehicular platooning scenario where green vehicles form a platoon with almost same speeds and inter vehicle distances. Yellow and blue vehicles represents interference communication with the platoon.

When the California Partners for Advanced Transportation Technology (PATH) program provided the platooning scenario [10], the previous assertions were shown to be accurate. Eight self-driving vehicles were platooned with inter-vehicle intervals of less than ten meters and drove in a single-lane formation guided by magnets buried in the roads. As a unit, the platoon exhibited its ability to start, halt, accelerate, and decelerate. Moreover, the PATH program demonstrated the ability to separate the platoon to allow vehicle ingress and subsequently reunite as one platoon. A Heads-Up-Display device was utilized to provide feedback to the user, such as speed, distance to destination, and the current maneuver the vehicle was doing. Agreeing with the premise of the previous notion, vehicle platooning may be defined as a method of improving the current transportation system both economically and technologically [8].

Another example of platooning can be found in [11], in which the author mentioned a vehicle platoon as a "tightly spaced string of vehicles, where the inter-vehicle distances were appropriately maintained as low as three to one meter at highway speeds, depending on what sensors and communication devices were used." Such small distances were safe enough for the vehicles since each vehicle

knew the dynamics of its leading vehicle and may also know the dynamics of the platoon's leading vehicle. Typically, vehicles must utilize a radar or laser sensor to directly measure the speed and distance between themselves and the previous vehicle. Inter-vehicle communication was also used to send needed signals in several modern systems. It was critical to ensure that V2V communication was robust for the platoon's safety. For example, all following vehicles were in touch with the lead vehicle and receive the same information.

The controller-area network (CAN) is a wired communication bus standard that allows microcontrollers and devices in automobiles (also known as nodes) to interact with one another. A vehicle may have many CAN buses for various functional areas such as the engine or body functions [12]. Separate functions of the platooning application, such as control algorithms, human machine interface (HMI), sensor fusion, and V2X, are handled via a dedicated CAN bus embedded into the nodes. The V2X node, or vehicle on-board unit (OBU), serves as a wireless gateway to the CAN bus of other vehicles and infrastructure. This node allows vehicles in the platoon to share local vehicle signals like speed and sensor data. The platoons control algorithms take advantage of the shared signals. IEEE 802.11p [13] or LTE-V2X, operating in the dedicated $5.9\ GHz$ radio frequency channel, are expected to be used for wireless communication in the V2V communication system.

However, these technologies suffer from performance deterioration owing to congestion, Radio-Frequency (RF) bandwidth shortage, and security concerns [14, 15, 16]. In contrast, VLC is a promising alternative technology that has the ability to overcome the above-mentioned issues. In 2016, Ucar et al. [14] analyzed a hybrid RF/VLC communication security vulnerabilities and hazards connected with the platoon attackers through simulation. The authors demonstrated that, despite the reduced influence of the adversary on platoon stability, hybrid RF/VLC systems were nevertheless vulnerable to packet falsification and replay assaults. Vehicles can be subjected to packet falsification due to a lack of security protocol, which disrupts platoon stability.

In 2016, Abualhoul et al. [17] present a low-cost, low-latency, and simple outdoor VLC prototype that may be placed as a vehicle tail lighting system. They tested the VLC prototype's performance in daylight and in a Line Of Sight (LOS) situation. A Simulink model was used to evaluate the performance of platooning control, which employed the VLC platform for inter-vehicle communication. The platform looked solid in terms of end-to-end communication performance for platoon safety standards such as Packet Delivery Ratio (PDR) and latency. In [18], Ucar et al. propose a hybrid security protocol for platoon communication based on IEEE 802.11p and VLC, with the purpose of assuring platoon stability and safeguarding platoon movements against data packet injection, channel overhearing, jamming, and platoon maneuver assaults.They show that their hybrid protocol causes a difference in speed and distance between platoon members under secu-

rity assaults of less than 0.1 percent, compared to 25% and 10% for previously suggested IEEE 802.11p and IEEE 802.11p-VLC hybrid protocols, respectively.

In 2018, Abualhoul et al. [19] suggest using the lane-centering approach to improve the VLC inter-connectivity of autonomous vehicle platoon members. By integrating both systems, the reliance on communicating vehicle status and Global Positioning System (GPS) locations to relocate platoon members and assure direct LOS is eliminated. When the road lanes are discernible, the findings validated the reduction in misalignment between platoon members and ensured the VLC connection stability independent of any collaboration needs. Other instances of detecting uncertainty or transient lane-marking insufficiency can be tolerated and may result in a temporary VLC suspension.

In a more recent work, Boukhalfa et al. [20] present an evaluation of radio and VLC technologies for platooning application. They demonstrate a novel RF architecture capable of supporting platooning applications, which is based on a completely distributed Time Division Multiple Access (TDMA) and satisfies the Quality of Service (QoS) criteria for platooning communication. Second, they attempted to assess the maturity of the vehicular VLC standard by performing large-scale simulations of dynamic road situations in which vehicles may use VLC technology, such as platooning versus interfering automobiles.

Nevertheless, the authors in [21] investigate cooperative vehicle platooning under various communication techniques and provide a new dynamic control strategy based on Predicted Cooperative Adaptive Cruise Control (PCACC). They carry out a performance comparison of several communication technologies, such as VLC and V2V, with or without relaying through Road-Side Unit (RSU), and evaluate their applicability to completely cooperative and semi-autonomous control methods. In terms of the influence of communication technologies, their findings reveal that conveying leader information through RSU produces the optimum performance, provided the network is appropriately dimensioned to ensure a low Packet Error Rate (PER).

1.2 . Why a vehicular communication system ?

Vehicles on the road have progressed from being metal surfaces on wheels to sensing and computation-capable machines nowadays, as can be appreciated in Figure 1.2. Hundreds of embedded processors and sensors are now standard on high-end versions of previous-generation vehicles, allowing them to see their surroundings and interact with them in semi-autonomous and ultimately fully autonomous ways. The road infrastructure has also developed with adaptive traffic signals and communication-capable pay tolls installed on roadways. Adopting the notion of communication and enabling information exchange between vehicles and infrastructure is expected to be the next stage in the evolution of transportation

systems.

The authors grouped the network applications of vehicular environment into three primary areas in the literature : road safety, traffic monitoring, and entertainment delivery [22] :

— Road safety : safety applications are always crucial in order to drastically minimize the number of accidents, with the primary goal of preventing accidents from occurring in the first place. The primary goal of these apps is to alert drivers about traffic conditions in their immediate vicinity and farther down the road via vehicular communications. This can be accomplished, for example, by reducing the number of lane changes and/or speed modification. Also, platooning allows vehicles to move more closely. Fuel-efficient vehicles benefit from reduced aerodynamic drag as vehicle headway is tightened. When combined with an adaptive cruise control system and V2V communications, a vehicle collision caused by human mistake can be avoided.

— Traffic monitoring and management : traffic monitoring and management are critical for avoiding traffic congestion and increasing road capacity. Crossing junctions on city streets may be hazardous and difficult at times. Thus, traffic signal timing can assist vehicles in crossing junctions. Allowing regular, steady traffic reduces travel time and increases vehicle throughput. Drivers, on the other hand, may plan their journeys more efficiently. With knowledge of real-time traffic conditions, the problem of highway traffic congestion may therefore be greatly minimized.

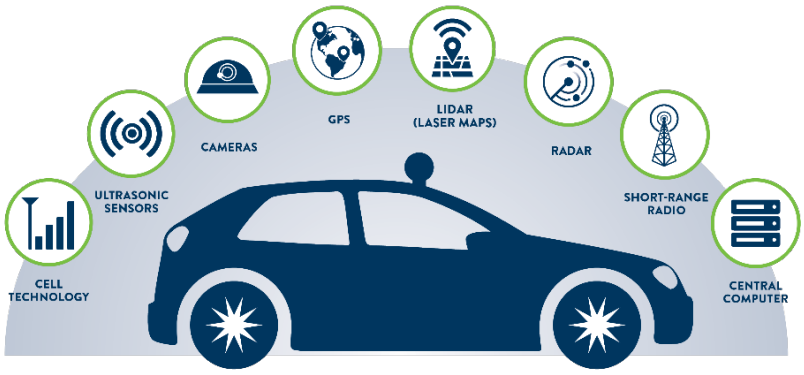

Figure 1.2 – Complexity of a modern vehicle : ultrasonic sensors, cameras, GPS, LIDAR, central computer, radar and communication systems

— Infotainment delivery : the purpose of infotainment apps is to give both drivers and passengers with ease and comfort. For example, the ability to produce peer-to-peer file sharing tools and games while traveling. A real-time parking guidance system is also suggested to alert vehicles to available parking spots. For marketing and warning, digital display panels for VANETs devices and users are proposed. Internet access may be simply provided through V2I communications.

A vehicular communication system will maximize the capabilities of next-generation transportation systems while also altering the paradigm from autonomous to cooperative driving. Vehicle and infrastructural capabilities that have recently been developed open the door for a slew of new applications. As a response, various authorities and regulatory bodies throughout the world have developed standards and strategies for deploying such systems, which are commonly referred to Intelligent Transportation Systems (ITS) [23]. RF communication is used in the majority of ITS applications proposed so far. The European Telecommunications Standards Institute (ETSI) C-ITS [24], and IEEE 1609 Wireless Access in Vehicular Environments (WAVE) [25] sets of standards, for example, offer entire ITS stacks for Europe and the United States, respectively, and are based on radio access technologies particularly ITS-G5, IEEE 802.11p, and C-V2X.

1.2.1 . Why a multi-technology RF and light based for communications ?

Lighting technology is another sector that has seen a significant change in the previous decade. VLC has developed as a viable communication method, fueled by substantial advancements in Solid State Lighting (SSL) technology and the widespread usage of Light Emitter Diode (LED) for indoor and outdoor illumination. VLC is a new technique that allows data to be sent by changing the intensity of light generated by LEDs. VLC uses the visible light spectrum (wavelengths between 780 and 375 nm) as a communication medium. Because VLC is done directly utilizing vehicle headlights and taillights, it is a quick, safe, and low-cost solution.

Furthermore, using LED instead of a xenon or halogen bulb provides several advantages, including long usable life, low power consumption, high environmental tolerance, and high-efficiency [26]. Finally, because radio and light communications do not interfere with one another, VLC may coexist and complement radio communications flawlessly. Indeed, the Institute of Electrical and Electronics Engineers (IEEE) has specified VLC standards, including IEEE 802.15.7[27] and IEEE 802.15.7r1[28], released in 2011 and 2018, respectively, and current work on IEEE 802.11bb[29].

VLC physical layer configurations primarily emphasize the IEEE 802.15.7 standard, and its revision IEEE 802.15.7r1 for indoor and outdoor LED to Photodiode (PD) or LED to camera VLC communications. The standards essentially carried

over the Wireless Personal Area Network (WPAN) solutions in the Medium Access Control (MAC). IEEE 802.11bb [29], on the other hand, aims to include Light Fidelity communication (LiFi) into Wireless Local Area Networks (WLAN) technologies.

In the next chapter, we go deeper into VLC technology, its theory, and the most relevant advances in the vehicular VLC field. Having defined what is meant by vehicular platooning and VLC communication, we now discuss the objectives and motivations of this research work.

1.3 . Objectives and Outline of the Thesis

1.3.1 . Objectives of this work

As mentioned above, early studies on VLC technology have shown that the technology can be well applicable for communications necessary to maintain a stable platoon of vehicles [30]. The studies are restricted to the Physical layer aspects for information encoding and decoding and distance measurement when vehicles are strictly in line-of-sight positions [17, 31]. While platooning is an application to which VLC fits naturally, other applications such as lane merging, parking, motorway tolling, and electric vehicle charging can also be imagined. Using VLC for such different applications first requires a smooth integration of the technology into the protocol stack.

The first question is how an application module can be aware that a VLC link is available, how it can discover the neighbors, and how it can find the intended communication peer. In WLANs, for instance, the MAC layer beaconing and the IPv6 Neighbor Discovery Protocol (NDP) play critical roles in neighbor/route discovery at both the MAC and network layers, allowing data transmission to the intended neighbor [32]. Unfortunately, to our knowledge, there is no work that has been done on neighbor discovery for VLC networks, and the WLAN/IPv6 protocols cannot be plugged efficiently into VLC, mainly because of the unidirectional and narrow FOV characteristics. More specifically, to make VLC operational in natural vehicular environments, it is necessary to design a Medium Access Control (MAC) protocol that ensures continuous V2V information exchange under the challenging situations coming from the vehicle mobility dynamics, multi-users interferences, and environmental noise.

The main objective of this Ph.D. work is then to develop MAC layer techniques for VLC for ITS applications. It will be shown in Chapter 2 that there are very few work on MAC protocol for VLC in vehicular scenarios. The United States Department of Transportation (USDOT) - Vehicle Safety Communications project [33] in 2005 recognized 34 DSRC safety applications, including platooning. The project identified the communication requirements of each of these applications. According to this study, for platooning, the communication system must provide one-way or

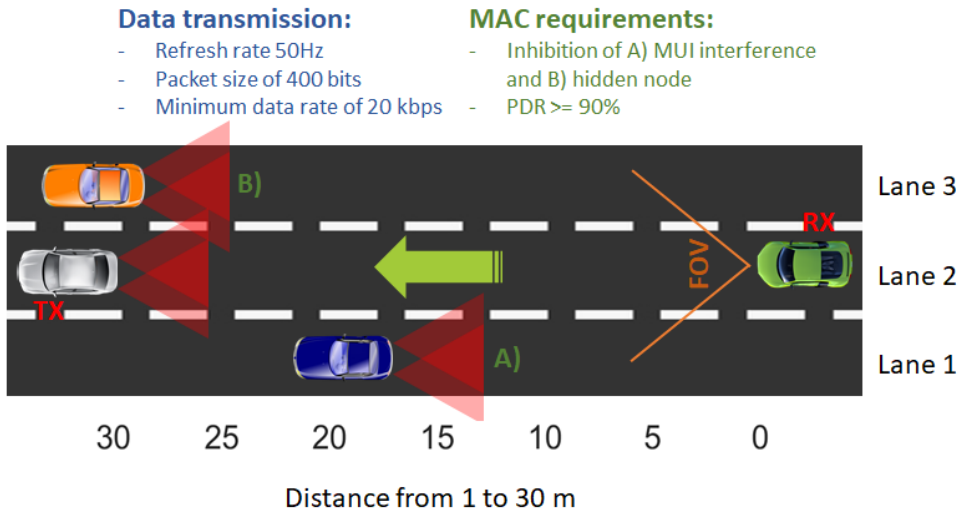

Figure 1.3 – Vehicular VLC system requirements for highway platooning

two-way communication and point-to-point or point-to-multipoint communication in a periodic transmission mode with a 50 Hz update rate and a range of 100 meters. The vehicle's location, velocity, acceleration, direction, and yaw-rate must be broadcasted, and each packet must be received at the destination at a latency of no more than 20 milliseconds. To summarize, for platooning application, a VLC system must

— enable one-way or two-way point-to-point communication,

— establish periodic transmissions at 50 Hz,

— provide a communication range at least 15 m, ideally up to 30 m, given an optimal inter-distance of 6 to 8 m for autonomous vehicles [34, 35, 36, 37],

— transmit packets of at least 400 bits,

— meet the latency requirement of maximum 20 milliseconds and the minimum throughput of 20 kbps, and

— set up a link with an error rate below to 10%.

In addition, the MAC protocol must have the following set of requirements.

— support multiple transmitters at the same time, despite the relative movement of the vehicles forming the highway platoon,

— reduce the impact of the signal interference generated by vehicles outside the platoon,

— provide a PDR of at least 90%

Those performance requirements are presented in Figure 1.3.

1.3.2 . Manuscript outline

The overall structure of this work takes then the form of five chapters. Since the vehicular VLC exposes a single application of an entire technology, its design and development are pretty similar to a most straightforward VLC system. Consequently, Chapter 1 introduces the principles of vehicular platooning. This chapter also introduces the VLC technology as a communication technology for autonomous vehicle platoon. We will also present the motivation of investigating the PhD subject and our work goals based on the previous assessments.

The main characteristics of VLC technology, its requirements, as well as the benefits of its implementation are presented in Chapter 2. Although, a summary of the most important developments along the past decades is presented in this chapter, including a brief summary about the history of Optical Wireless Communications systems and the typical communication schemes. This analysis details how some MAC protocols have been implemented and some physical designs that improve the performance of the VLC link. Thus far, we have established the reference point from where our work departs, we conclude this chapter with the well studied channel model equations of the VLC systems intended to establish comprehension of the channel, lighting on the differences against the radio communication, and the challenges for developing a MAC protocol.

Chapter 3 analyzes the multi-users interference impact on the vehicular VLC. While some MAC protocols have been proposed for VLC, there is no study showing the impact of multi-users interference, and hence, the need of MAC for VLC in the vehicular scenario. Therefor, this chapter presents an analytical model on the interference zone in VLC for different data rates. Simulations on VLC systems performance are carried using two different platforms, Veins VLC and Matlab, analysing the VLC communication range affected by the MUI in different traffic densities. Finally, an experimental demonstration of those interfering zones is presented, exhibiting the capabilities of our VLC prototype. The results shows that its undeniable that MAC is necessary to achieve a reliable outdoor VLC.

Chapter 4 presents the research findings and evaluates the possibility to adapt a MAC protocol based on the results obtained on the previous chapter. Therefore, this chapter presents the principles of a vehicular VLC MAC protocol, summarizing the essential points and the essential features it must contemplate to prevent or suppress the interference generated in the scenario. Also, this chapter presents relevant attention to the MAC protocol proposed for vehicular VLC communication. We test the protocol behavior with different configurations, showing the key parameters, and exposing the efficiency of the protocol through simulations. Nonetheless, the PDR simulation results of different CDMA codes in synchronous and asynchronous transmissions are presented in this chapter. At the end of this chapter, we introduce the time requirements on simulation for CDMA codes, intending to show the resources consumed by each of them.

Finally, Chapter 5 summarizes and identifies the key contributions of the work described throughout this thesis. The identification of crucial properties of the MAC layer for vehicular VLC and the proof of concepts by simulations make part of them. Some observations on the improvements of the developed platform are presented, based on the experimental results. It is clear that automotive VLC still faces several challenges for the future years. Some perspectives describe these challenges at the end of this work.

1.4 . Context of works

This thesis work has been carried out in collaboration between the ISA team of the Laboratoire d'Ingénierie des Systèmes de Versailles (LISV) [38] and the VEDECOM Institute [39].

The ISA team is structured around the problem of characterizing the behavior of so-called advanced systems, modeling the behavior of components to understand the role of environmental parameters, then instrumentation and metrology of the component or the system as a whole block to validate its performance.

The VEDECOM institute, established in February 2014 as an Institute for the Energy Transition (ITE) under the French Government's Future Investments Program (PIA), is committed to personalized, carbon-free, and sustainable transportation. The objective of VEDECOM is to create breakthrough technologies and a transversal vision of new uses for more ecological, autonomous, and shared mobility and to deliver significant competitive benefits to their members and the environment.

Moreover, during the development of this thesis, I collaborate with the University Stephan Cel Mare of Suceava, Roumania, in the PHC Brancusi project "Development of adaptive vehicle-to-vehicle communication systems with range finder capabilities, based on visible light communication technology." During this collaboration, I effectuated a short internship from 11^{th} to 16^{th} of November of 2019 in the Romanian laboratory to share technical information about the VLC platforms developed for both universities. This collaboration concludes with the publication of a conference paper [40]. It was also planned a full month in Suceava but the situation did not allowed it.

2 - State of the art : vehicular VLC

Sommaire

A large number of R&D studies and standardisation efforts suggest VLC as a candidate solution for increasing reliability and security for V2X communications. The majority of those works focuses on VLC physical layer solutions, including modulation techniques and filtering strategies [41, 42, 43]. There have also been several real-world demonstrations of VLC prototypes for V2V communication [2, 3, 43]. In contrast to the extensive literature on physical layer solutions, there has been a very little attention on MAC for VLC [44, 45, 46, 47]. Conceivably, the reason behind the lack of attention on MAC for VLC are due to the fact that VLC is directional and requires a LOS condition, one could question whether Multi-Users Interference (MUI) is present in VLC, thereby overlooking the relevance of MAC.

2.1 . Brief historical of OWC systems

Free Space Optical communication (FSO) is a centuries-old method that involves transmitting data-laden optical radiation across the air from one place to another. Ancient Greeks and Romans utilized fire beacons for signaling around 800 BC, and by 150 BC, American Indians were employing smoke signals for the same purpose [48]. Other optical signaling systems, such as the semaphore, were employed by French sea navigators in the 1790s. However, Alexander Graham Bells photophone experiment in 1880 [1], illustrated in Figure 2.1, may be considered the first optical communication in an unguided channel. In his experiment, Bell modulated the solar radiation with a voice signal and transmitted it across a distance of roughly 200 meters. A parabolic mirror with a selenium cell at its focal point served as the receiver. However, due to the crude nature of the gadgets employed and the sporadic nature of the solar radiation, the experiment did not proceed well.

With the discovery of optical sources, most notably the laser, Optical Wireless

Communication (OWC) fortunes altered in the 1960s and early 1970s. The spectacular transmission of a television signal was demonstrated over a 48 km distance using Gallium - Arsenide (GaAs) LED by researchers working in the MIT Lincolns Laboratory in 1962 ; a 190 km transmission of voice modulated into a Helium - Neon (HeNe) laser between Panamint Ridge and San Gabriel Mountain was performed in USA in May 1963 ; and the first TV-over-laser demonstration by a group of researchers working in the North Lab in March 1963 were just few examples. Nippon Electric Company (NEC) constructed the first laser connection to handle commercial traffic in Japan about 1970. The connection was a 14-kilometer full-duplex $0.6328\mu m$ HeNe laser FSO between Yokohama and Tamagawa [49].

OWC has been developed and utilized mainly through the military for stealth communications since that period. National Aeronautics and Space Administration (NASA) and the European Space Agency (ESA) have both conducted extensive research into the technology for deep-space applications, with programs such as the Mars Laser Communication Demonstration (MLCD) [54] and the Semiconductor-Laser Intersatellite Link Experiment (SILEX) [55], respectively. Despite outer space OWC is beyond the scope of this study ; it is interesting to note that near-Earth FSO has been successfully demonstrated in space between satellites at data rates of up to 10 Gbps during the previous decade [56].

OWC has seen a renaissance as a result of the fast growth and maturity of optoelectronic devices. In addition, as the demand for additional bandwidth grows in response to new and developing applications, the previous approach of depending on a single access method to connect end-users must be abandoned. These factors

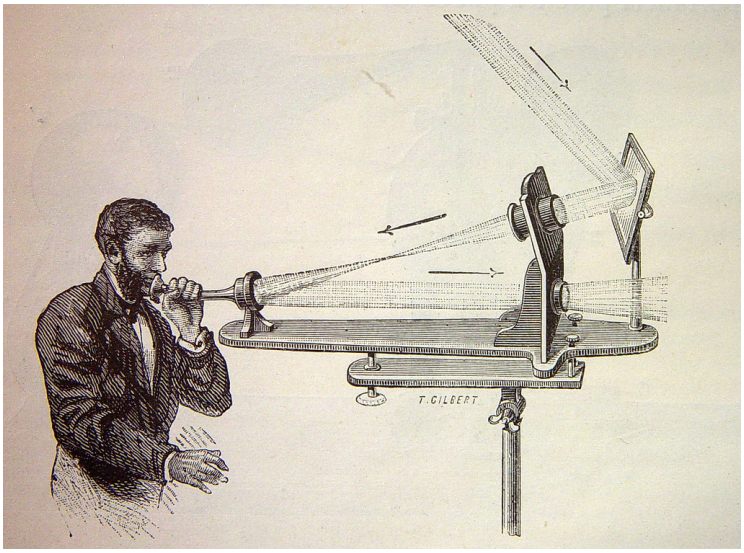

Figure 2.1 – Alexander Graham Bell's photophone experiment in 1880 [1]. Considered the first optical communication in an unguided channel

Table 2.1 – History of FSO systems.

Date	*Device / Standard / System*
800 BC	Fire beacons - by the ancients Greeks and Romans
150 BC	Smoke signal - by the American Indians
1790	Optical telegraph - by Claude Chappe, France [50]
1880	Photophone - by Alexander Graham Bell, USA
1960	Laser
1970	FSO mainly used in secure militar applications
1979	Indoor OWC systems - F. R. Gfeller ang G. Bapst [51]
1993	Open Standard for IR data communications - The Infrared Data Association (IrDA) [52]
2003	The Visible Light Communication Consortium (VLCC) - Japan [53]
2008	Global standards for home networking (infrared and VLC technologies) - Home Gigabit Access Project (OMEGA) - EU
2009	IEEE 802.15.7 - First standard on VLC [28]
2021	IEEE 802.11bb - Standard on VLC compatible with IEEE 802.11 standard (Ongoing work) [29]

and their demonstrated effectiveness in military use reignited interest in its civil applications inside the access network. A summary of this technological evolution is presented in table 2.1. Recently, light emitting diodes (LED) have been able to replace conventional lighting for both indoor and outdoor use due to its low energy

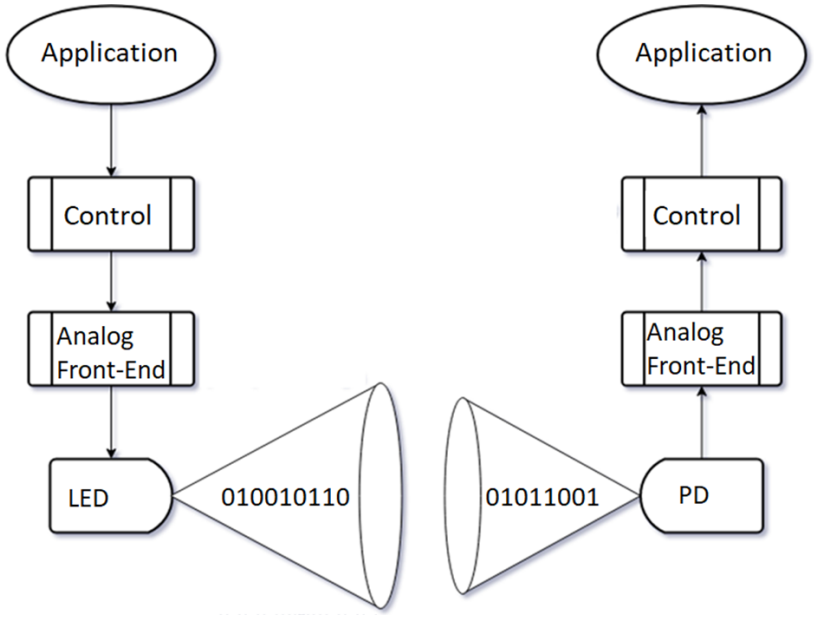

Figure 2.2 – Block diagram of a general VLC system

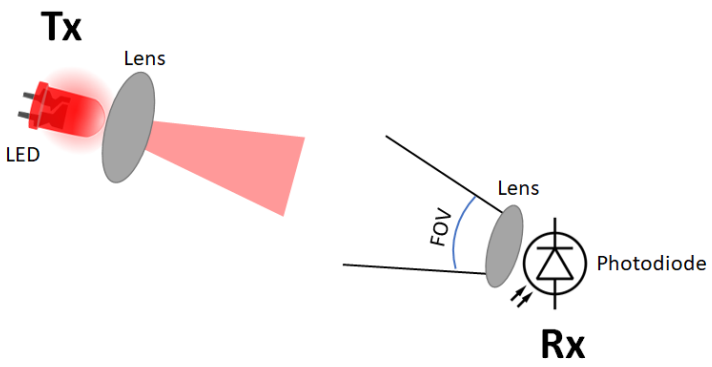

Figure 2.3 – Directed LOS VLC link configuration

consumption, extended lifetime, and cheaper cost per unit brightness [57, 58]. Furthermore, the LED's relatively fast modulation speed allows for short-range communication using visible light. As a result, VLC may be separated from RF communication to enable EMI-free and license-free communications [59, 60, 61]. The use of LED lighting systems for VLC is gaining popularity [62].

2.2 . VLC Link Configuration

We must consider various aspects such as environmental noise and channel conditions to build high-speed optical links using VLC technology. This is particularly true because the light will reflect off the ceiling, walls, roads, and most other objects but will not penetrate through opaque barriers ; however, the light will be dispersed and absorbed owing to air conditions in an outside setting. Figure 2.2 illustrates a block diagram of a VLC system.

There are several methods to construct an optical connection physically. Typically, these are divided into four configurations [48] :

— Directed LOS

— Non-directed LOS

— Diffuse

— Tracked

Directed LOS

The most well-known link architecture is directed LOS, illustrated in Figure 2.3, which is used for many years in low data rate, simplex remote control applications for household electrical devices like televisions and audio equipment. There has

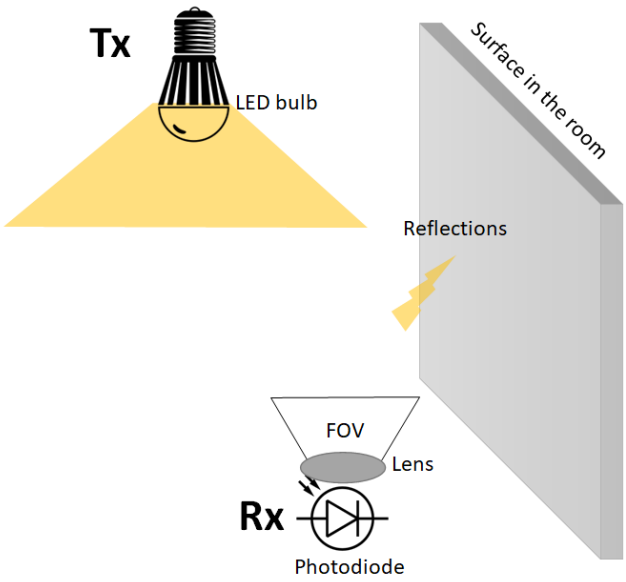

Figure 2.4 – Non-directed LOS VLC link configuration

been a surge in interest in using LOS connections for various outdoor applications in recent years. The optical lens concentrates the light on a narrow beam with minimal power consumption and a high power flux density on the photodiode. In addition, the directional connections in the LOS system do not suffer from multi-path distortions, and, when employed by a restricted FOV receptor, noise from ambient light sources is also substantially rejected [63]. Consequently, the data rate is restricted by a loss of free space instead of the effects of multi-path dispersion [64]. However, the directionality of this setup might instead limit the communication range of an indoor application, which would make it challenging to cover all the room space. Directed LOS connections require the transmitter and the receiver to be almost perfectly aligned, and hence difficult to be applied to mobile communications.

Non-directed LOS

Non-directed LOS considered the most versatile option for indoor applications, employs wide beam transmitters, and wide FOV receivers. Dispersion from surfaces within the room to provide a larger coverage area (Figure 2.4), thereby enabling an optical system comparable to RF with data rates above $150\ Mbps$ [61, 62]. Non-directed connections are appropriate for point-to-multipoint broadcasting. They are resistant to shadowing and blocking and do not demand alignment or tracking. They can be less sensitive to signal blockage than to reflections on the surfaces of objects in that area, result in a high proportion of transmitted light being detected at the photodiode from different directions. However, they suffer from significant

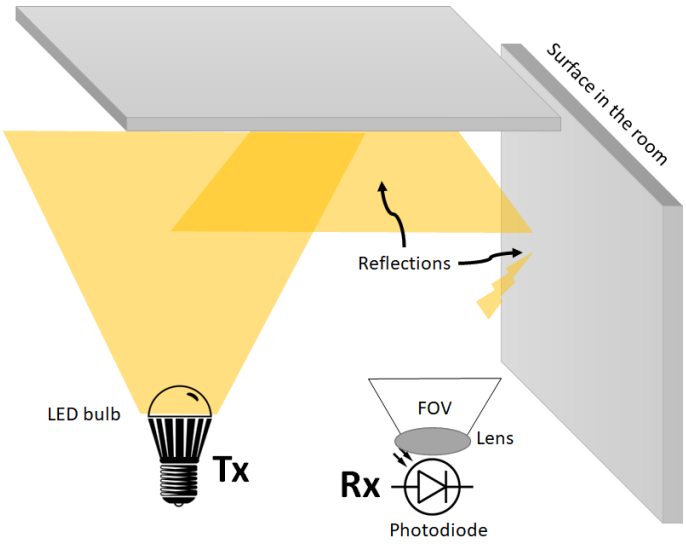

Figure 2.5 – Diffuse VLC link configuration

optical path loss thus, needing higher transmit power to cope with multipath-induced dispersion. VLC connections should present a good performance, even in settings with high ambient light levels, which usually degrades link throughput.

Diffuse

The diffuse VLC indoor topology is the most suitable for LAN ad hoc networks because it does not require accurate alignment of the transmitter and receiver modules, does not require a LOS path, and is essentially immune to transmission path obstruction as showed in Figure 2.5. It generally comprises a transmitter that emits a broad beam of light while pointing directly at the ceiling. Unfortunately, diffuse connections have substantial path loss with a horizontal spacing of 5 m, generally 50–70 dB [25]. The path loss is enhanced further if a momentary barrier, such as a human, masks the receiver, obstructing the primary signal path, a condition known as shadowing [25]. The received signal may also suffer from severe multi-path dispersion, which occurs when the transmitted pulses are distributed out in time over alternative routes of varying lengths, restricting the maximum unequalized bit rate attainable. Furthermore, with diffuse systems, single or several transmitters must illuminate the whole space. After a few reflections, diffused light propagation can do this but requires a significant amount of transmitted optical power.

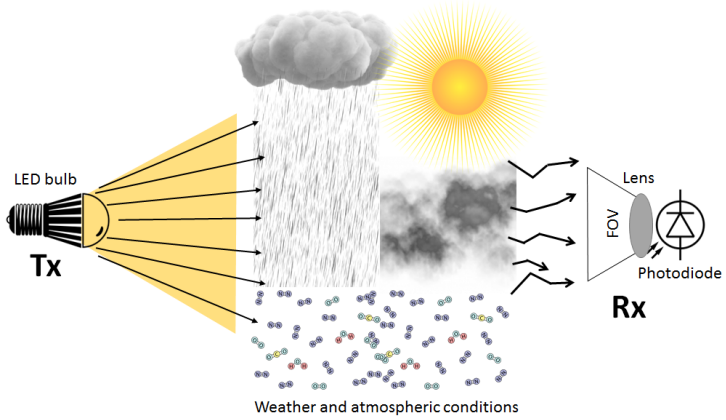

Figure 2.6 – Outdoor VLC link configuration

Outdoor communication

VLC connections can provide equivalent performance to optical fiber communication in an outdoor setting, with a link range from a few meters to a few kilometers in the case of a laser as transmitter. The optical transmitter output can reach $100\,mW$ or even several watts, with enough power margin at the receiver to handle attenuation effects of atmospheric and climatic circumstances, including fog, snow, rain, drizzle, turbulence, and structural thermal expansion, as illustrated in Figure 2.6. The received signal fades more than the RF waves due to atmospheric and climatic circumstances. When compared to rain and snow, fog is the most difficult to deal with because of its significant attenuation.

Following an explanation of the different configurations for the VLC systems, the next section addresses the related work produced in the field of vehicular communication, with a focus on VLC.

2.3 . Vehicular communication

Vehicular communication and vehicle automation are the key research domains on which automotive industries have been put a great effort in the past decades [65]. For example, advanced driver assist systems (ADAS) that automate the Vehicle's longitudinal and lateral movements, such as the Tesla Autopilot and Cadillac Super Cruise systems, are becoming available as an option in an increasing number of production vehicles. Furthermore, V2V communication technology is currently integrated in Cadillac CTS vehculars [66] and Volkswagen Golf 8 [67].

Vehicle-to-vehicle communication allows surrounding vehicles to coordinate their mobility and form vehicle platoons : a group of vehicles traveling at the same speed and at a small inter-vehicle distance. As mentioned earlier, vehicle pla-

tooning has two key advantages : improving traffic efficiency due to its capability of driving vehicles at shorter inter-vehicle distance at relatively high speed, increasing fuel consumption due to lower aerodynamic drag forces acting on platooning vehicles, particularly heavy-duty vehicles.

Indeed, a microscopic simulation study in [68] indicates that increasing the density of vehicles with cooperative adaptative cruise control (CACC) will improve highway capacity since it allows the driver to choose smaller time headways. The authors of [69] developed a mathematical model that estimates that vehicle platooning in the urban highways should double the traffic throughput. The estimation has been validated by simulation analysis. The minor separation between two heavy-duty vehicles reduces fuel consumption, according to experiments published in [70]. Vehicle platooning has already been demonstrated to be technically feasible. The California PATH team, for example, performed Vehicle platooning on the I-18 freeway in San Diego, California, between 1994 and 1997 [71]. Other highway-based experimental assessments include [72], which develops a platooning system architecture for heavy-duty trucks. Over varied degrees of road slope, the system is assessed in terms of controller tracking performance and fuel usage. String stability [73], defined as the capacity of preceding vehculars to attenuate traffic disruptions downstream, is a fundamental controller performance parameter in these studies (for example, changes in velocity).

The activities of creating, merging, and separating platoons, in addition to maintaining a platoon formation, need organized coordination between vehicles that in principle realised via V2V communication. In [74], the authors present a negotiation protocol between vehicles that explain the sequence of actions during merge, split and change lane operations. After a protocol terminates successfully, the vehicle actions become coordinated via V2V communication, and the maneuver begins. In [75], a message set is suggested to allow linked vehculars to coordinate more complicated moves in merging, junction, and emergency vehicle scenarios for a 2016 Grand Cooperative Driving Challenge [76].

Furthermore, the majority of current VLC standardization and R&D efforts are focused on improving physical layer architecture. According to the IEEE 802.15.7 standard, Physical Layer Type I (PHY-I) is intended for outdoor applications using On - Off Keying (OOK) and Variable Pulse Position Modulation (VPPM) coding methods, which are moderately durable in severe outside conditions. The authors of [41, 42] presented several transmission modulation methods (Manchester, Orthogonal Frequency Division Multiplexing (OFDM), Miller, and others) as well as sophisticated reception filtering algorithms.

Belle et al. [77] presented an IEEE 807.15.7 VLC prototype that builds on their earlier work [78] on IEEE 802.15.4 [79]. The authors created software libraries for PHY and ZigBee MAC that were not built particularly for VLC. Wang et al. [80] evaluated VLC performance in outdoor/indoor environments for different types of

VLC systems : high/low power LED to PD or LED to LED, using a VLC platform, in terms of communication speed, communication distance, and low power LED/PD saturation for different types of VLC systems : high/low power LED to PD or LED to LED. The authors of [2] recommended that visible light be used not just for V2V communications but also for measuring inter-vehicle distance. Finally, a number of VLC-based V2V communication demonstration have been done [2, 3].

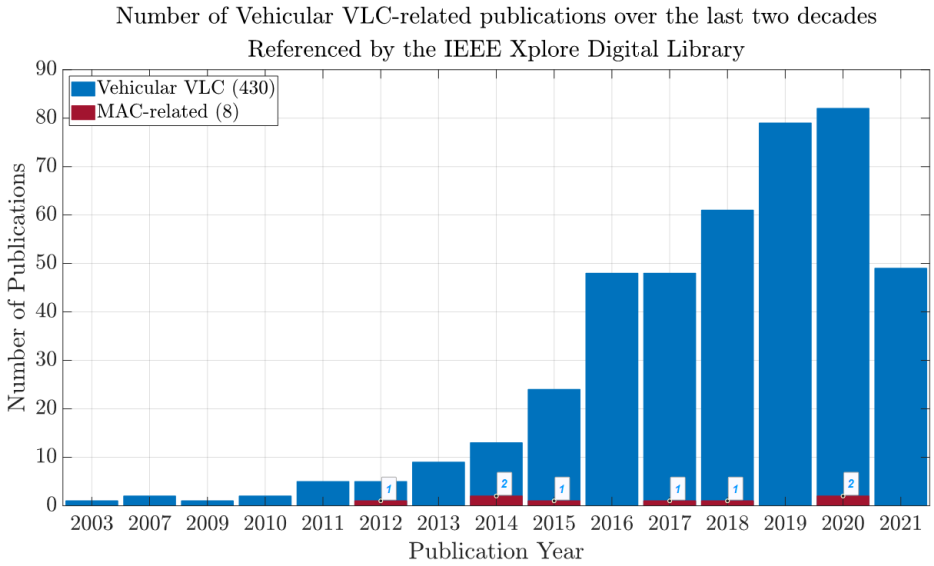

Figure 2.7 – Evolution over the years of the number of academic publications referenced by the IEEE Xplore Digital Library when searching the term 'Vehicular Visible Light Communication'.

In contrast to the large number of studies on PHY, there are few papers on MAC in the literature, outlined by Figure 2.7, where the exponentially growing interest in vehicular VLC in the last two decades is presented and compared against the vehicular VLC MAC related works. VLC offers various physical layer options, but the lack of a MAC design prevents it from being utilized in Vehicular Ad-hoc Network (VANET). In a recent paper [81], we showed that in medium to dense traffic circumstances, multi-users interference (MUI) may significantly degrade the packet delivery performance of V2V VLC. The research clearly shows that MAC is required for VLC in automotive applications. Non-beacon mode without CSMA/CA, non-beacon mode with CSMA/CA, beacon-enabled mode without CSMA/CA, and beacon-enabled mode with CSMA/CA as MAC for VLC are the four random access techniques defined by current standards [28, 82].

In beacon-enabled mode, nodes employ the slotted random channel access technique with the backoff slots aligned with the beginning of the beacon broadcast. A device with data to broadcast first locates the boundary of the next backoff slot, then waits for a random number of backoff slots and determines whether or not the channel is idle. If the channel is not in use, the device broadcasts on the

next available backoff slot boundary. It's also conceivable that the carrier detect mechanism is turned off because it is optional. In such situation, the node begins a transmission immediately after backoff. An acknowledgment can be used to certify the successful reception and validation of a data or MAC control frame. Without the use of a random access mechanism, acknowledgement and beacon frames are delivered. A non-beacon-enabled MAC employs an unslotted random channel access mechanism, in which each time a device desires to send data, it first waits for a random backoff period before transmitting its data frame. With CSMA/CA, the same carrier sense techniques are used [28, 46].

VLC is characterized with a highly directional communication link, FOV and the differences in the transmission power from different sources such as low and high beam of headlights, taillights, or semaphore light generate variable channel conditions. Therefore, carrier sensing at the VLC transmitter is ineffective since the channel condition at the transmitter can be very different from that of at a VLC receiver. As a result, only carrier sensing at the VLC receiver makes sense, but the receiver must communicate the information to the VLC transmitter implementing a feedback communication link.

Because it is challenging to create bi-directional links in a dynamic network topology like VANET, this information exchange cannot occur over the same VLC channel. In this scenario, one of the intuitive reasons to use CSMA-CA for VLC is that the VLC receiver informs the channel state using, for example, RF technology. This method is expensive since it necessitates installing two technologies (VLC and radio) on each node merely to get VLC to operate.

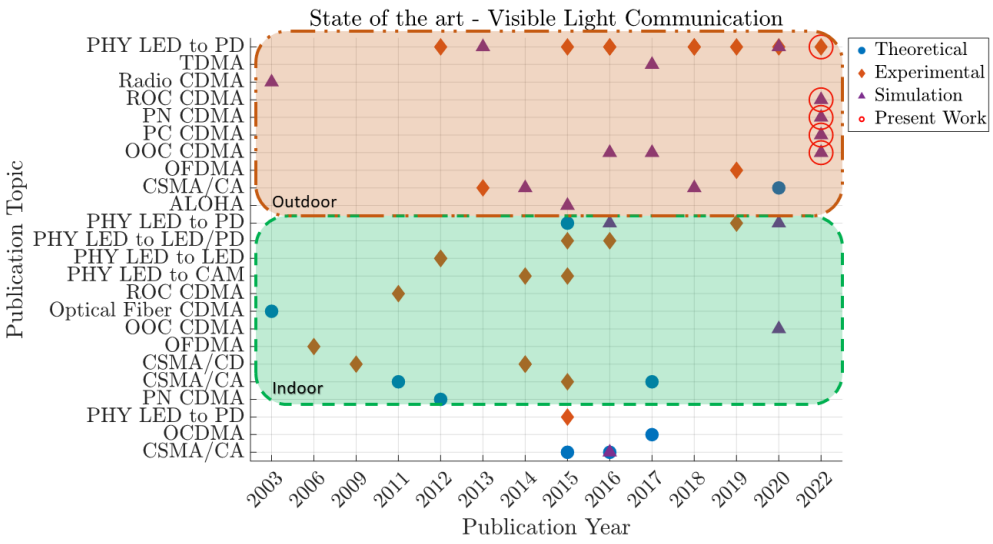

Figure 2.8 – State of the art of Visible Light Communications on the last two decades

The authors of [44] investigated CSMA/CA on top of the physical layer of IEEE 802.15.7 [27] with different priority levels (High, Medium, and Low Priorities), resulting in different back-off times, back-off exponents, and contention window sizes. Based on Markov modeling and MATLAB simulations of IEEE 802.15.7 VLC standard, Shams et al. [46] offered a performance evaluation of throughput, latency, power consumption, collision probability, transmission probability, access probability, and packet reject probability. The authors of [82] used a Markov chain model to assess the IEEE 802.15.7 standards service time distribution.

In addition, the authors presented an analytic and semi-analytic queue modeling technique. Ishihara et al. [45] presented a radio-visible light hybrid communication system for platooning applications, based on the IEEE 1609.4/802.11p radio frequency standard and the ALOHA MAC protocol for visible light communication. None of the previous attempts are based on MUI in VLC experiments that demonstrate MAC requirements. Furthermore, the logic for using CSMA/CA or ALOHA for VLC, which is intrinsically half-duplex and directional, is unclear.

Finally, Figure 2.8 groups the related works on MAC for VLC in terms of their intended scenario (indoor or outdoor), the implemented protocol, and the physical layer scheme. In the figure, we can observe that there is no specific tendency or a preferred protocol implementation. Nevertheless, for outdoor applications, the most studied physical layer is LED to PD, and for MAC protocol, only Optical Orthogonal Codes have been considered. Also, we can observe that the majority of experimental evaluations have been conducted on indoor scenarios.

2.3.1 . VLC research tools

Regarding VLC assessment tools, Wang et al. [80] proposed a low-cost, open-source VLC platform that allows researchers to build and evaluate their VLC systems. However, the Linux driver requires advanced coding skills as it is made in C and assembly language, and its modification must be carefully carried on. Although it is an open-source system, the developers do not produce any prototyping platform.

Researchers can use simulations and prototypes to investigate the different critical factors around VLC technology. Veins VLC is a simulation framework incorporating VLC transmitter, receiver, and channel models [83, 84]. Nevertheless, there is insufficient information about the VLC module and how to work with it, making it complicated and time-consuming to add new MAC codes for the simulation. Consequently, we opt to carry on our simulations on MATLAB and Simulink, based on previous works reported on the literature [2, 48, 85, 86, 87].

2.4 . VLC Channel model

To design, construct, and operate effective optical communication systems, the channel characteristics must be thoroughly understood. The channel impulse response is used to characterize a communication channel, which is subsequently used to analyze and mitigate the impacts of channel distortions. Much research on channel characterization has been published, encompassing experimental measurement and computer modeling of indoor and outdoor systems.

2.4.1 . Intensity Modulation with Direct Detection

Intensity Modulation with Direct Detection (IM/DD) is a widely used technique for optical communications. The LED produces the modulated signal $m(t)$, whose intensity varies in line with the data, as shown in Figure 2.9.

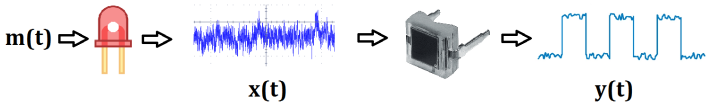

Figure 2.9 – VLC systems using intensity modulation direct detection (IM/DD).

The signal $x(t)$ is captured by the PD of the receiver after it has propagated across the wireless channel. The latter produces a current, $y(t)$, proportional to the power of the light incident on the PD's active region. To model such a VLC, we must first express the angular distribution ($R_o(\phi)$) or intensity pattern generated by the LED [2, 3, 48]

$$R_o(\phi) = \begin{cases} \frac{(m_i+1)}{2\pi}\cos^{m_i}(\phi) & \phi \in [\frac{-\pi}{2}\ \frac{\pi}{2}] \\ 0 & \phi \geq \frac{\pi}{2} \end{cases} \quad , \quad . \tag{2.1}$$

The Lambert coefficient (m_i) associated with the LED semi-angle at half-power ($\phi_{1/2}$) as shown in Figure 2.10, is

$$m_i = \frac{-\ln 2}{\ln(\cos\phi_{\frac{1}{2}})} \quad . \tag{2.2}$$

Thus, the radiant intensity is given by

$$U(\phi) = P_t R_o(\phi) = P_t \frac{m_i+1}{2\pi}\cos^{m_i}(\phi) \quad , \tag{2.3}$$

and the receiver's effective reception area ($A_{eff}(\psi)$) is represented as follows

$$A_{eff}(\psi) = \begin{cases} A_r\cos(\psi) & 0 \leq \psi \leq \frac{\pi}{2} \\ 0 & \psi > \frac{\pi}{2} \end{cases} \quad , \quad , \tag{2.4}$$

where Ar is the active region that collects light beams at ψ angles (see Figure 2.10). Although a large-area detector would be ideal for OWC to gather as much power as possible, it would pose many issues in practice, including increased manufacturing costs, greater junction capacitance, and therefore a reduced receiver bandwidth well as increased receiver noise. As a result, using a non-imaging concentrator to enhance the total effective collecting area is a cost-efficient approach. An ideal non-imaging concentrator with an internal refractive index of n has an optical gain of

$$g(\psi) = \begin{cases} \frac{n^2}{sin^2(\psi_c)} & 0 \leq \psi \leq \psi_c \\ 0 & \psi > \psi_c \end{cases} \quad , \quad , \tag{2.5}$$

where $\psi_c \leq \pi/2$ is the FOV.

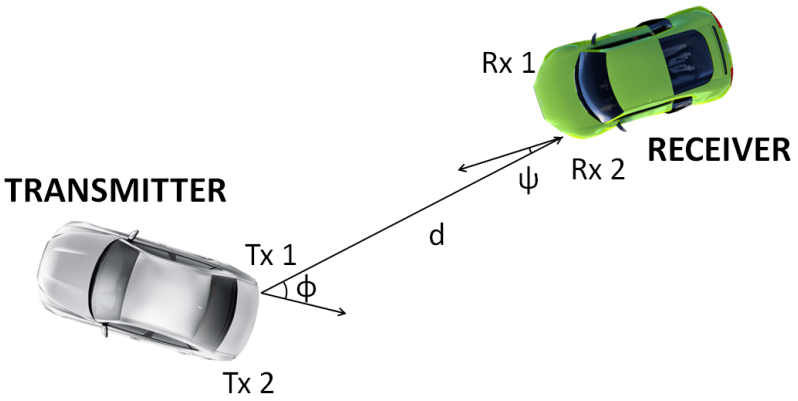

Figure 2.10 – VLC link between a transmitter (left vehicle) and a receiver (right vehicle).

For a PD positioned at d distance from a transmitter with an irradiance (ϕ), with an optical band-pass filter of transmission $T_s(\psi)$, a non-imaging concentrator of gain $g(\psi)$ and an incidence FOV (ψ_c), the DC gain ($H(\phi, \psi)$) is expressed as follows [2, 3, 48] :

$$H(\phi, \psi) = R_o(\phi) \cdot A_{eff}(\psi) \cdot T_s(\psi) \cdot g(\psi) \quad 0 \leq \psi \leq \psi_c \quad , \tag{2.6}$$

$$H(\phi, \psi) = \begin{cases} \frac{A_r(m_i+1)}{2\pi d^2} \cos^{m_i}(\phi) T_s(\psi) g(\psi) \cos(\psi) & 0 \leq \psi \leq \psi_c, \\ 0 & \text{elsewhere} \end{cases} \quad . \tag{2.7}$$

The receiver power P_r, is hence :

$$P_r = H(\phi, \psi) P_t = \frac{H_0(\phi, \psi)}{d^2} P_t \quad , \tag{2.8}$$

where, P_t is the transmission power, thus $P_r(\phi, \psi)$ is :

$$P_r(\phi,\psi) = \begin{cases} \frac{A_r(m_i+1)}{2\pi d^2} P_t \cos^{m_i}(\phi) T_s(\psi) g(\psi) \cos(\psi) & 0 \leq \psi \leq \psi_c, \\ 0 & \text{elsewhere} \end{cases} \quad . \tag{2.9}$$

Subsequently, Figure 2.11 depicts the IM/DD model, where R is the photodetector responsivity, $h(t)$ is the baseband channel impulse response obtained by Eq. (2.7), and $n(t)$ is the signal-independent shot noise, which is represented by the Additive White Gaussian Noise (AWGN) with a double-sided power spectral density (PSD) of $N_0/2$.

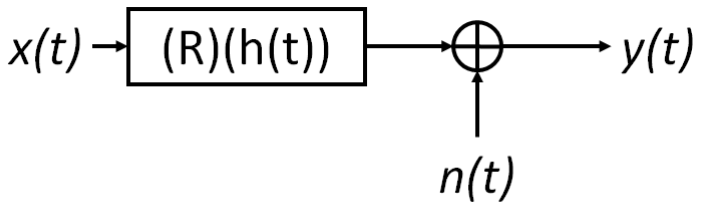

Figure 2.11 – Model for an OWC system using IMDD.

2.4.2 . Photodetection noise

The additive noise $\sigma(t)$ produced by the PD is a significant cause of distortion in FSO channels. It comes in two forms : shot noise and thermal noise. The shot noise is proportional to the number of photons captured and consequently grows in proportion to the incoming light flux. This noise source is dominating in outdoor situations, because the light source of interest is inevitably surrounded by a variety of ambient light sources, both natural and artificial. The sun, which emits a powerful and diffuse wide-band light, clearly dominates natural light sources. Artificial light sources, moreover, are classified as follows : street lights, neon signboards, and LED displays [88]. The influence of each source is inextricably linked to the proportion of light emitted that is captured by the PD. As a result, the shot noise is represented as an AWGN with variance σ^2_{shot} by the equation 2.10.

$$\sigma^2_{shot} = 2qRP_rB + 2qI_{bg}I_2B \quad , \tag{2.10}$$

where q denotes the electronic charge, R is the photodetector responsivity, B is the bandwidth of the electrical filter that follows the photodetector, I_{bg} represents the background photocurrent, and I_2 signifies a noise bandwidth factor equal to 0.562 [49, 48]. The first term is P_r-dependent and hence represents the contribution of the light source of interest. The dominant background noise, on the other hand, is represented by the second term. If the only background light examined is sunshine, then I_{bg} may be approximated to be $5100\ \mu A$ in the case of direct exposition or $740\ \mu A$ in the event of indirect exposition [89].

Thermal noise, in contrast, indicates the movement of charge carriers at a specific temperature and is highly dependent on the type of preamplifier employed. Although a front-end based on bipolar junction transistors (BJT) consumes less power than a front-end based on field-effect transistors (FET), the noise generated is greater. As we do not have any power constriction, and we intend to implement a system with low noise, a FET-based trans-impedance amplifier (TIA) is taken into account here. The thermal noise is likewise treated as a signal independent Gaussian noise with variance $\sigma^2_{thermal}$ detailed in 2.11.

$$\sigma^2_{thermal} = \frac{8\pi k T_K}{G_{ol}} C_{pd} A_r I_2 B^2 + \frac{16\pi^2 k T_K \Gamma}{g_m} C^2_{pd} A^2_r I_3 B^3 \quad , \tag{2.11}$$

where k is Boltzmann's constant, T_K is absolute temperature, G_{ol} is open-loop voltage gain, C_{pd} is photodetector fixed capacitance per unit area, Γ is FET channel noise factor, gm is FET transconductance, and I_3 is noise-bandwidth factor equal to 0.0868 [49, 48]. The total noise variance (σ^2_{Tot}) is just the sum of the shot noise and thermal noise variances :

$$\sigma^2_{Tot} = \sigma^2_{shot} + \sigma^2_{thermal} \quad . \tag{2.12}$$

In addition, because the received optical power is $P_r = H(\phi, \psi) P_t$, the signal power at the receiver side S for a PD responsivity (R) is :

$$S = R^2 H(\phi, \psi)^2 P_t^2 \quad . \tag{2.13}$$

Therefore, the SNR will be equal to :

$$SNR = \frac{S}{\sigma_{Tot}} = \frac{R^2 H(\phi, \psi)^2 P_t^2}{\sigma^2_{shot} + \sigma^2_{thermal}} \quad . \tag{2.14}$$

It is worth noting that the received optical power is proportional to the square of the photodetector area (A_r^2) The variation of shot noise is proportional to the detector area. As a result, if shot noise is the major source of noise, the SNR is proportional to the detector area. Because thermal noise is a complex function of A_r, noise variance is also a convoluted function of photodetector area.

2.5 . Conclusion

This chapter provides a quick overview of OWC systems and the most common VLC-system setups. Furthermore, we offer an overview of the most current state-of-the-art automotive VLC systems, as well as several VLC research tools like the OpenVLC system and the Veins simulator. Even while research into VLC technology and its uses in-vehicle situations has increased in recent decades, Figure 2.7 illustrates that this has not been the case for MAC-protocol investigations. Figure

2.8 depicts the most significant MAC-protocol-related works and the configurations that have been applied to them. As the figure illustrates that the current studies do not reveal a clear preference for a particular MAC protocol, and only a few researchers examine this technology's outdoor applications. At the end of this chapter, we provide the well-studied channel model for VLC systems.

3 - Vehicular VLC : Multi-Users Interference

Sommaire

This chapter first formulates an analytical model of a multi-users interference zone, i.e., the zone from which interfering signals can arrive to a target VLC receiver. This model is based on the channel model presented in the previous chapter. The aim is to protect a continuous VLC communication between an intended transmitter and receiver. This analysis help us define and understand the scope of the VLC V2V communication and the impact of the interference nodes close to the intended transmitter and receiver. Then, we demonstrate the effects of those interferences through experimentation. We introduce the platform developed for this purpose and the procedure to carry on the experiments. Concluding the chapter, we present the plots of the test results, which prove the necessity of the MAC layer in VLC vehicular application.

3.1 . Impact of Multi-Users Interference

3.1.1 . Computation of the SINR threshold

As shown in the previous chapter, a standard method for VLC communications is IM/DD, and the power received $P_r(\phi, \psi)$ at irradiance ϕ and incidence ψ angles by the PD is hence

$$P_r(\phi,\psi) = \begin{cases} \frac{A_r(m_i+1)}{2\pi d^2} P_t \cos^{m_i}(\phi) T_s(\psi) g(\psi) \cos(\psi) & 0 \leq \psi \leq \psi_c, \\ 0 & \text{elsewhere} \end{cases} \quad . \tag{3.1}$$

We assume that no error-correction coding is used for the sake of simplicity. In such a scenario, assuming that multipath fading is ignored in VLC [90], the ability of the receiver to decode the received signal, PDR correctly is determined by the Bit-Error Rate (BER) and the packet size, L_b bits [91] :

$$PDR = (1 - BER)^{L_b} \quad . \tag{3.2}$$

The following shows the relationship between BER and the Signal to Interference Noise Ratio (SINR) for OOK [48].

$$BER = Q(\sqrt{SINR}) = Q\left(\frac{P_r}{MUI + \sigma_{Tot}}\right) \quad , \tag{3.3}$$

where Q-function is often used to compute the area under the tail of a Gaussian probability distribution function and is denoted as

$$Q(z) = \int_z^\infty \frac{1}{\sqrt{2\pi}} e^{-y^2/2} dy \quad . \tag{3.4}$$

In (3.3), σ_{Tot} denotes the noise power, including shot and thermal noise defined in the previous chapter (2.12). MUI is the overall interference power. The received $SINR$ must be greater than a specified threshold $(SINR_{th})$ to receive the sent data accurately, set by the modulation method.

$$\frac{P_r^2}{MUI^2 + \sigma_{Tot}^2} \geq SINR_{th} \quad . \tag{3.5}$$

We can calculate the $SINR$ threshold $(SINR_{th})$, determined by the required communication quality, i.e., the PDR requirement. Because $PDR = 1 - PER$, we can determine the $SINR_{th}$ for a binary modulation system using equations (3.2) and (3.3) as follows

$$SINR_{th} = \left(Q^{-1}(1 - \sqrt[L_b]{PDR_{req}})\right)^2 \quad . \tag{3.6}$$

Q^{-1} is the inverse Q function in this case. Computing (3.6), Figure 3.1 depicts $SINR_{th}$ in dB for various PDR criteria and packet sizes. As seen in the figure, the SINR threshold rises significantly as the PDR threshold rises, taking $11.37,\ 12.57,\ 13.52$ and $14.30\ dB$ for a PDR requirement of 90% for a $1,\ 10,\ 100\ kb$ and $1\ Mb$ of payload respectively.

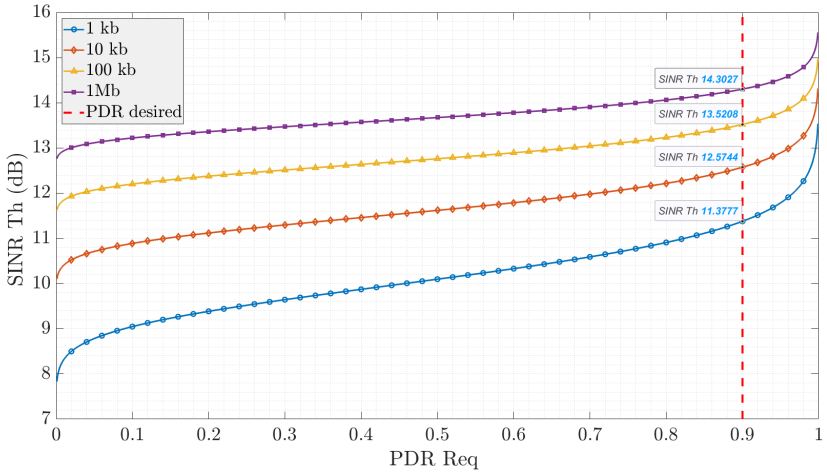

Figure 3.1 – $SINR_{th}$(dB) vs. PDR_{req}. Mathematical computation of the SINR threshold as a function of the PDR requirement. Here $L_b = 1K$, $10K$, $100K$ and $1M$ Bits.

3.1.2 . Estimation of interference zone based on the SINR threshold

We are now interested in finding the geographical zone from which interferences have to be surveyed, i.e., the MUI zone, for a given pair of the intended transmitters and one receiver as depicted in Figure 3.2. In other words, we will compute the distance (d_{ir}) between an interfering node and the intended receiver that meets the following criteria

$$P_i^2(d_{ir}) \geq \frac{P_r^2(d_{tr})}{SINR_{th}} - \sigma_{Tot}^2 \quad , \tag{3.7}$$

where d_{tr} is the distance between the intended transmitter and the receiver, d_{Lx} refers the longitudinal distance inside the MUI zone for each lane, and L_w represents the width of each lane. P_i denotes the interference power or the power received from the interfering node. Because VLC is directional, the transmitter and the interfering node must be in the FOV of the receiver (PD) while obeying the irradiance and incidence angle requirements (see Figure 2.10). We may safely ignore σ_{Tot} in the equation (3.7) because $P_r/SINR_{th} \gg \sigma_{Tot}$ (indeed, we can see $P_r/SINR_{th} \approx 1\ \mu W$ while $\sigma_{Tot} \approx 50\ nW$) (3.7). Furthermore, because (3.1) expresses P_r and P_i using d_{tr} and d_{ir}, respectively, the highest d_{ir} meeting condition (3.7) is determined to be

$$d_{ir} = d_{tr}\sqrt{SINR_{th}} \quad . \tag{3.8}$$

Because the interfering nodes as well as the intended transmitter, must be inside the receivers FOV, the MUI zone for a given pair of intended transmitter (Tx) and receiver (Rx) is the circular sector with a radius d_{ir} and center angle 2ψ, as illustrated in Figure 3.2.

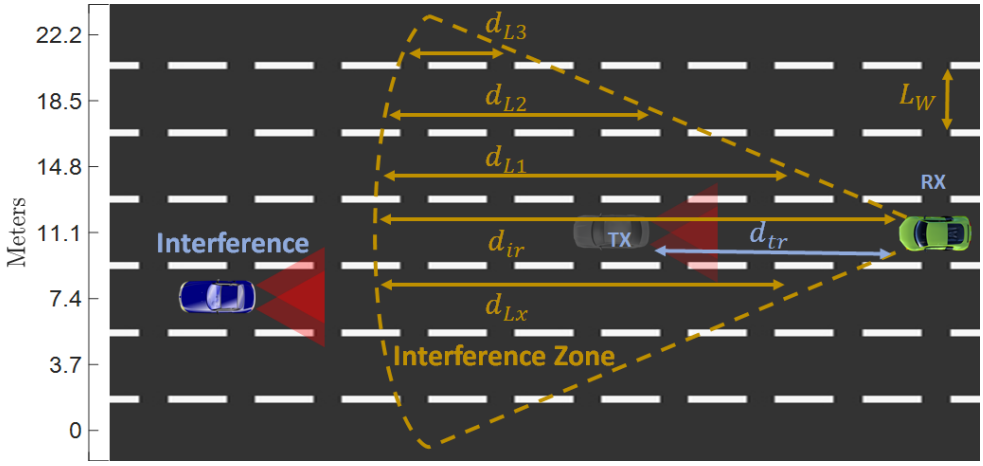

Figure 3.2 – Schematic scenario for MUI zone estimation for a given pair of transmitter (Tx) and receiver (Rx) of VLC.

Table 3.1 – Simulation Parameters.

Parameter	*Value*
PD reference	SFH-206 k [92]
A_r	7.02 mm^2
PD efficiency	0.62 A/W
Reciver FOV (ψ_c)	60°
LED half angle (α)	$20°$
LED-PD lateral distance (d_L)	3 m
Vehicle width (d_w)	2 m
Vehicle length (d_{len})	4.5 m
PD capacitance	72 pF/m^2
Transmission frequency	500 kHz
Transmission power	2 Watt (vehicle taillight)
Packet size (L_b)	100 Bits
Lane width (L_w)	3.7 m

We now proceed to compare the estimate MUI zone against a simulation carried on Matlab. The parameters of this simulation are summarized on Table 3.1. We first assess PDR for VLC communications from the intended emitter to the receiver in the absence of interfering nodes. The simulations are carried out on a seven-lane straight road, with the receiver (Rx) placed in the middle lane (lane 4) and the planned transmitter (Tx) along all the scenario lane by lane as illustrated in Figure 3.3.

The acquired findings are shown in Figure 3.4, where the horizontal and vertical axes represent the longitudinal (i.e., distance from the receiver) and lateral (i.e., lane number) locations of Tx, respectively. The color plate represents the achieved

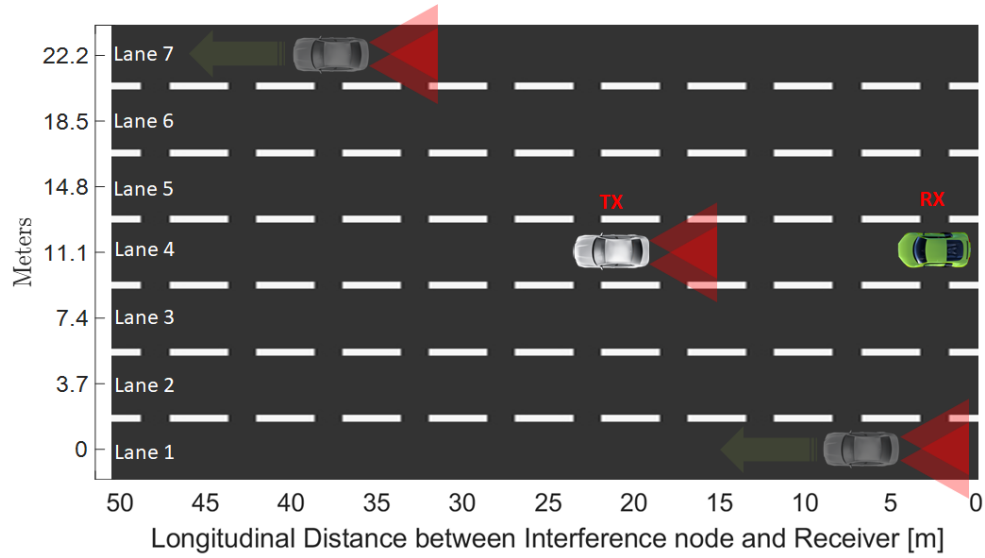

Figure 3.3 – Proposed scenario to estimate the communication zone for a given pair of transmitter (Tx) and receiver (Rx) of VLC on a seven lane road.

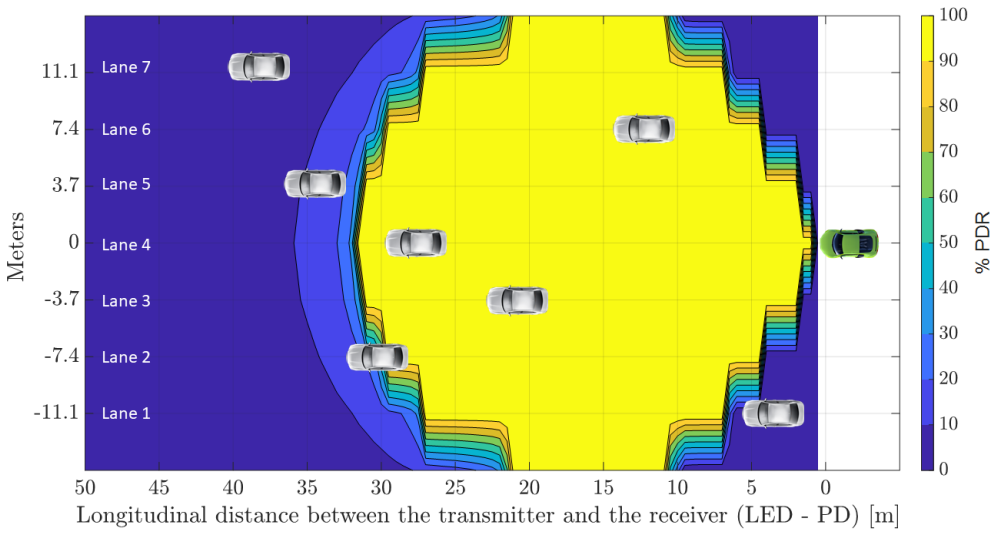

Figure 3.4 – Vehicle-to-vehicle communication range (PDR) when transmitter (white vehicle) and receiver (green vehicle) are on a seven-lane road with no interference.

PDR result for each Tx location. The longest communication distance is attained when the transmitter and receiver are on the same lane (i.e., the lateral distance is $0\ meters$). A $PDR > 90\%$ is achieved up to $32\ meters$ of longitudinal distance. When the transmitter is in the adjacent lanes to the right or left, more than 90

percent of PDR may be achieved over 2 to 31 $meters$ of longitudinal distance. For 5 to 30 $meters$ longitudinal lengths, a PDR over 90 percent may be reached when the transmitter is in a second adjacent lane. Finally, > 90 percent PDR is obtained for 8 to 27 $meters$ if the transmitter is in the third adjacent lane.

Then, we proceed to add the interference vehicle and launch the simulation to get the PDR map presented on Figure 3.5a. The transmitter and receiver vehicles

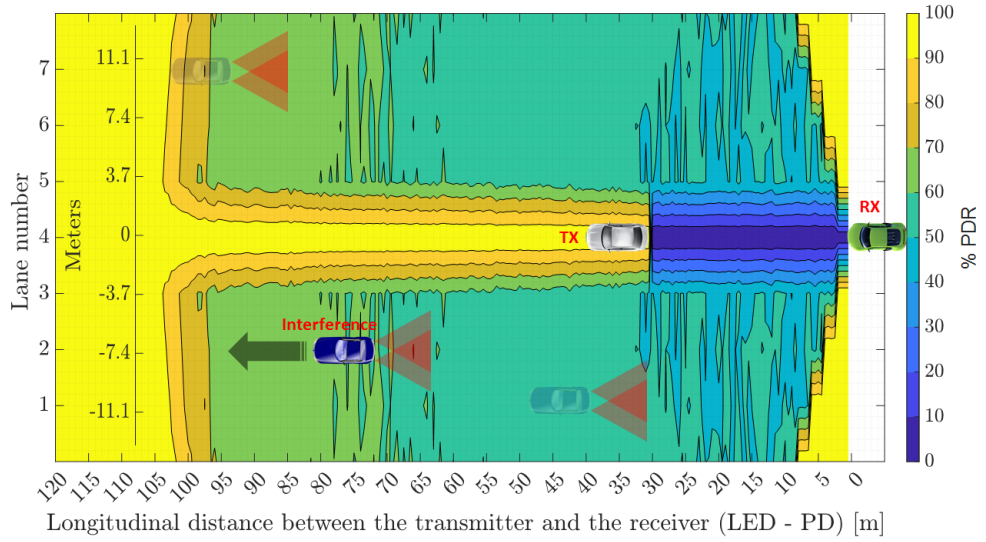

(a) Interference mapping.

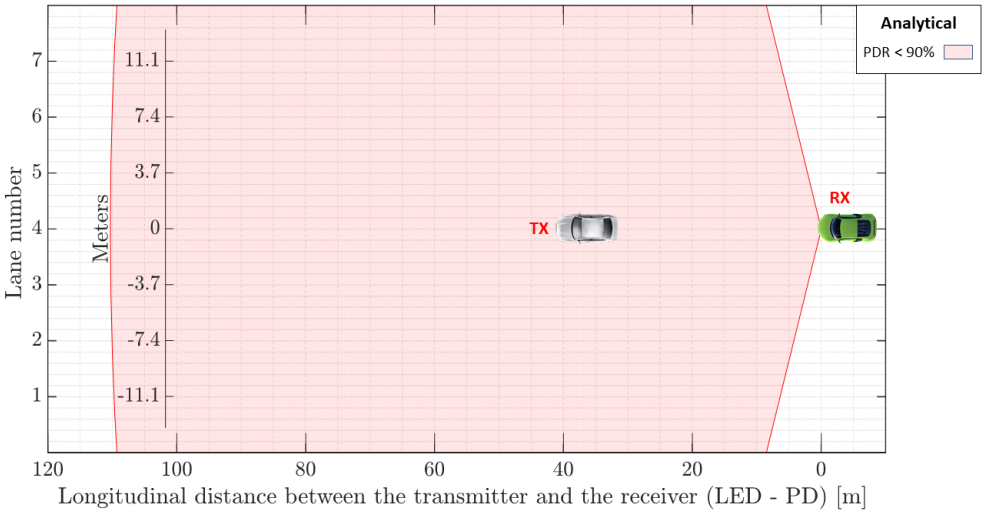

(b) Result analytic vs result simulation

Figure 3.5 – Interference simulation results for a 7 lanes road a) PDR mapping and b) analytical model estimation of MUI zone.

are fixed at the middle lane (lane 4) with a separation of $30\ m$ to get the most critical case when the Tx is at the limit of the communication zone ; thereby, the interference zone will demonstrate for the worst case. The interference transmitter changes the position by steps of $0.5\ m$ within all the scenario lane by lane. Subsequently, we discretize the results to have two unique zones, more or equal to 90% PDR and less to 90% PDR. Finally, we compare the simulation results against the analytical model as illustrated in Figure 3.5b. The difference between both results can be related to the fact that we do not consider the transmittance angle and, by consequence, the path loss related to it in the analytical model.

In addition, vehicles can only be in individual lanes when considering V2V communication on a multi-lane straight route. In such a case, we now compute the lengths of each lane in the MUI zone (see Figure 3.2). Because d_{ir} is the distance from the receiver to the MUI zone limit (see (3.8)), we may assume $d_{ir} \gg L_w$, where as illustrated in Figure 3.2, L_w is the lane width, and the lengths of individual lanes d_{Lx} in the MUI zone are :

$$d_{Lx} = d_{ir} - j \cdot L_w \cdot cot(\psi) \qquad 0 \leq j \leq Lx \quad , \tag{3.9}$$

where Lx is the number of lanes on the receivers right or left side. The total length of lanes inside the MUI zone is then calculated as

$$L_{Tot} = d_{ir} + \sum_{Lx=1}^{Lx_l} d_{Lx_l} + \sum_{Lx=1}^{Lx_r} d_{Lx_r} \quad . \tag{3.10}$$

Here, Lx_l (resp. Lx_r) is the number of adjacent lanes on the receivers left (resp. right) side.

We now compute the probability of getting interfering vehicles on the lanes in the MUI zone by addressing an intended transmitter and a receiver at d_{tr} distance

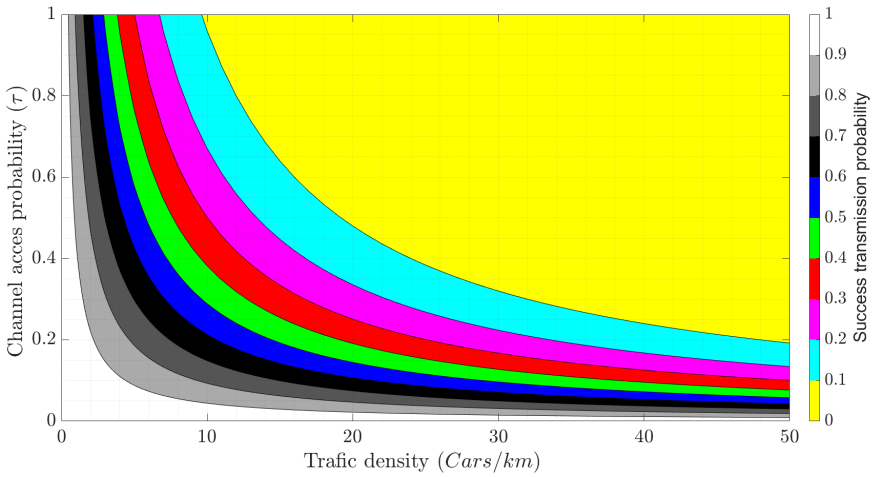

Figure 3.6 – Success transmission probability on a 7-lanes road.

with the LOS condition. We consider that automobiles on a highway follow the Poisson distribution with a density β $(vehicles/meters/lane)$, which is frequently used for highway traffic [93], and that the possibility of getting i vehicles on an l-kilometer stretch of road is [94].

$$P(i,l) = \frac{(\beta l)^i e^{-\beta l}}{i!} \quad . \tag{3.11}$$

The channel access probability at individual vehicles is denoted by τ, and is determined by assuming that vehicles generate messages (beacons) on a regular basis and using T_{tx} as the average packet transmission time. Therefore,

$$\tau = \frac{T_{tx}}{T_{interval}} \quad . \tag{3.12}$$

$T_{interval}$ is the message generating interval in this case. The findings illustrated in Figure 3.6 reveal that when there is no MUI control, i.e., no MAC, satisfactory PDR performances are only achieved at extremely low traffic density and shallow message creation rate. In particular, to achieve 90% PDR with a message production rate of 0.8, the traffic density for a 7-lane scenario must be less than two $vehicles/Km$.

Otherwise, to achieve greater than 90% PDR at 50 $vehicles/km$ density, the message generation rate τ must be less than 0.01 for the 7-lanes scenario. Although the obtained values are relatively pessimistic, they demonstrate the need for a MAC protocol for VLC.

3.1.3 . Multi-Users Interference : potential number of interfering signals

The model presented in the previous subsection ignores the signal occlusion in the interference zone. Consequently, the obtained results were rather pessimistic. This subsection determines the maximum number of simultaneous VLC connections that a given receiver may have by taking into account of the signal occlusion created body of vehicles. For sake of simplicity, we pass from 7-lanes route to 3-lanes route. Precisely, we analyze positions of transmitter vehicles that have VLC connections with a specific receiver, the green vehicle in the center lane, on a three-lane straight road depicted in Figure 3.7. Vehicles may broadcast VLC signals by their rear lights, and the receiver receives signals through a PD placed in the center of the front bumper. A communication link exists for VLC if just the two requirements listed below are satisfied.

— The transmitter and receiver have a LOS route from each other.

— The LOS route between the transmitter and receiver is inside the receiver's FOV (ψ_c).

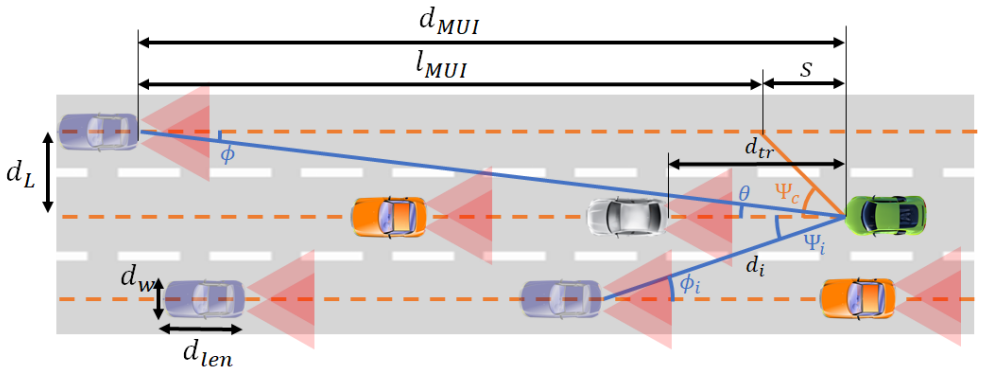

Figure 3.7 – Target scenario

The preceding requirements are satisfied for the emitting vehicle (grey vehicle), which is just in front of the target vehicle (green vehicle), as shown in Figure 3.7. Because these vehicles are on the same straight lane, zero irradiance and zero incidence angles are shared by these two vehicles. The vehicles in front of the emitting vehicle and behind the receiver vehicle (orange vehicles) do not fulfill the LOS requirement and do not have a VLC link with the intended receiver.

We will look for vehicles in neighboring lanes with a VLC link to the target receiver and might thus be interfering transmitters. We can say that the vehicles sharing VLC connection with the target receiver must be in the front left or right side of the target receiver due to the FOV condition. Allowing l_{MUI} to be the length of the left (or right) lane, we may locate vehicles having a VLC link to the target receiver. l_{MUI} is restricted by d_{MUI} distance due to the LOS condition (see Fig.3.7), where :

$$\tan(\theta) = \frac{d_w/2}{d_{tr}} = \frac{d_L}{d_{MUI}} \quad . \tag{3.13}$$

d_{tr} is the distance between the green and grey vehicles from bumper to bumper, d_w is the vehicle width, and d_L is the lateral distance between the receiver and transmitters on the next lane (see Figure 3). The longitudinal distances s from which the LOS route enters the FOV receiver are obtained as follows due to the FOV condition :

$$s = d_L \times \frac{1}{\tan(\psi_c)} \quad . \tag{3.14}$$

Both requirements must be met in order to have a VLC connection, and therefore we can finally determine l_{MUI} on which the interfering nodes may be found :

$$l_{MUI} = \max(0, d_{MUI} - s) \quad . \tag{3.15}$$

Any vehicle i on the adjacent lane with a VLC link to the target receiver must have irradiance ϕ_i and incidence ψ_i angles that satisfy the following condition :

$$\psi_c \geq \phi_i = \psi_i \geq \theta \quad . \tag{3.16}$$

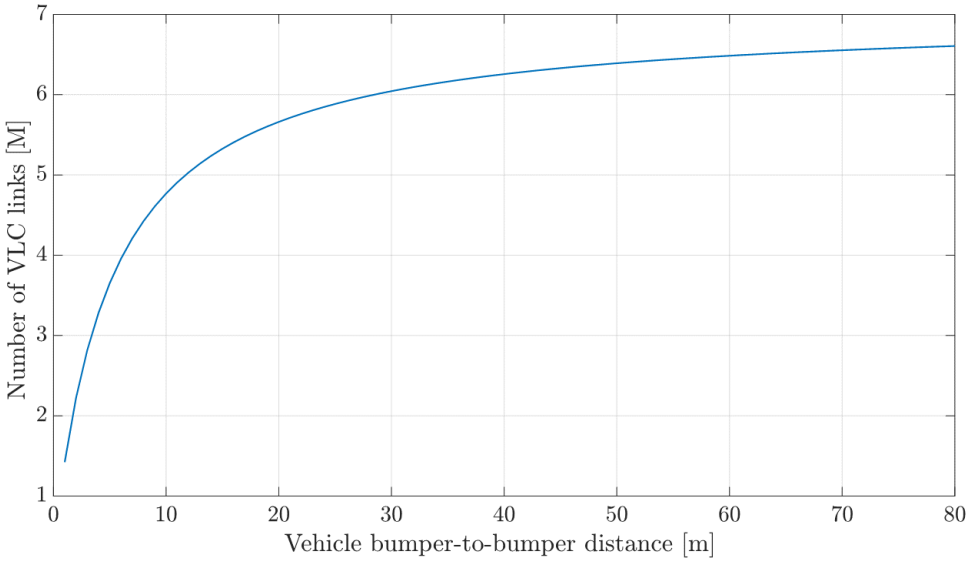

Figure 3.8 – Number of VLC links.

Now we can figure out the average total number of vehicles with VLC connections to the target vehicle :

$$M = 2 \times \left(\frac{l_{MUI}}{d_{tr} + d_{len}} \right) + 1 \quad . \tag{3.17}$$

The vehicle length is denoted by d_{len}. The predicted number of vehicles with a VLC link to the target VLC receiver is shown in Figure 3.8. Table 3.1 lists the parameters utilized in the computation. The results demonstrate that in the target highway situation, a receiver can have up to 6 VLC connections and hence can have interference from up to 5 vehicles for a given, intended signal.

3.2 . Simulation of MUI zone

The number of interfering VLC links was mathematically determined in the preceding section. As a result, the signal quality must be sufficient compared to the overall interference power to have successful communication. The influence of multi-user interference on the packet delivery ratio between a particular transmitter and receiver on a 7-lane straight road is evaluated using Veins VLC and Matlab in the following. Because the focus of the assessment is on multi-user interference, noise due to meteorological conditions and sun, atmospheric attenuation, and visible light reflection have been omitted for simplicity [95, 96].

3.2.1 . Veins VLC simulation

Veins [97] is a free and open-source framework for simulating vehicular networks. It is built on the foundations of two well-known simulators : OMNeT++,

an event-based network simulator, and SUMO, a road traffic simulator. It expands on them to provide a comprehensive set of models for simulating inter-vehicular communication.

The Veins framework offers a complete set of models designed to make vehicular network simulations as realistic as possible while remaining fast. The OMNeT++ and SUMO GUIs and IDEs may be used to set up and execute simulations interactively quickly.

SUMO, a well-known software in traffic engineering, does road traffic simulation. OMNeT++ simulates networks in conjunction with the physical layer modeling toolkit MiXiM, allowing for precise models for radio interference and shadowing by static and moving objects.

Both simulators are bi-directionally connected, and simulations are carried out in real-time as shown in Figure 3.9. The impact of vehicular networks on road traffic may be studied, and intricate connections between the two domains can be investigated. On this foundation, domain-specific models for automotive networking are built to give a comprehensive framework that is nonetheless simple to understand and use.

Veins VLC adds channel models for V-VLC to the Veins vehicular network simulation framework. It allows for the analysis of many elements of V-VLC networks, such as a variety of different applications (for example, platooning), upper-layer protocols (for example, medium access), and heterogeneous networks integrating V-VLC and IEEE 802.11p DSRC as presented in Figure 3.10. Exploring the behavior of the simulator and, to get the communication zone, we carried on the simulation described in the scenario proposed in Figure 3.3.

The results illustrated in Figure 3.11 show the communication zone between two vehicles using headlamp (right side of the plot) and taillight (left side of the plot) as a transmitter. The receiver is fixed at the center of the scenario. Two PDs are placed at the front and back of the vehicle with the proposal to

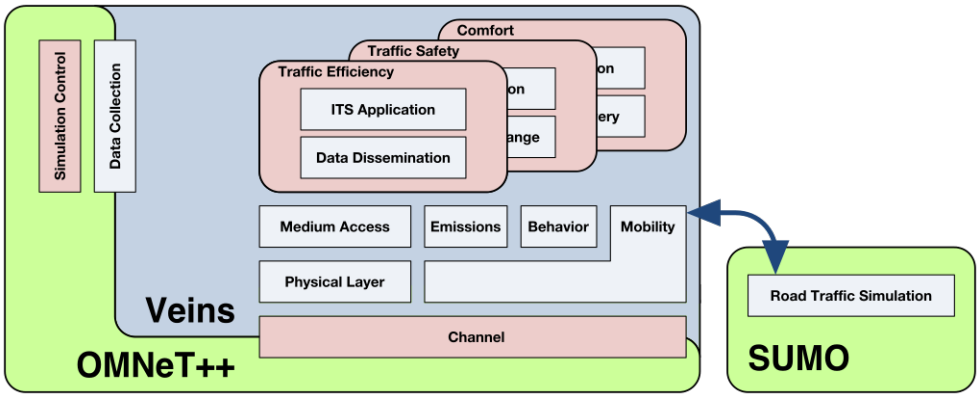

Figure 3.9 – Veins architecture between OMNeT++ and SUMO.

receive information from both sides. As expected, the communication zone is not symmetric, especially if we compare the longitudinal coverage area achieved by the headlamp against the fulfilled with the taillight. It is also interesting to remark the realistic model of the headlight implemented on the simulation, resulting into a communication zone not as symmetric as the taillight region, generating a larger communication zone at the rear right side of the receiver vehicle.

After we know the communication zone, we introduce a third vehicle to disturb the intended communication and generate an interference zone. As illustrated in Figure 3.11, the most critical area for the interference is from the adjacent lanes because a transmitter placed there can achieve a $100\ \%$ of PDR. To determine the impact of an interfering vehicle on the adjacent lane, we simulate a 2-lane road where the intended transmitter and receiver are placed at $17\ m$ one from the other. The interference vehicle passes aside them, transmitting with the headlamp and taillight simultaneously. The PDR impact on the communication link between the intended vehicles is presented in Figure 3.12

As illustrated in Figure 3.12, the interferences zones presented seem to be binarized. In other words, PDR changes from 0% to 100% from a particular position to the next, even when the displacement steps of the interference vehicle are $10\ cm$. Therefore, we analyze the different modules of the simulator to find out the parameter responsible for these binary results. Nevertheless, due to the lack of information about how the VLC module is constructed and how to modify it, we conclude that Veins VLC simulator is ineligible to carry out our desired simulations. It is necessary to mention that Veins VLC has an impressive development, resul-

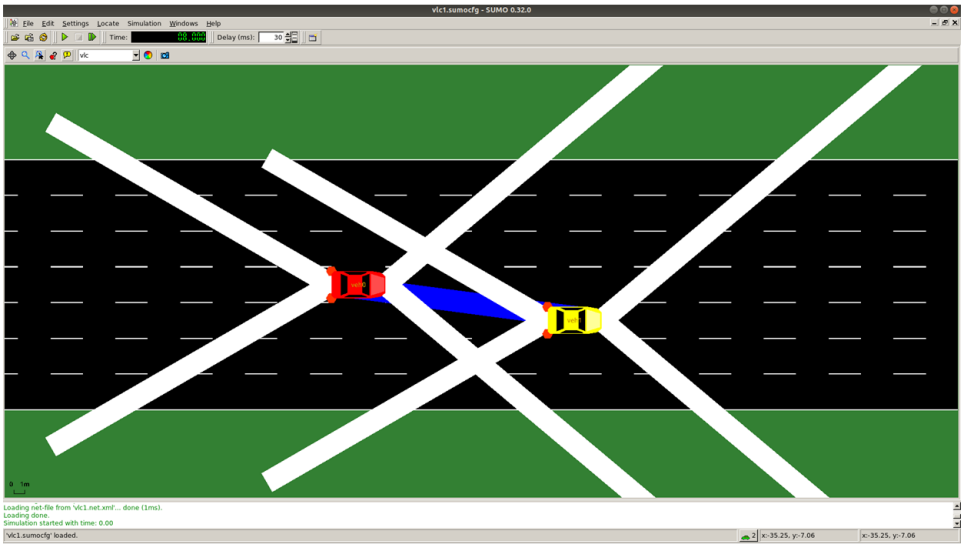

Figure 3.10 – VLC Veins simulation - graphical user interface (GUI). White lines represent the emission VLC angles.

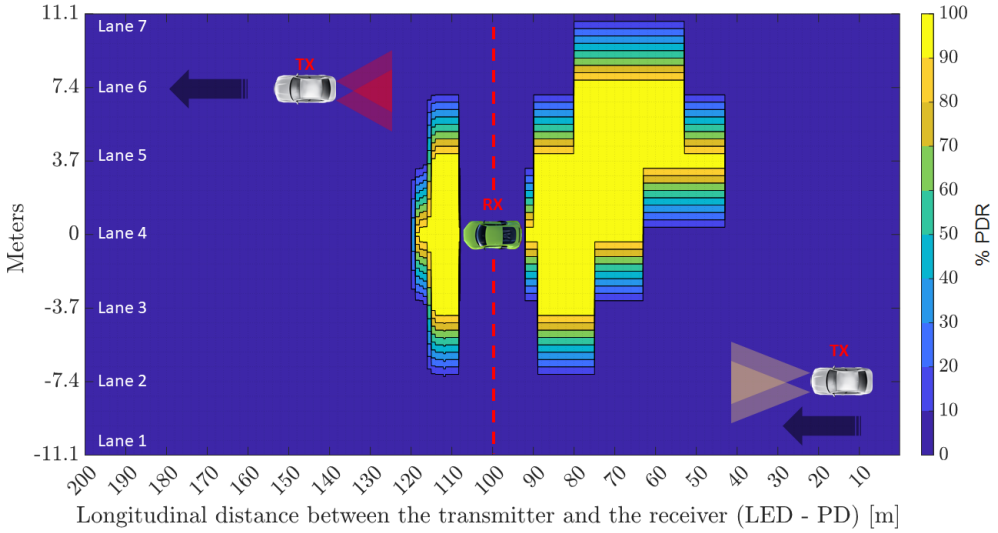

Figure 3.11 – Veins simulation - communication zone using headlamp (right side) and taillight (left side) as transmitters.

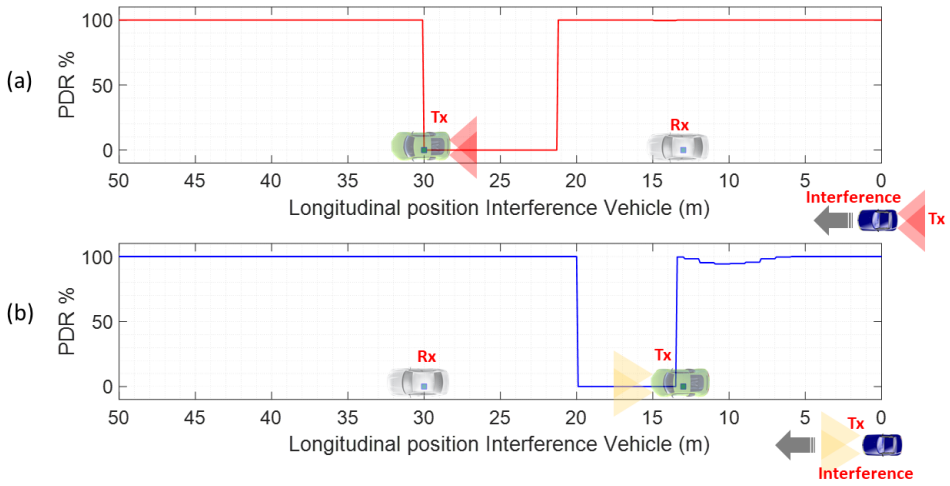

Figure 3.12 – Veins simulation - Interference zone for an intended transmitter/receiver using (a) taillight and (b) headlamp as transmitters.

ting in the fusion between traffic and network simulators. Veins and his different modules, including VLC, become helpful for the scientific community who study the adaptability of this new technology to different scenarios. Also, the possibility of simulating a hybrid communication stack makes Veins an essential development tool.

However, the lack of information regarding the construction of additional mo-

dules and their connection with the existing VLC module makes the deployment of this simulator difficult for novice users. Finally, due to the time limitation for developing this research work, we proceed to the development of a Matlab simulation. The vast catalog of tools like Simulink and the support of the scientific community makes Matlab an easy-to-implement simulator.

3.2.2 . Matlab VLC simulation

Many engineers and scientists use MATLAB to analyze data, design algorithms and build models. MATLAB is a desktop environment that is optimized for iterative analysis and design processes and a programming language that directly represents matrix and array mathematics. It allows us to write scripts that merge code, output, and formatted text into an executable notebook. MATLAB toolboxes are professionally developed, rigorously tested, and thoroughly documented.

We used Matlab/Simulink to create models of the VLC transmitter, receiver, and interfering nodes for simulation assessments. A message generator, Digital to Analog Converter (DAC), and LED drivers are included in the transmitter and interference nodes, as shown in Figure 3.13. The planned transmitter (white vehicle) and receiver (green vehicle) are traveling in the middle lane (lane 4) with a distance of $20\ meters$ between them as shown in Figure 3.14. Table 3.1 summarizes the most important parameters of this simulations. We assume that the vehicles are traveling at a comparable speed, resulting in a platoon. After then, the Doppler effect is ignored. At $50\ km/h$, the $20\ m$ corresponds to a suitable braking distance for an autonomous vehicle [37, 36, 35, 34].

The third interfering vehicle (blue vehicle) is introduced to assess the impact of its signal on the communication link between the intended transmitter and receiver,

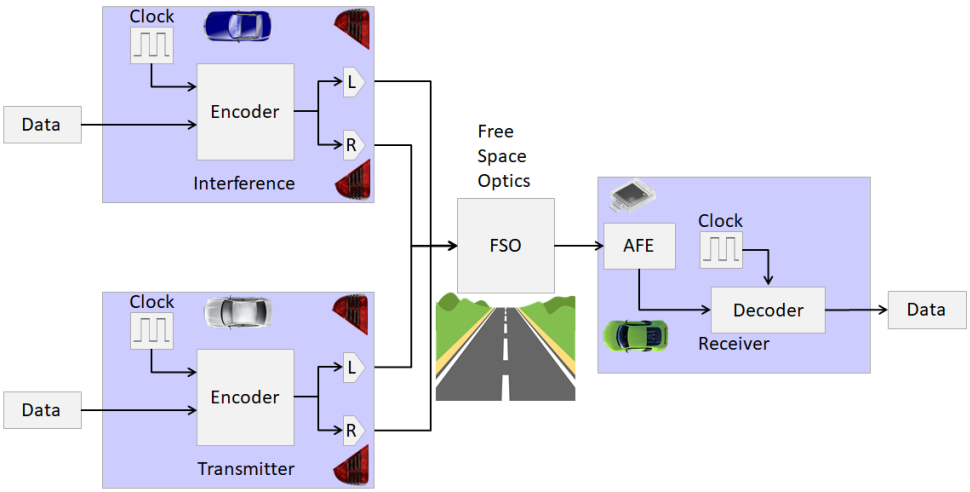

Figure 3.13 – Simulink model for simulation evaluations

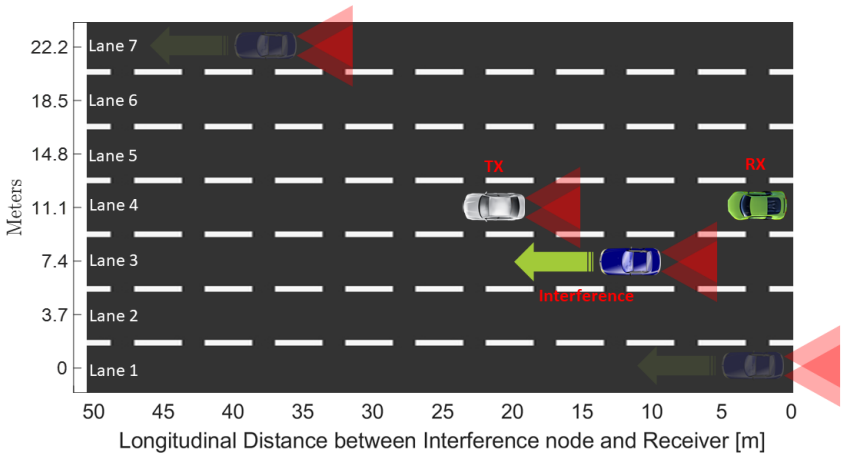

Figure 3.14 – Target scenario : The intended transmitter (Tx : white vehicle) and receiver (Rx : green vehicle) are in the center lane at a set distance, but the interfering vehicle (blue vehicle) is at various places across the lanes.

depending on the interfering vehicle's position (see Figure 3.14). More specifically, the position of the interfering vehicle was changed by 10 cm increments in each lane. Figure 3.15 depicts the acquired results. The results provide us with the following insights :

— Figure 3.15a presents at the limits a step shape because we fix the interference vehicle at the center of each lane ; in other words, we discretize the lateral axis on steps of $3.7\ m$.

— When an interfering vehicle is between the transmitter and the receiver, PDR is 0 (no communication is possible between the intended emitter and the receiver). This is due to the interfering vehicles body obscuring the signal. We are interested in using MAC to address the problem of multi-users interferences ; therefore, the current case is outside the scope of our effort (we cannot solve the issue with MAC).

— When the interfering vehicle is in the same lane as the transmitter and receiver but not between the two, PDR is $100\ \%$.

— If the interfering vehicle is in adjacent lanes, PDR might be as low as $50\ \%$, even for the furthest lanes.

Because VLC is planned to be employed for safety-critical applications like platooning, lane shifting, and lane merging assistance, a PDR performance of 50% to 90% is inadequate. The above results highlight the importance of a MAC protocol for V2V communications to avoid MUI.

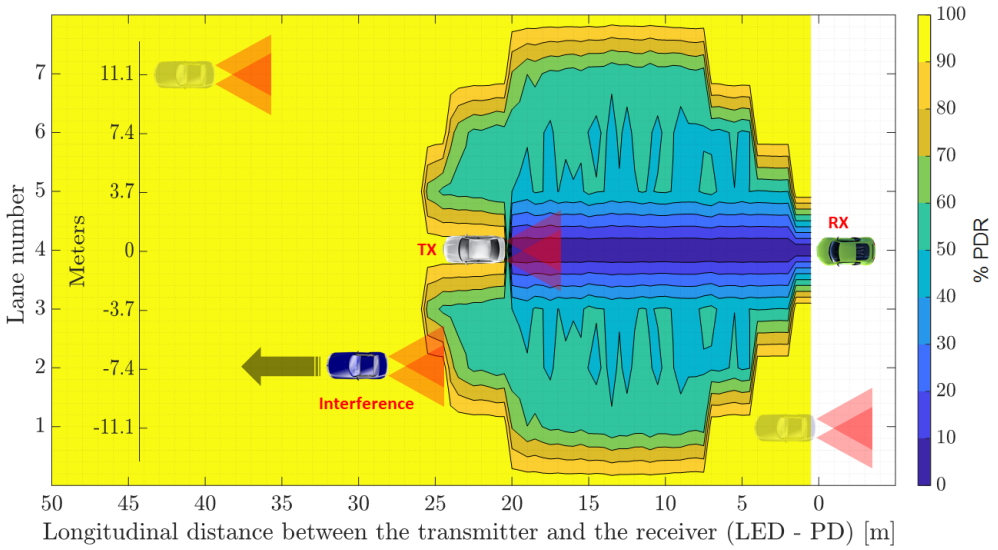

(a) Results for a 7 lanes road PDR mapping.

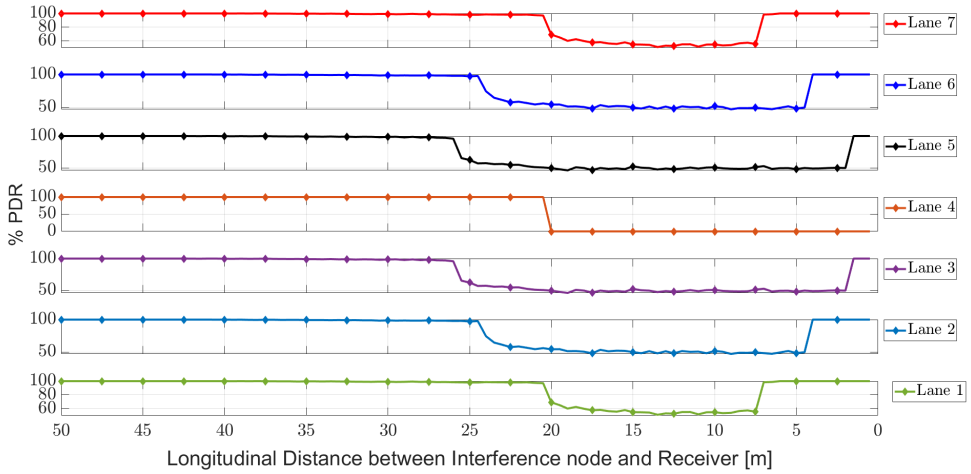

(b) Results for a 7 lanes road PDR per lane.

Figure 3.15 – Interference simulation results for a 7 lanes road. (a) Total PDR map with top view, (b) Details for PDR for each lane

3.3 . Experimental study on interference in vehicular VLC

In order to have a more realistic panorama about interference in the vehicular scenario, we conducted several measurements with our developed platform. This section describes the main characteristics of our test platform, the different tests carried on, and the results obtained.

(a) Vehicular VLC Tx integration (b) Vehicular VLC Rx platform

Figure 3.16 – Beagle Bone Black board a) connected to a vehicular taillight through our developed AFE, and b) integrated with our AFE solution for the reception of VLC signals.

3.3.1 . Vehicular VLC platform

The test platform consists of two main parts : the Beagle Bone Black (BBB), a low-cost, community-supported development platform for developers.[98] This board is in charge of all the digital tasks as networking, coding, and decoding the information, taking advantage of the Operating System (OS) Linux and the driver developed by the open-source project *OpenVLC* [99]. The software solution is developed as a Linux driver that directly communicates with the cape and the Linux networking stack. The VLC interface is configured in OpenVLC as a new communication interface that can take advantage of a wide range of Linux utilities. The driver makes use of the BBB platform's programmable real-time units (PRU) [42]. The second component of our vehicular VLC platform is the Analog Front-End (AFE) which is then responsible for converting the digital signals generated by the BBB into beams of modulated light on the transmitter, and again to digital signals representing the variations on this light intensity on the receiver side. Although the OpenVLC project offers an open-source AFE design, this last is not conceived to support a vehicular light into an outdoor scenario. Therefore, we decided to develop our AFE to integrate it with a real vehicular headlight/taillight, as illustrated in Figure 3.16 Platform characteristics are summarized on Table 3.2.

The challenges to developing this AFE for vehicular VLC lie in the correct

Figure 3.17 – Emitter and receiver structures used for the VLC experiments.

Table 3.2 – Platform characteristics

Beaglebone Black		*AFE*	
Parameter	*Value*	*Parameter*	*Value*
Power supply	$5v$ - USB	Power supply	$12v$ max.
Processor	$AM335x$[100]	PD wavelength	400 - $690\ nm$
PRU	2×200 MHz	PD sensitive area	$7.02\ mm^2$
Memory	4Gb 8-bit	PD sensitivity	0.37 A/W
USB port	2	OpAmp BW	3 GHz
Ethernet	1	ADC Sample rate	3 MHz
HDMI	1	ADC Resolution	12-bit
I/O pin	2×46	ADC Interface	48-MHz
Operative System	Debian	LED output power	$100v$ / $32A$
		LED turn-on time	83ns max.
		LED turn-off time	75ns max.

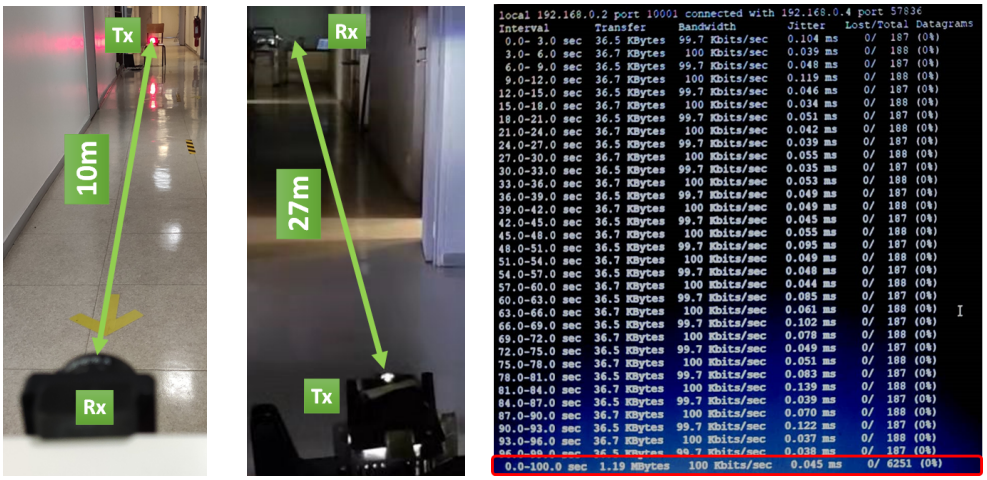

(a) (b) (c)

Figure 3.18 – Experimental results of communication range with (a) taillight intended transmitter at $10\ m$ from the intended receiver, (b) headlamp intended transmitter at $27\ m$ from the intended receiver on indoor environment without outdoor noise (no windows). (c) Screenshot of iperf test with a $100\ kbps$ bandwidth and no lost datagrams.

tuning of parameters as the trans-impedance amplifier gain against the parasite capacitance of the circuit, as the properties of the selected components (photodiode, operational amplifier, etc.) like internal capacitance, wavelength response, FOV, the bandwidth of operation.

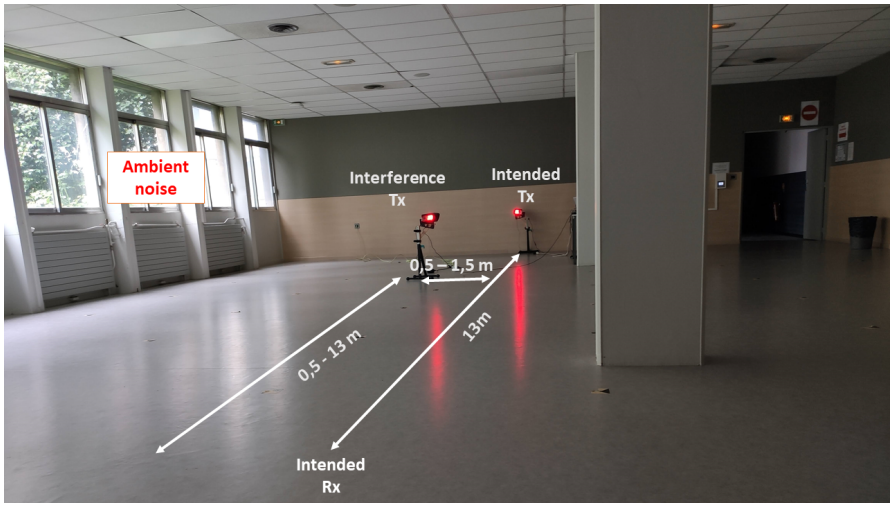

Figure 3.19 – Emitter and receiver structures used for the VLC experiments.

Experimental Set-Up

All the experiments carried out in this section are based on the same setup. Figure 3.17 demonstrates how the various basic bricks described earlier were put together to create a VLC system that operates at 100 kbps and uses OOK with Manchester coding, as required by the IEEE 802.15.7 standard.

Communication range

We first get access to the BBB board through the SSH service. Once connected, the OS shows the VLC interface set up as a new communication interface. The iperf utility is used to calculate the achievable throughput and the lost packets over a certain transmission period. To do this, we run iperf in client mode at the TX and server mode at the RX with the User Datagram Protocol (UDP) setup.

The first test discovers the achievable communication distance with the vehicular VLC platform. To this end, iperf tests were launched at a fixed bandwidth of $100\ kbps$ and packet size of $36.6\ kb$ datagrams (Figure 3.18c). Then we increase the distance between the transmitter and receiver without changing the lateral distance. As illustrated in Figure 3.18a, the maximum distance attainable with these parameters is approximately $10\ m$. It is important to remark that the test was conducted in an enclosed environment, and no external light perturbs the test. Furthermore, it is notable in Figure 3.18 that the reflections on the walls and floor could improve those results.

Before launching the second test, we add a large surface Fresnel lens to the system to collect a significant quantity of light and increase the communication

distance from $10\ m$ to $13\ m$ for a taillight transmitter and from $15\ m$ to $27\ m$ for a headlamp transmitter (Figure 3.18b), within the same scenario. Although we achieve a communication distance of $13\ m$ in a room with windows across the wall and less reflective surfaces, the FOV becomes critically narrow, getting significant looses of datagrams due to misalignment as illustrated in Figure 3.20, making the system unusable for a dynamic scenario as the vehicular.

Interference test

For the interference test, we install the system at the center of a room of $20\ x\ 10$ meters with windows which let come outdoor noise as shown in Figure 3.19. Due to this external noise and the lack of optical filters, the communication range of our vehicular VLC system was reduced to $3.5\ meters$ with taillight as a transmission source.

We conducted the test by adding a second transmitter called an interference transmitter. As in the interference simulation, we fix the position of the intended transmitter and receiver and change the position of the interference transmitter by steps of $0.5\ m$, over three different lateral distances, $0.5,\ 1,\ and\ 1.5$ meters.

Figure 3.21 show the PDR performance of a taillight intended transmitter placed at $3.5\ m$ from the receiver, whereas Figure 3.22 presents the results of the same test but with a headlight intended transmitter at $13\ m$ from the receiver. In both tests, the interference transmitter was a taillight placed at the right of the

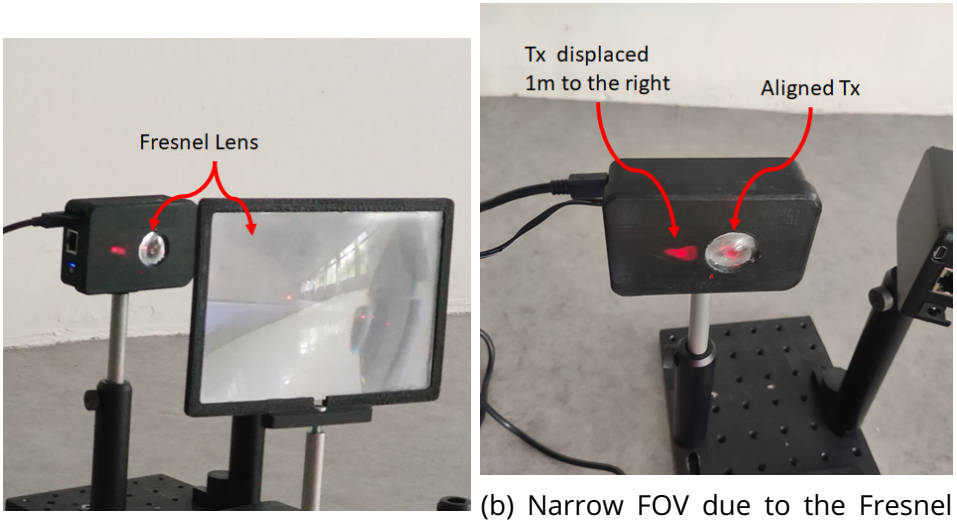

(a) Fresnel lens configuration.

(b) Narrow FOV due to the Fresnel lens.

Figure 3.20 – Experimental results of communication range with an arrangement of Fresnel lens. Lost of communication link due to misalignment

intended transmitter.

From Figures 3.21 and 3.22 we can observe that the interference has a critical impact on the communication link, even when the intended transmitter is closer to the receiver than the interference transmitter.

Furthermore, we demonstrate that some level of interference can be suppressed by optical configuration. We drive our test with a Fresnel lens of $25\ mm$ of diameter with a focal at $10\ mm$ and observe that the communication range increase a few meters and the interference comes from a lateral displacement of $1.5\ m$ disappears.

Also, we conducted some tests with a $190\ mm \times 130\ mm$ Fresnel lens. Although this lens helps to catch more light, increasing the communication range, the FOV is critically closed, solving the interference problem as illustrated in Figure 3.20. Nevertheless, this narrow FOV generates losses due to misalignment of the Tx with the Rx. Furthermore, the ambient noise becomes problematic as the system can catch more light due to the lens.

3.4 . Conclusion

The necessity of a MAC protocol to manage interference generated from the same and adjacent lane is proved in this chapter. The major contribution of this chapter is the theoretical demonstration of the interference impact to the vehicular

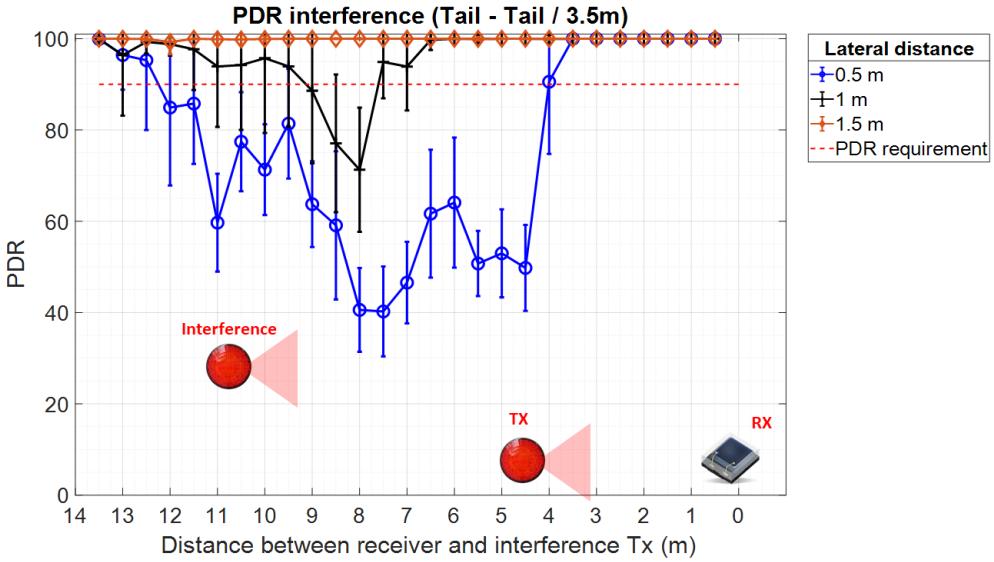

Figure 3.21 – Experimental results mean value for 5 samples per point, error bars variation due to the misalignment and different ambiance noise levels for interference with intended transmitter taillight at 3.5 m from the intended receiver and interference transmitter (taillight) moving in parallel at 0.5,1, and 1.5 m from 0 to 13 m

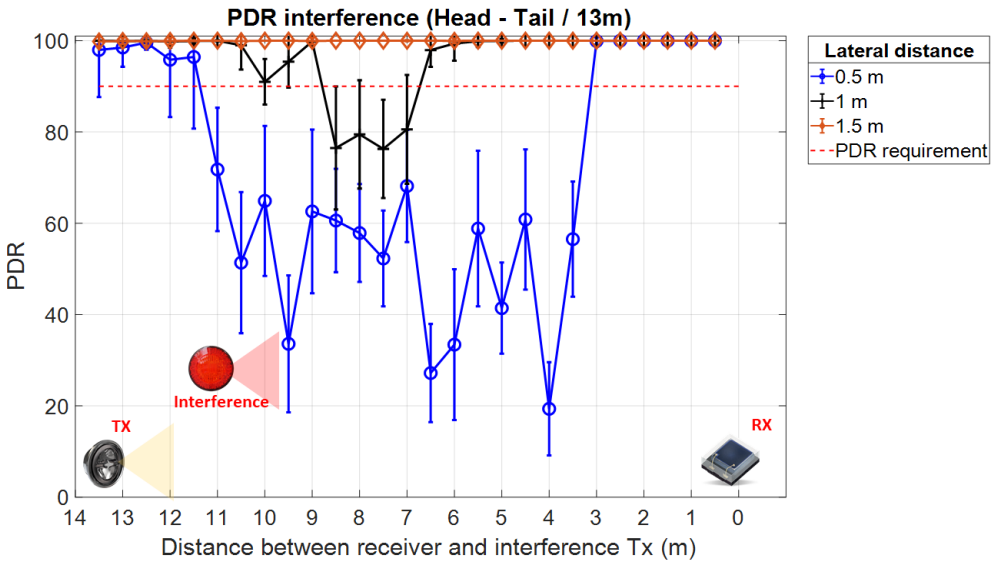

Figure 3.22 – Experimental results mean value for 5 samples per point, error bars variation due to the misalignment and different ambiance noise levels for interference with intended transmitter headlamp at 13 m, from the intended receiver, and interference transmitter (taillight) moving in parallel at 0.5 ,1 and 1.5 m from 0 to 13 m

VLC link through simulation and experimentation. The research has also shown that, for a 3-lane road, a maximum of 6 VLC links can be attained for a single VLC receiver.

It is clear from the results that our vehicular VLC platform needs improvements beyond the aims of this work to be suitable for a realistic scenario. We associate the significant variance of the PDR results to the differences in the alignment of the interference transmitter against the receiver. The most important limitation lies in the fact that the simulation results and tests carried on do not match in values and ranges due to the lack of development on the physical layer and the miss consideration of some physical parameters on the simulations. Nevertheless, we evaluated the vehicular VLC platform to demonstrate that vehicles can not use a typical VLC platform for dynamic scenarios, demanding more development. Furthermore, even when the values are different, simulations and test results conclude the necessity of a MAC protocol to manage the interference efficiently, minimizing the losses of information and increasing the capability of the autonomous vehicle platoons.

4 - Vehicular VLC : MAC protocol

Sommaire

4.1 . Vehicle-to-Vehicle VLC MAC protocol

4.1.1 . VLC MAC insights

Various MAC methods, including TDMA, CDMA, CSMA/CA, and ALOHA, have been investigated for VLC systems, as shown in Chapter 1, Figure 2.8. The following are the advantages and disadvantages of the various solutions :

— Although ALOHA and CSMA/CA cannot guarantee collision-free channel access [45], they are reliable in dispersed networks. Although ALOHA does not need channel sensing, it is reported to perform worse than CSMA/CA. CSMA/CA, on the other hand, is an enhanced version of ALOHA that is extensively utilized in distributed radio technologies, such as IEEE 802.11. However, as previously stated, CSMA/CA is not feasible in unidirectional VLC since it needs the transmitter to be aware of the receiver's channel

situation. The TDMA MAC protocols suggested for distributed radio access networks, such as those presented by Mao et al. [47] need nodes to reach an agreement through information sharing.

— When the nodes are entirely time-synchronized, TDMA can offer collision-free channel access. With TDMA, the difficulty is to assign unique slots to specific nodes (users), and the slot allocation is dynamically changed in response to node mobility (nodes join and leave the network) and demands (nodes need more or fewer resources). For centralized networks (cellular networks), where slot allocation is done by a central coordinator, such as a base station, a near-optimal TDMA MAC can be built. However, it is considerably more difficult in distributed mobile networks since nodes must independently choose slots while guaranteeing that other nodes do not select these spaces. In VLC, like in CSMA/CA, such a solution is challenging to implement or expensive.

— In contrast to ALOHA, CSMA/CA, and TDMA, where nodes share resources in the time domain (i.e., only one node may access the channel at a time), CDMA allows nodes to access the channel concurrently utilizing spread-spectrum technology. Each node, in turn, uses a spreading code to distribute the continuing message. There are two different types of spreading codes : orthogonal and non-orthogonal. Gold codes, for example, offer robust cross-correlation characteristics. They can use a different code to eliminate the propagation of interference signals as long as the signals are perfectly time-synchronized. Non-orthogonal codes, such as PN codes, on the other hand, have lower cross-correlation characteristics but do not require node time synchronization. Code allocation is the most challenging aspect of CDMA MAC systems. We propose a CDMA MAC protocol in which nodes pick CDMA codes independently based on their position and orientation in this section. Information sharing between potential interfering nodes is not required by the method.

— Frequency division multiple access (FDMA) might potentially be a solution, but it is a complicated solution due the complexity of the electronics. In the other hand, to develop this solution we must split the light in multiple bandwidths making it harder to build and deploy a functional platform [101].

4.1.2 . Vehicular VLC MAC proposal

The suggested MAC is optimized for vehicle-to-vehicle communication in platoons [30], which is the primary application of VLC. The following are the primary goals :

— To guarantee that vehicles in neighboring lanes use separate codes, reducing, if not eliminating, interference from adjacent lanes (depending on the code type),

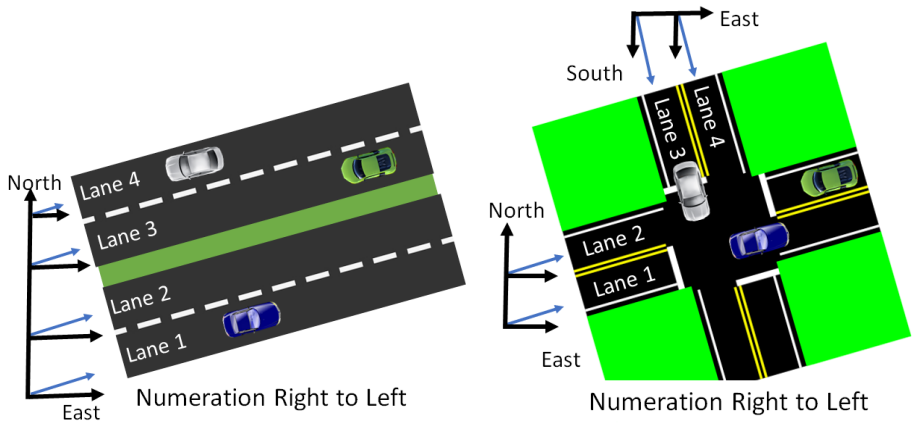

(a) Highway lane numbering. (b) Intersection lane numbering.

Figure 4.1 – Examples of lane numbering for different road configurations.

— To decrease the likelihood of vehicles in the same lane or non-adjacent parallel lanes sharing the same code.

Individual vehicles, especially automated vehicles, are assumed to be aware of their locations, and the road lane (i.e., the lane id) [102, 103, 104]. Individual lanes have different identifications, as seen in Figure 4.1. We split the total number of possible spreading codes, N_c, into n_c code groups in the suggested method, with each code group assigned to vehicles in specific lanes. Each code group includes four codes when $N_c = 16$ and n_c is 4. Code groups are assigned to vehicles in specific lanes; for example, code group 1 is assigned to lanes 1, 3, and 6.

The suggested MAC protocol is shown in Figure 4.2. To send a packet using VLC, the vehicle first determines its location and lane ID, then picks one code at random from the lane's code group. All the vehicles within the communication zone can transmit at the same time. The receiver must save the complete frame into a buffer to recover the information sent by the intended transmitter. Then, the receiver should compare the received frames with the codes assigned to the lane where it circulates. Once the frame on the buffer matches with one code, the receiver sets this code as the first of the code list. Henceforth, the receiver will try to decode the information received with this code until it does not match anymore, and the process to discover the main code reboot.

4.2 . Optical codes for VLC

4.2.1 . Random Optical Codes (ROCs)

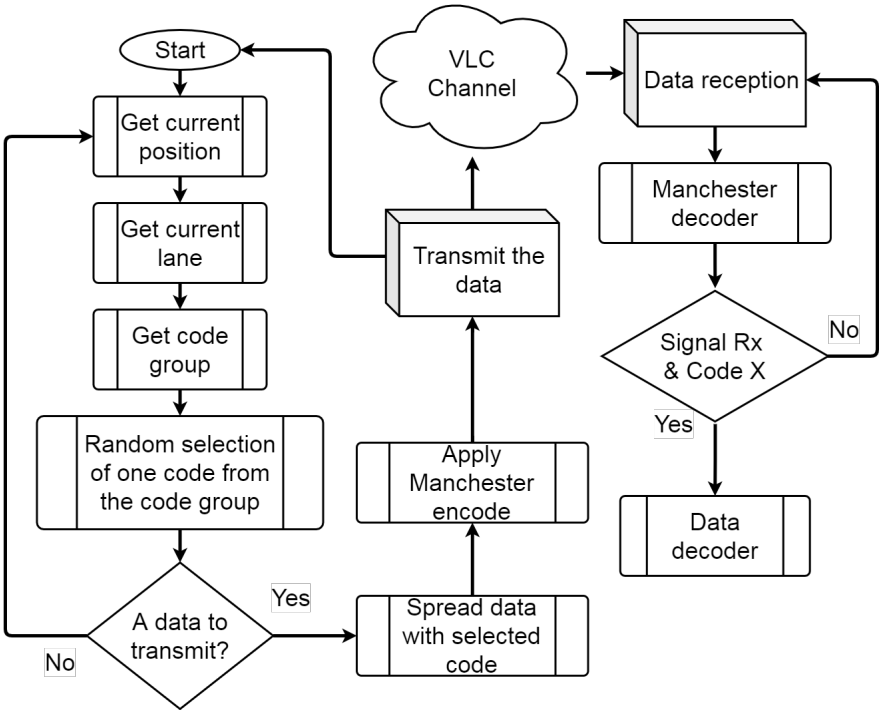

Figure 4.2 – Optical Code Division Multiple Access proposed protocol.

ROCs are well-suited to applications like wireless sensor networks, where many users use the same channel. Although ROCs correlation functions are not perfect, they are excellent enough to allow many users to share a single VLC channel. Each user in a VLC-CDMA system is granted a unique signature code. L_b bits are split into L_{sc} chips, with L_{sc} being the length of the ROC.

Only w_c chips with a non-zero power level are communicated, where w_c is the

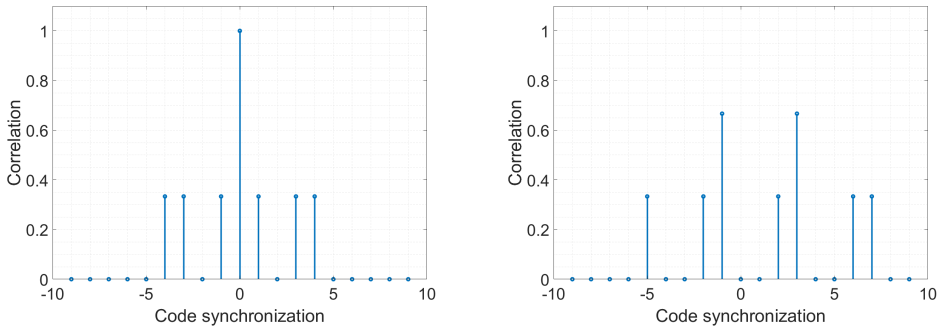

(a) ROC - auto-correlation property. (b) ROC - cross-correlation property.

Figure 4.3 – Example auto-correlation properties of ROC code 3 and cross-correlation of ROC code 3 against ROC code 5.

Table 4.1 – Random Optical Codes implemented on this work. $L_{sc} = 10, w_c = 3, Users = 5$

Code	*Value*
ROC1	0110010000
ROC2	1010000001
ROC3	0001001100
ROC4	0101000001
ROC5	1000100010

coding weight, and the placements of w_c non-zero chips appear randomly in L_{sc} chips. An example of those codes is presented in Table 4.1, and the correlation between codes on Figure 4.3. The magnitude of the cross-correlation signal indicates how closely the received signal resembles the target signal. As in this case, the codes are not orthogonal ; the cross-correlation shows that the similitude is significant for some points. Furthermore, when the data bit is one, these code sequences convey data. So far, several ROC codes have been proposed, including one application in audio experiment systems in [101, 105]. A cyclic shift can be used to change the original ROC to gain extra codes. To minimize interference, various shifts were given to distinct transmitters, and to recover the broadcast signals ; a receiver employs a shift register to execute a matched-filter operation.

4.2.2 . Prime Codes (PCs)

Because of the advantages of a simple code generation method and relatively straightforward encoder/decoder construction, PCs have been widely used in non-coherent OCDMA and wavelength hopping OCDMA systems. However, PC's correlation functions are not ideal, and its auto-correlation signals are often massive, making reliable synchronization for both transmitters and receivers problematic. As a result, it is unsuitable for asynchronous VLC-CDMA systems, and PC enhancements were recommended.

Based on modified prime sequence codes, [106] generalized modified prime sequence codes (GMPSC) and inverted GMPSC (MPSC). By improving its correlation functions, GMPSC may be employed in MUI cancellation systems. Table 4.2 presents the 4 (w_c) main codes and their sub-codes implemented for [106] and its correlation results corresponds to the following equation :

$$(C(n_{c_1}, N_{c_1}) \star C(n_{c_2}, N_{c_2}) = \begin{cases} w_c & ; n_{c_1} = n_{c_2} \; and \; N_{c_1} = N_{c_2} \quad , \\ 0 & ; n_{c_1} = n_{c_2} \; and \; N_{c_1} \neq N_{c_2} \quad , \\ 1 & ; n_{c_1} \neq n_{c_2} \end{cases} \quad . \tag{4.1}$$

As we can observe in the Table 4.2, the sub-codes implemented split the main codes on 4-bits frames and then re-organize the position of those frames, thus

results in the correlation properties described on Equation 4.2. If the correlated codes are the same code, the correlation value is equal to w_c. If the codes are different but from the same group (n_c), the correlation value is almost 0. Finally, if the codes are of different group (n_c), the resulting correlation is equal to 1. Figure 4.4 show an example of the normalized correlation.

Table 4.2 – Prime Codes implemented on this work.

n_c	N_c	*Code*
0	0	1000 1000 1000 1000
	1	0100 0100 0100 0100
	2	0010 0010 0010 0010
	3	0001 0001 0001 0001
1	0	1000 0100 0010 0001
	1	0100 1000 0001 0010
	2	0010 0001 1000 0100
	3	0001 0010 0100 1000
2	0	1000 0010 0001 0100
	1	0100 0001 0010 1000
	2	0010 1000 0100 0001
	3	0001 0100 1000 0010
3	0	1000 0001 0100 0010
	1	0100 0010 1000 0001
	2	0010 0100 0001 1000
	3	0001 1000 0010 0100

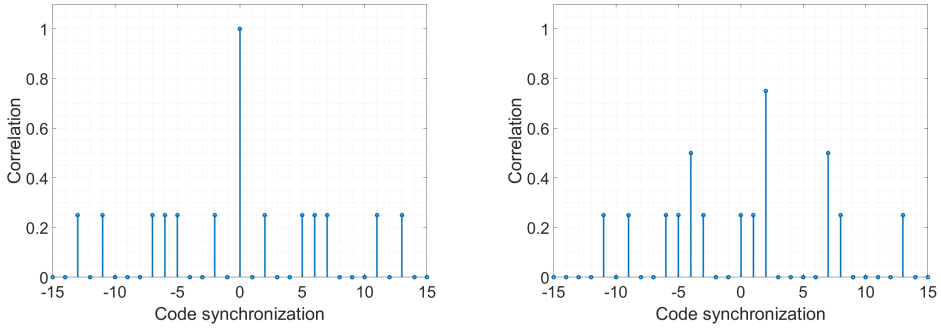

(a) PC - auto-correlation property. (b) PC - cross-correlation property.

Figure 4.4 – Example auto-correlation properties of PC code $(2, 2)$ and cross-correlation properties of PC code $(2, 2)$ against PC code $(1, 2)$.

4.2.3 . Pseudo Noise codes (PN)

PN codes are deterministic codes of 0s and 1s that looks like channel noise but have a deterministic structure. The codes are often created using feedback shift registers and are generated using a method that uses a seed value as a beginning value ; the process is deterministic and creates a series of integers that is not statistically random. However, if the method is suitable, the resultant sequences will satisfy many plausible randomness tests. These numbers are known as pseudo-random numbers, or PN sequences [107, 108].

The authors of [109] propose PN codes as a solution for an optical-fiber CDMA MAC protocol. According to Mollah et al. [110], PN codes must meet the following constraints :

— Sequences must be constructed from two leveled integers (0 and 1 for this work).

— To allow code synchronization, the codes should have a crisp (1 chip wide) auto-correlation peak.

— The cross-correlation value of the codes must be small. With a lower cross-correlation, the system can accommodate more users. This criterion applies to both full-code and partial-code correlation. Because there will seldom be a full-period correlation of two codes, it is more likely that they will only correlate partially due to the random-access character of the data [108].

— The code's differences between ones and zeros should be balanced ; this final criterion stands for good spectral density qualities (equally spreading the energy over the whole frequency band).

— The linear feedback shift register (LFSR) is a circuit that consists of XOR gates and a PN generator for spread spectrum. The total number of runs for a maximum-length sequence generated by a linear feedback shift register of length L_c is $(N_c + 1)/2$, where $N_c = 2^{L_c} - 1$ [108].

Table 4.3 – Pseudo-noise Codes implemented on this work.

Code	*Value*
PN1	100000100
PN2	001100010
PN3	100111101
PN4	000111001
PN5	001011011
PN6	101100110
PN7	101011111

The PN codes implemented in this work are introduced in Table 4.3 and an example of their auto- and cross-correlation are depicted in Figure 4.5. As illustrated on the plot, the code auto-correlation is well differentiated from the cross-correlation if the two codes are synchronized. Nonetheless, this example presents a maximum correlation value of almost 0.5 for auto- and cross-correlation if the signal is not synchronized.

4.2.4 . Optical Orthogonal Codes (OOCs)

The authors explained the basic features and mathematics underpinning the OOC design in [111, 112] in 1989. The OOC codes are built from chips (0s, 1s) of length L_c and weight w_c, with the requirement that they are orthogonal. Auto-correlation and cross-correlation are two of these characteristics.

$OOC(L_c; w_c; \lambda_a; \lambda_c)$ denotes this binary sequence, where L_c is the spread code length (number of chips), w_c is the weight (number of ones in the sequence), and λ_a and λ_c are the auto-correlation and cross-correlation constraints, respectively [111]. The following criteria apply for given OOCs u and v [112] :

$$u \star u = \sum_{j=0}^{L_c-1} u_j u_{j+w_c} \begin{cases} = w_c & ; w_c = 0 \\ \leq \lambda_a & ;1 \leq w_c \leq L_c - 1 \end{cases} , \tag{4.2}$$

$$u \star v = \sum_{j=0}^{L_c-1} u_j v_{j+w_c} \leq \lambda_c \; ; \; 0 \leq w_c \leq L_c - 1 \quad . \tag{4.3}$$

The auto-correlation of u and the cross-correlation of u and v, respectively, are denoted by $u \star u$ and $u \star v$. In reality, when IM/DD signal transmission is employed, strict orthogonality between two spread codes is not possible. We have $\lambda_a = \lambda_c = 1$ for OOCs, which results in the smallest MUI. The maximum number

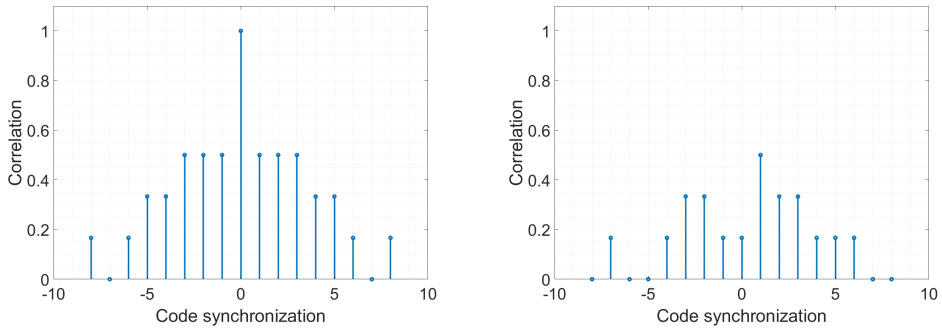

(a) PN - auto-correlation property. (b) PN - cross-correlation property.

Figure 4.5 – Example auto-correlation properties of PN code 3 and cross-correlation properties of PN code 3 against PN code 2.

Table 4.4 – Optical Orthogonal Codes $(49, 4, 1, 1)$ implemented on this work.

Code	*Value*
OOC1	1100100 0000000 1000000 0000000 0000000 0000000 0000000
OOC2	1010000 1000000 0000000 0000010 0000000 0000000 0000000
OOC3	1000001 0000000 0000100 0000000 0000010 0000000 0000000
OOC4	1000000 0100000 0001000 0000000 1000000 0000000 0000000

of users N_c that may be managed using $OOC(L_c; w_c; 1; 1)$ codes is upper limited by [112] :

$$N_c \leq \frac{L_c - 1}{w_c(w_c - 1)} \quad . \tag{4.4}$$

Error-free data recovery for an "ideal" connection (i.e., without noise impact and only from an MUI standpoint) is achievable for these kinds of codes if w_c satisfies the required conditions [111, 112] :

$$w_c > N_c - 1 \quad . \tag{4.5}$$

The auto-correlation of each code must display impulsive behavior to differentiate one code from another (see Figure 4.6a). On the other hand, the cross-correlation between different codes must be significantly lower, near-zero (see Figure 4.6b). The OOC codes implemented in this study are introduced in Table 4.4

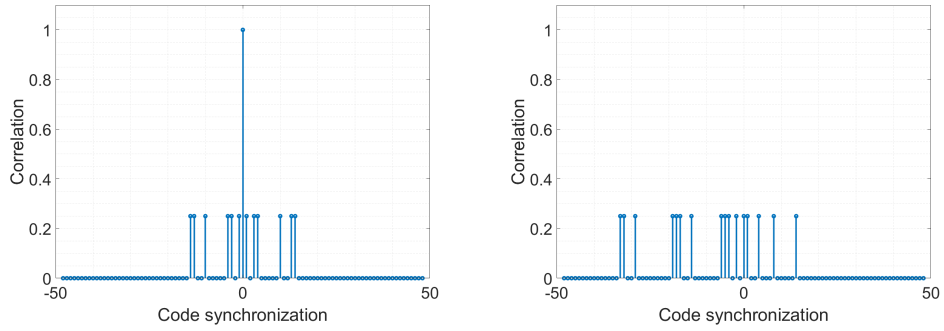

(a) OOC - auto-correlation property. (b) OOC - cross-correlation property.

Figure 4.6 – Example auto-correlation properties of OOC code 1 and cross-correlation properties of OOC code 1 against PN code 3.

4.2.5 . Comparison between codes

The correlation characteristics of the codes studied in this work are shown in Figures 4.3, 4.4, 4.5 and 4.6. The well-studied OOC codes exhibit an auto-correlation and cross-correlation always less than 0.3 unless the auto-correlation is synchronized $(correlation = 1)$, presenting them one of the best solution for the CDMA protocol. Finally, Table 4.5 summarize the relevant data about proposed codes.

Table 4.5 – Correlation comparison of OCDMA codes

Code	L_{sc}	N_c	*Min cross-correlation*	*Max cross-correlation*
OOC	49	4	0.25	0.25
PC	16	16	0.25	0.75
PN	9	7	0.16	0.83
ROC	10	5	0.33	0.66

4.3 . Simulation of OCDMA

This section assesses the proposed MAC protocol performance for the 7-lane highway situation depicted in Figure 3.14. In a Matlab simulator, we constructed the proposed VLC MAC and VLC physical layer and assessed the PDR performance of the proposed MAC codes described in the previous section. The suggested MAC outcomes were compared to the scenario when no MAC was used (from now on, no-MAC solution).

The Matlab script updates the interfering vehicle's position in 10 cm increments each iteration, while the intended Tx and Rx stay fixed at the same position. The script encodes the random data generated using the codes, and sends the packet using Manchester modulation. After it passes through the FSO channel, the receiver filters the signal, demodulates, decodes, and saves the data received for later comparison with the broadcast data. We manually assigne the codes to each lane for controllability sake and run the simulation numerous times, altering the code of the relevant lane each time. We establish the capability for each code to be repeated every three lanes. The simulation is conducted for each code described before, and the results are presented in the followings.

4.3.1 . Simulation of OCDMA with ROC codes

We first analyze the correlation of the codes, as it can be appreciated in Figure 4.7. We choose the ROC code 2 as the main code for the results reported on this document. Nevertheless, we launch the simulation with different code arrangements and with other codes as intended transmission code.

As shown in Figure 4.7, normalized cross-correlation of the ROC code 2 with the rest of the codes is almost the same, a cross-correlation of almost 0.35, except

for code four where the maximum value is around 0.7. In any case, the difference against auto-correlation is remarkable when the codes are synchronized, in which case, the value of the correlation is 1. The following codes are allocated to each lane for the simulation results :

— Lane 1 - ROC code 2,

— Lane 2 - ROC code 5,

— Lane 3 - ROC code 4,

— Lane 4 - ROC code 2,

— Lane 5 - ROC code 1,

— Lane 6 - ROC code 3,

— Lane 7 - ROC code 5.

Figure 4.8a contrasts the PDR efficiency of the suggested MAC with ROC codes to the no-MAC alternative when the intended and interfering signals are precisely synchronized. Nonetheless, in Figure 4.8b it is possible to see the PDR variations designed by color zones. As previously discussed, the PDR is equal to zero if the interference vehicle is in the zone between the intended transmitter and receiver and equal to 100% if it is in front of the intended transmitter because the MAC protocol does not solve shadowing problems.

As expected, the worst PDR obtained is when the interference transmitter uses code 4 in lane 3, getting in almost all the lane a $PDR = 95\%$. Moreover, a PDR equal to 95% on lane 6 but with less frequency is also observable. For the rest of the plot, the results goes between 96 and 100%.

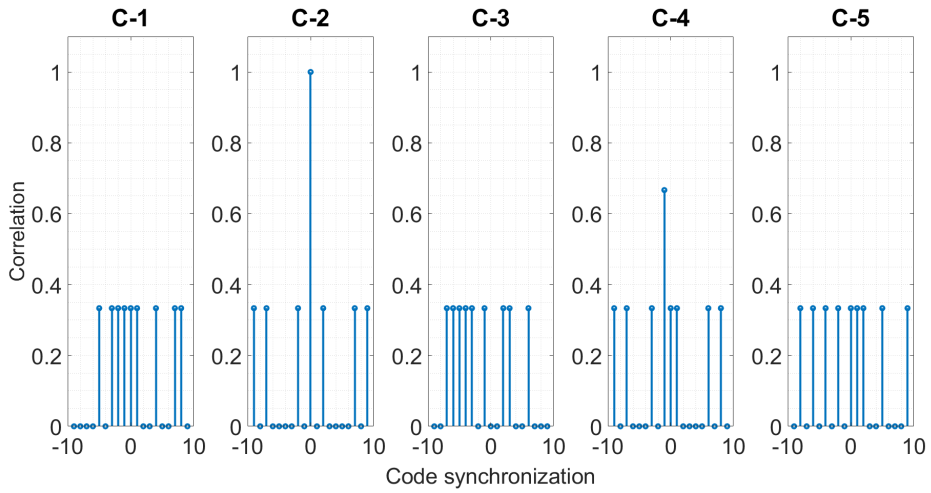

Figure 4.7 – ROC code 2 correlation against the rest of the codes.

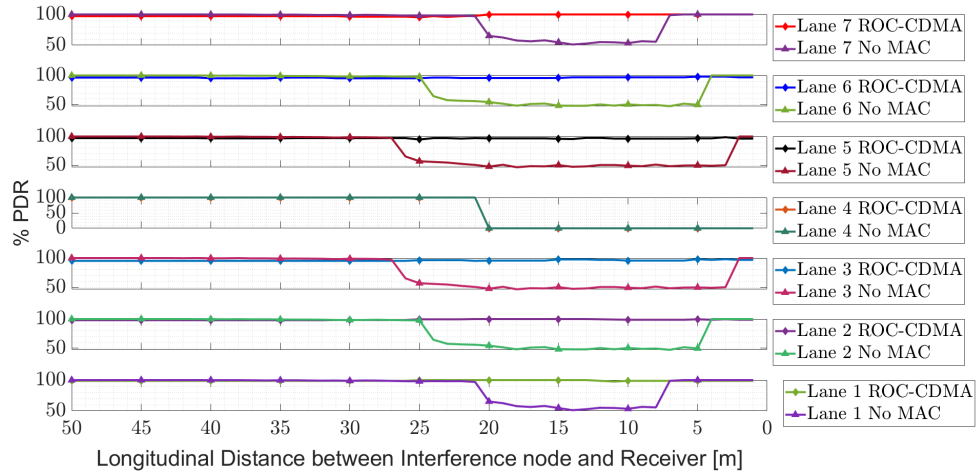

(a) OCDMA ROC codes per lane performance.

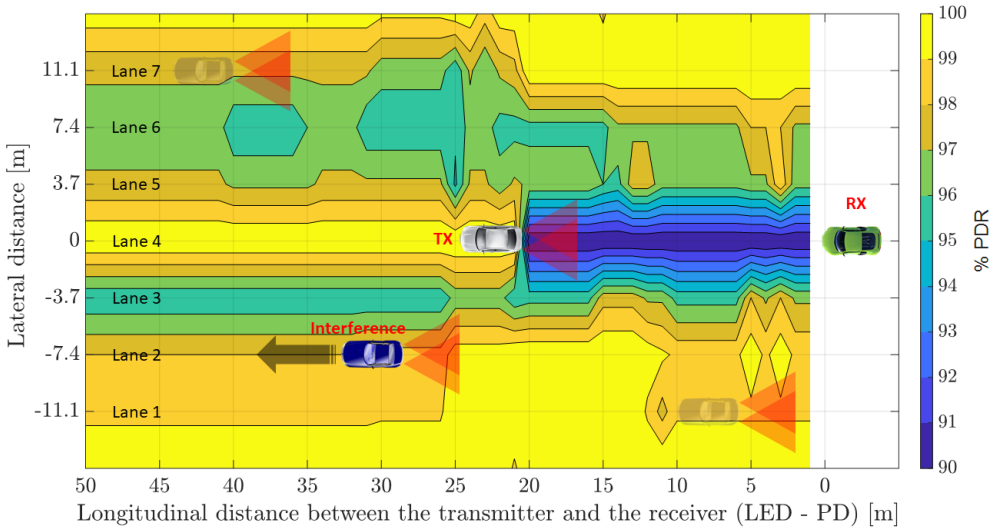

(b) OCDMA ROC codes mapping performance.

Figure 4.8 – ROC OCDMA MAC protocol simulation results for a 7 lanes road (a) per lane performances and (b) PDR mapping.

4.3.2 . Simulation of OCDMA with PC codes

Let us now consider the PC codes for the next simulation. As in the previous section, we begin showing the correlation of the proposed codes. As previewed by the equation 4.2, Figure 4.9 presents the normalized values of the correlation of PC code 11 against the rest of the codes.

The correlation plot shows that the PC code 11, selected for this example, have a low cross-correlation with the codes 1 to 4, a correlation of 0.5 with codes 5, 6, 8, 9, 10, 14, 15, and 16, and a maximum cross-correlation value of 0.75

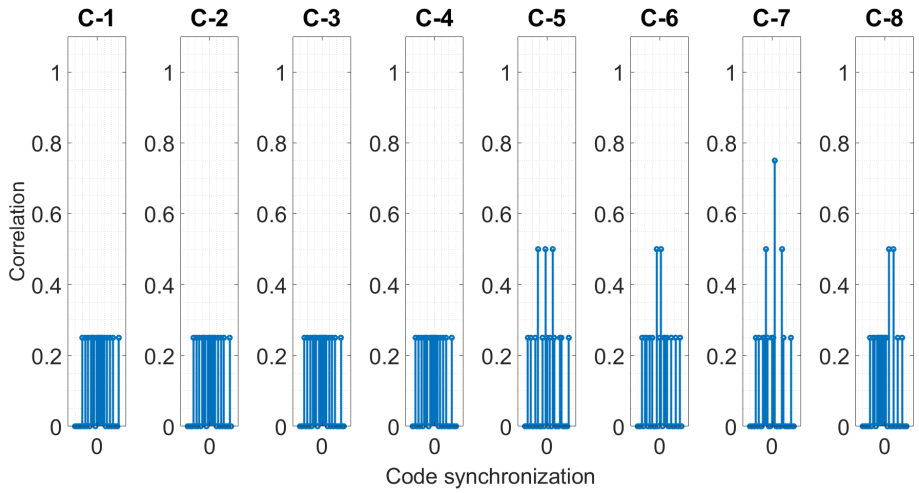

(a) PC code 11 correlation against PC code 1 to 8.

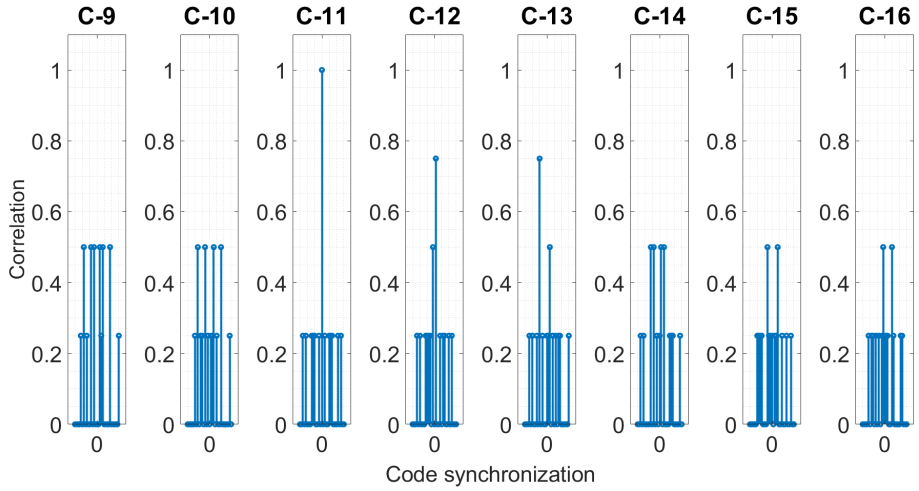

(b) PC code 11 correlation against PC code 9 to 16.

Figure 4.9 – PC code 11 correlation against the rest of the codes.

with codes 7, 12, and 13. For the simulated data, the following codes are assigned to each lane :

- Lane 1 - PC code 12,
- Lane 2 - PC code 9,
- Lane 3 - PC code 10,
- Lane 4 - PC code 11,
- Lane 5 - PC code 5,
- Lane 6 - PC code 4,
- Lane 7 - PC code 3.

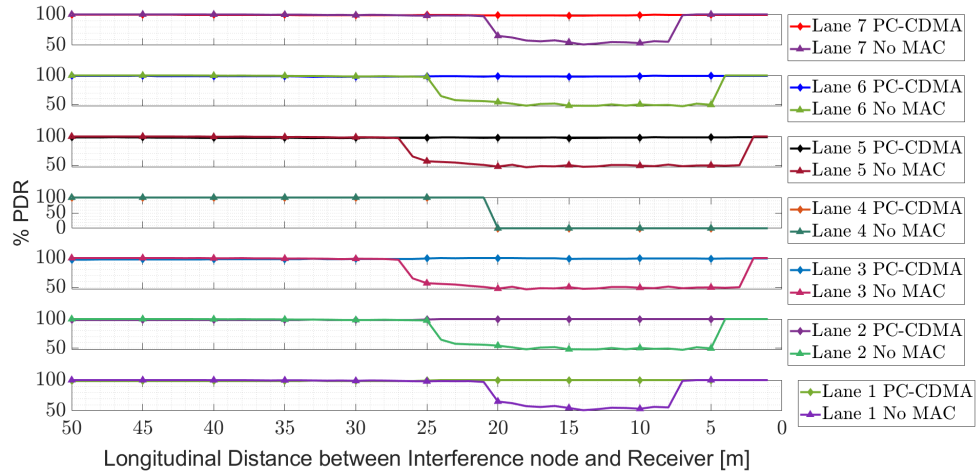

(a) OCDMA PC codes per lane performance.

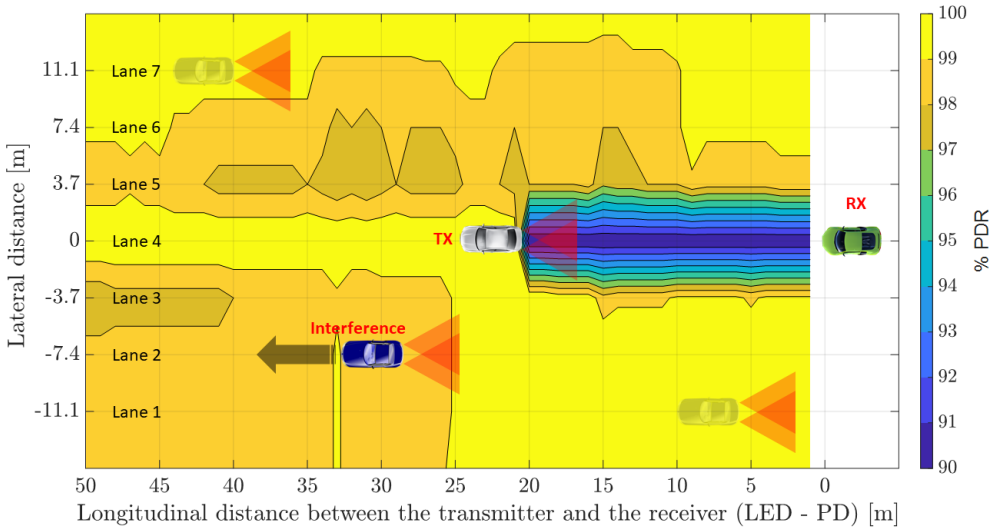

(b) OCDMA PC codes mapping performance.

Figure 4.10 – PC OCDMA MAC protocol simulation results for a 7 lanes road (a) per lane performances and (b) PDR mapping

When the intended and interfering signals are precisely synchronized, Figure 4.10a compares the PDR performance of the proposed MAC with PC codes to the no-MAC option. More in detail, Figure 4.10b presents the PDR mapping where color zones represent the different PDR values. The plot shows that the minimum PDR value on the adjacent lanes is around 97%. Also, there are zones, i.e., the region from $0\ m$ to $25\ m$ on lane 1 and 2 where the PDR is almost 100%. The correlation properties of this code make its implementation on CDMA protocol result in a desirable PDR performance.

4.3.3 . Simulation of OCDMA with PN codes

The suggested MAC protocol employing PN codes is the third proposition we study. The following PN codes are assigned to each lane :

— Lane 1 - PN code 6,

— Lane 2 - PN code 4,

— Lane 3 - PN code 5,

— Lane 4 - PN code 3,

— Lane 5 - PN code 7,

— Lane 6 - PN code 2,

— Lane 7 - PN code 1.

In lane 4, PN code three is assigned to the planned transmitter. Figure 4.11 shows the correlation values of this code with the rest of them. We can observe from the figure that there is not a low correlation value constant as it exists with the previously analyzed codes, i.e., PC code 1 to 4, and ROC code 1, 3, and 5. Nonetheless, the correlation remains 1 only when the code is correlated against itself, allowing us to distinguish it from the rest of the codes. The closest correlation value is around 0.85, obtained against the code 7.

The suggested MAC results are compared to the outcomes of the no-MAC solution in Figure 4.12a. As illustrated in Figure 4.12b, the proposed MAC protocol with PN codes has a sufficiently high PDR ($PDR > 90\%$) for all lanes in the intended scenario. However, we saw considerable oscillations due to the codes cross-correlation features, mainly when the interfering vehicle was in lanes 3 and 5. The worst PDR zone is located on lane three from 38 to 50 m, where the PDR value is around 93%. Furthermore, we can highlight from the mapping that PDR

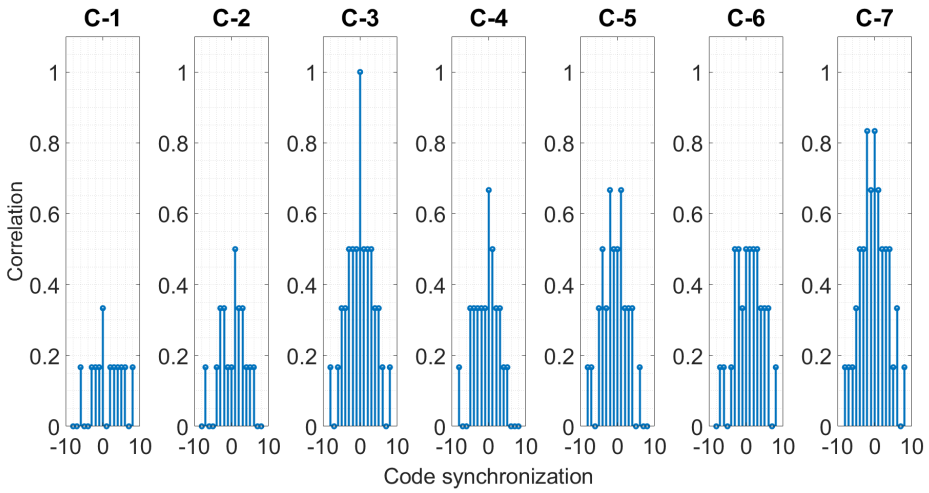

Figure 4.11 – PN code 3 correlation against the rest of the codes.

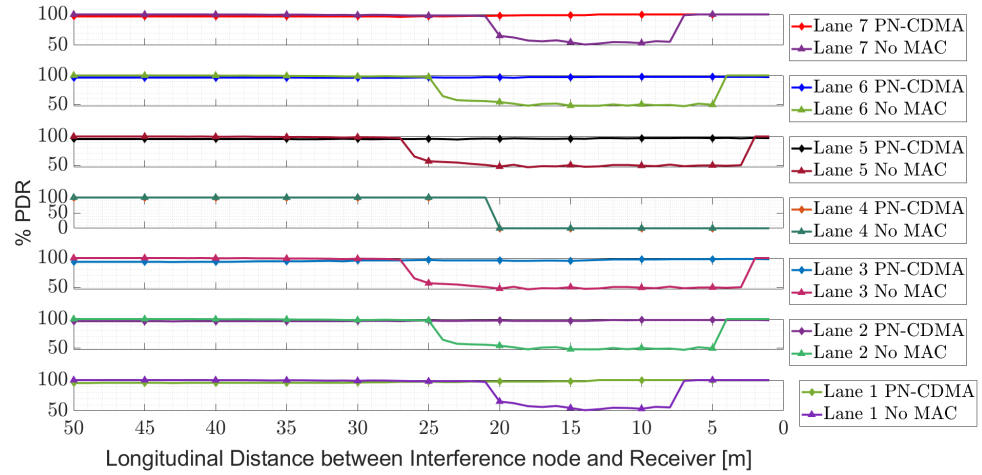

(a) OCDMA PN codes per lane performance.

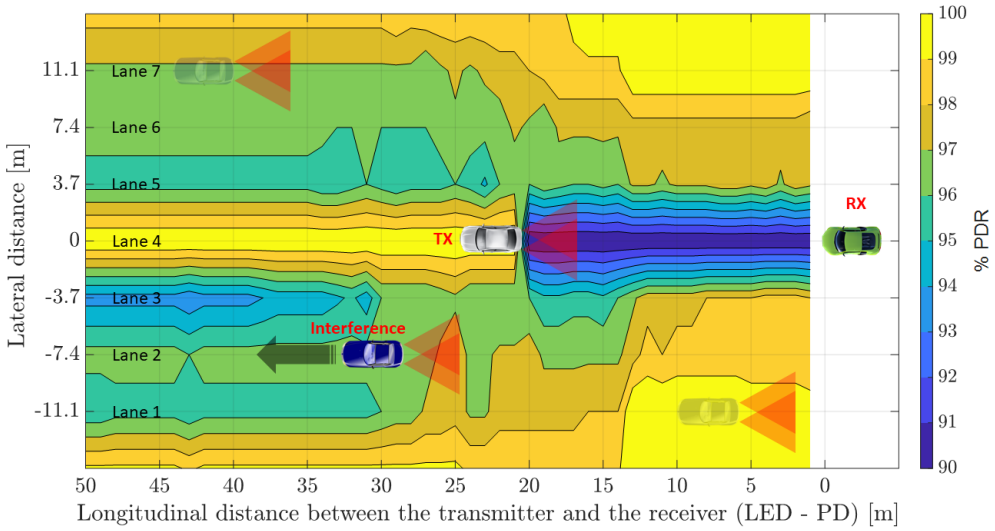

(b) OCDMA PN codes mapping performance.

Figure 4.12 – PN OCDMA MAC protocol simulation results for a 7 lanes road (a) per lane performances against no-MAC solution, and (b) PDR mapping.

degradation begins when the interference vehicle is farther than $15\ m$ concerning the receiver. Before $15\ m$, it does not matter where the interference vehicle is placed ; the PDR value is superior to 97%.

4.3.4 . Simulation of OCDMA with OOC codes

We now pass to evaluate an orthogonal code to later compare the results against the non-orthogonal codes. Figure 4.13 shows the correlation of OOC code

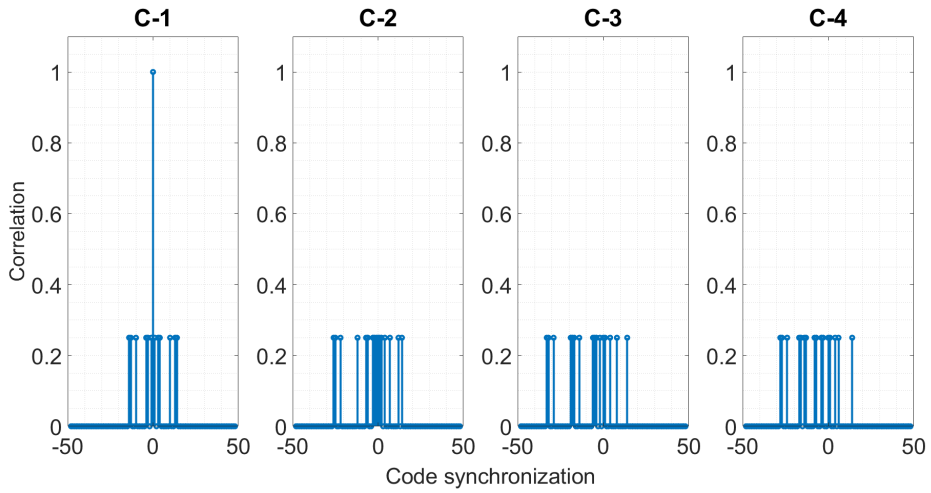

Figure 4.13 – OOC code 1 correlation against the rest of the codes.

1 with itself and the rest of the codes. When the codes are correctly synchronized, a very prominent auto-correlation peak can be seen, whereas for the rest of the codes the correlation value remains low (0.25). When the signals are synchronized, the difference between this peak value and the other values is substantial, suggesting OOCs decoding capacity. For this test experiment, the following codes are assigned :

- Lane 1 - OOC code 1,
- Lane 2 - OOC code 4,
- Lane 3 - OOC code 2,
- Lane 4 - OOC code 1,
- Lane 5 - OOC code 2,
- Lane 6 - OOC code 4,
- Lane 7 - OOC code 3.

When the intended and interfering signals are precisely synchronized, Figure 4.14a compares the PDR performance per lane of the proposed MAC with OOC codes to the no-MAC option.

In contrast to the no-MAC method, which achieves a PDR of 50% when conflicting nodes are in neighboring lanes, Figure 4.14b shows that the suggested CDMA code achieves a PDR of approximately 99% regardless of the position of the interfering vehicle. Only a small zone who involves the lanes 5 and 6 presents a small degradation to 98% for this specific case. As previously stated, when the interfering vehicle is situated between the intended transmitter and the receiver, the PDR is 0%, owing to the signal blockage problem. However, this is a VLC-specific problem that we cannot tackle with a MAC protocol.

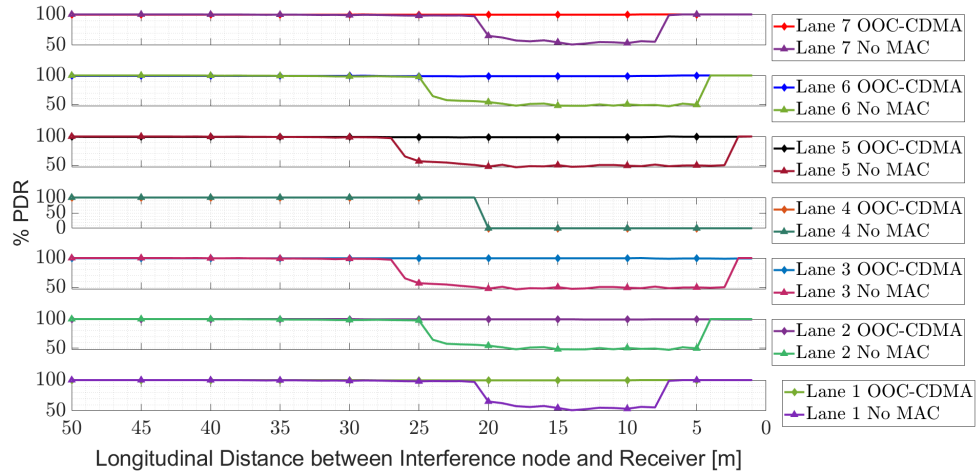

(a) OCDMA OOC codes per lane performance.

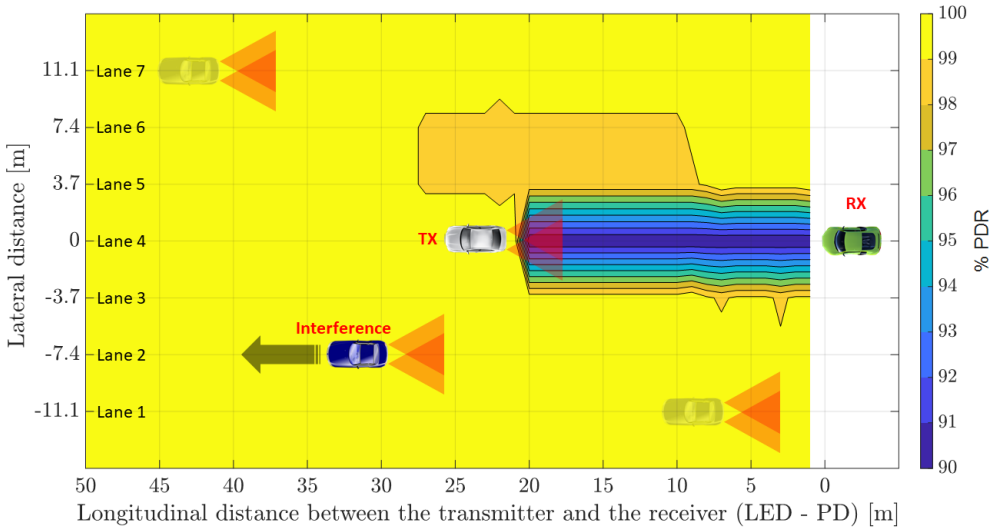

(b) OCDMA OOC codes mapping performance.

Figure 4.14 – OOC OCDMA MAC protocol simulation results for a 7 lanes road (a) per lane PDR performance and (b) mapping

4.4 . Performance comparison of OCDMA codes

In order to have a more precise idea about which code has better performance, in this section, we compare the most straightforward scenario of two lanes (Figure 4.15). In this scenario, the intended transmitter and receiver are placed as before, separating them by $20\ m$. Then, the interference vehicle moves along the adjacent lane with steps of $10\ cm$, transmitting a new random message encoded with a different code of the same group synchronized with the intended transmitter.

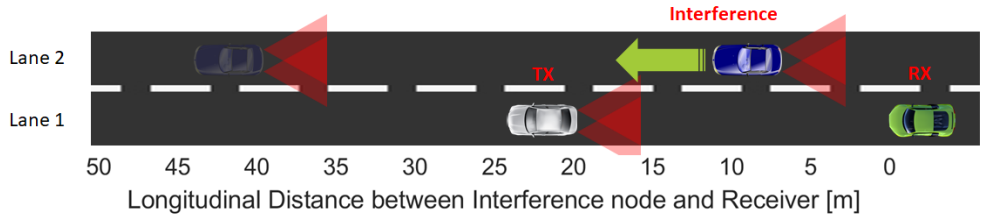

Figure 4.15 – Two lanes scenario to compare the different OCDMA codes performance

This simulation was launched 10 times with different code arrangements for each group, ROC, PC, PN, and OOC. The average results of those simulations with their respective error bar are illustrated in Figure 4.16a. The results show an upper PDR performance when the OCDMA protocol is implemented. Nevertheless, the OOC codes seem better than the others, but we can not appreciate the fundamental differences between the codes in this plot.

In Figure 4.16b, we remove the no-MAC solution from the plot and zoom in on the PDR axis. The plot lets us determine more precisely which code group performs better. We compute the PDR average each meter, from $1\ m$ to $50\ m$. Each distance is launched 10 times and codes are arbitrary allocated. For each point we calculate the PDR values and represent them as an error bar on the plot.

To summarize the performance of each code, we compute the PDR average of the mean value and the maximum and minimum PDR values from all the points (from 0 to 50 m). Those results are summarized on Table 4.6. As expected, OOC codes present the highest PDR mean of 99.2%, with the lowest variation between the points. The maximum PDR value for OOC results is 100%, and the minimum value is 97.6%. This result can be expected due to the same low correlation value between the intended transmitter code and the interfering OOC codes. On the other hand, for the non-orthogonal codes, we can observe that PC codes present the highest PDR means, with value of 97.9%, with a maximum and minimum values of 100% and 94.8% respectively. Those results are followed ROC codes which present the most variable performance ; even when the results are over the PDR requirement. The PDR average of ROC results is of 96.9%, with a maximum PDR value of 100% and a minimum PDR value of 94.8%. Finally, PN codes with lowest PDR values, an average PDR of 96.4, with a maximum and minimum PDR values of 99.6% and 93.2% respectively.

4.4.1 . Simulation of OCDMA asynchronously

In this section we analyze the proposed MAC protocol performance when interfering signals are not synchronized. The OOC, as previously stated, has highly code correlation qualities in comparison with the rest of the codes. Only the auto-correlation for code 1 equals 1 for OOC, while the cross-correlation with the other

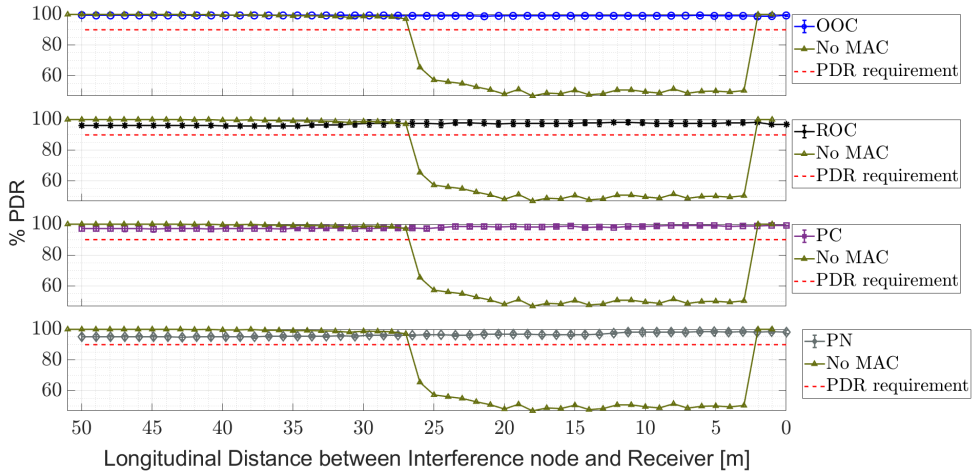

(a) PDR comparison of the OCDMA codes against no-MAC solution

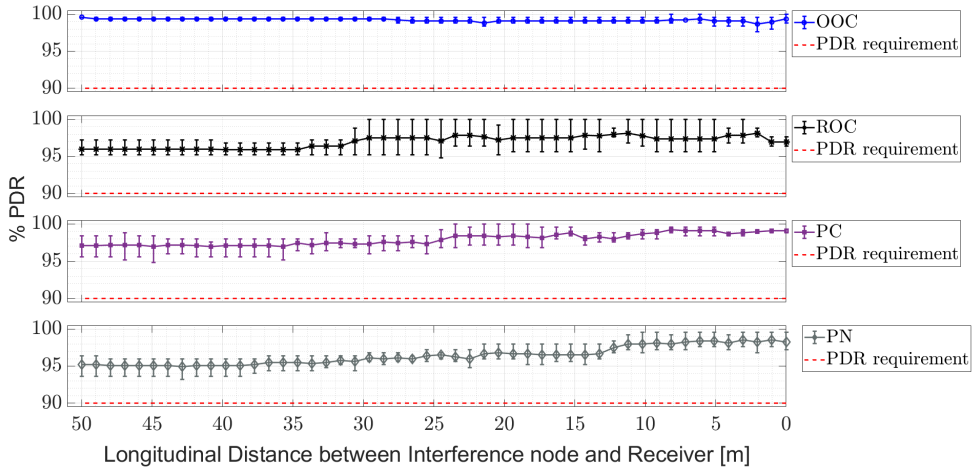

(b) PDR comparison between OCDMA codes.

Figure 4.16 – Comparison of the results of OCDMA MAC protocol with intended TX and RX at $20m$, on synchronous mode with OOC, ROC, PC, and PN codes. (a) Comparison with interference, (b) comparison between codes.

Table 4.6 – Performance comparison of OCDMA codes

Code	*Minimum PDR*	*PDR Mean*	*Maximum PDR*	*PDR variation range*
OOC	97.6%	99.2%	100%	2.4%
PC	94.8%	97.9%	100%	5.2%
ROC	94.8%	96.9%	100%	5.2%
PN	93.2%	96.4%	99.6%	6.4%

codes is a maximum of 0.25, indicating that the codes are orthogonal. However, the auto-correlation for code 1 is equal to 1 only when the signals are precisely synchronized.

For the non-orthogonal codes, if the auto-correlation is not synchronized the value can be even lower than the cross-correlation against other code, as illustrated in Figure 4.17. Because VANETs are distributed asynchronous networks, synchronizing the nodes is challenging and expensive. As a result, it is more reasonable to assume that the vehicles are not synchronized and can send packets whenever they choose.

The interfering signals are sent to the channel at random time intervals during the simulations, and the PDR of the intended communication is computed. Figure 4.18 shows how the protocols PDR performance do not differed when OOC, ROC, PC, and PN codes are employed. We can observe that the impact of the interference is lower for all the codes when it is not synchronized with the intended transmitter.

4.4.2 . Comparison of time simulation

Finally, to assess feasibility of the implementation of this proposed MAC protocol we compare the latency that can be estimated by the processing time (simulation time) for encode, transmit and decode a 32 $byte$ frame with ROC, PC, PN, and OOC code. The transmission time is the length of time it takes from the start until the end of a message transmission. The transmission time will change for each OCDMA code due to the length of each code and the complexity of the coding and decoding stage.

Furthermore, transmission time should not be confused with propagation delay, which is the amount of time it takes for the initial bit to travel from transmitter to

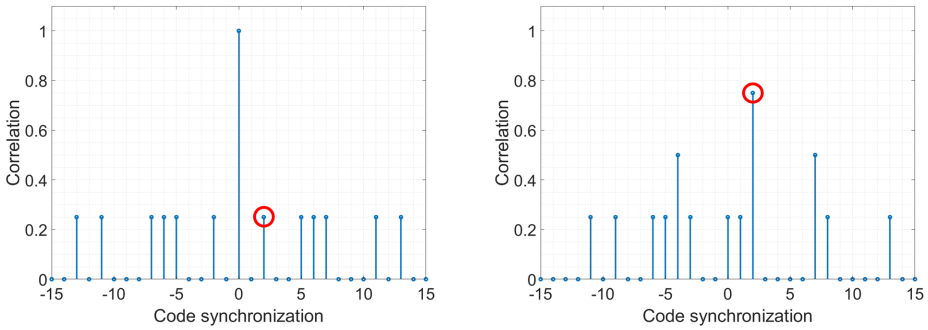

(a) Auto-correlation example of PC(2,2) code.

(b) Cross-correlation example of PC(2,2) code against PC(1,2) code.

Figure 4.17 – Correlation comparison between two PC codes. Red circles highlight auto and cross-correlation values for asynchronous transmission that can result on a decoding error.

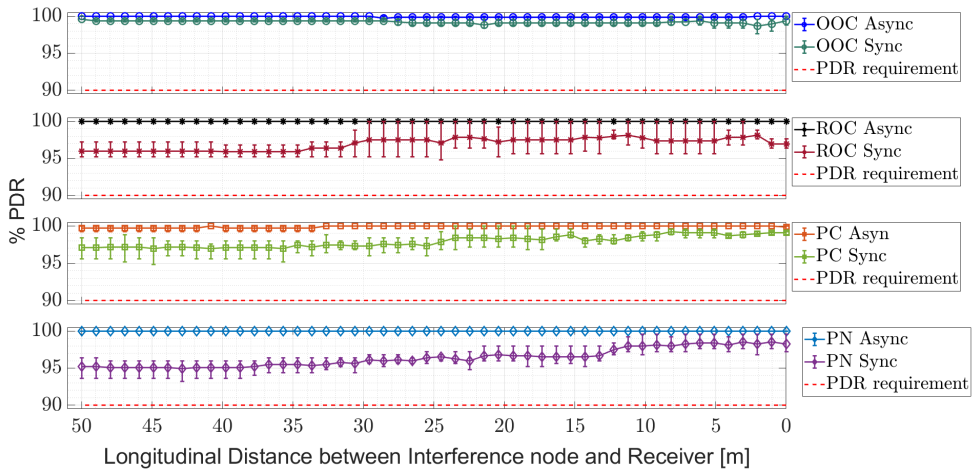

Figure 4.18 – Comparison of the results of OCDMA MAC protocol with intended TX and RX at $20\ m$, on asynchronous mode compared against synchronous results with OOC, ROC, PC, and PN codes.

the receiver, and it depends on the transmission frequency and the length of the transmitted frame (thus, the code implemented as showed in Table 4.7).

For wireless communication, the propagation speed depends on the physical channel of the link and is in the range of 3×10^8, which is equivalent to the speed of light ($66.79\ ns$ for the case of $20\ m$ of separation between the intended Tx and Rx). As a result, the packet delivery time (PDT) or latency is defined as the period between when the first bit leaves the transmitter and when the last bit is received. In the simulation, we add the coding and decoding time to highlight the impact of the complexity for code/decode the implemented OCDMA code. It is represented as follows :

$$PDT = 66.79\ ns + Transmission\ time + Coding/Decoding\ time \quad (4.6)$$

According to the findings, in Figure 4.19 we can observe that OOC codes take five times longer to process than the ROC, PC, and PN codes. The non-orthogonal

Table 4.7 – Comparison of transmission time of the proposed OCDMA codes

Code	*Transmission time*	*Transmission Frequency*	*Packet size*
OOC	$49\ ms$	$500\ kHz$	$256\ bits$
PC	$16\ ms$	$500\ kHz$	$256\ bits$
ROC	$10\ ms$	$500\ kHz$	$256\ bits$
PN	$9\ ms$	$500\ kHz$	$256\ bits$

PN and ROC codes present the lowest simulation time, even if the three non-orthogonal codes show a low simulation time value. Nevertheless, it is necessary to clarify that the time reported in the plot is not the latency of the network. Thereby, the values are presented to compare the differences between the codes and should not be taken literally as latency values. Due to the varying lengths of the codes, this finding can be predictable ; yet, it is critical to quantify it, especially for platooning applications of autonomous vehicles, where the reaction time of the following vehicles has a substantial influence on the platoon's performance.

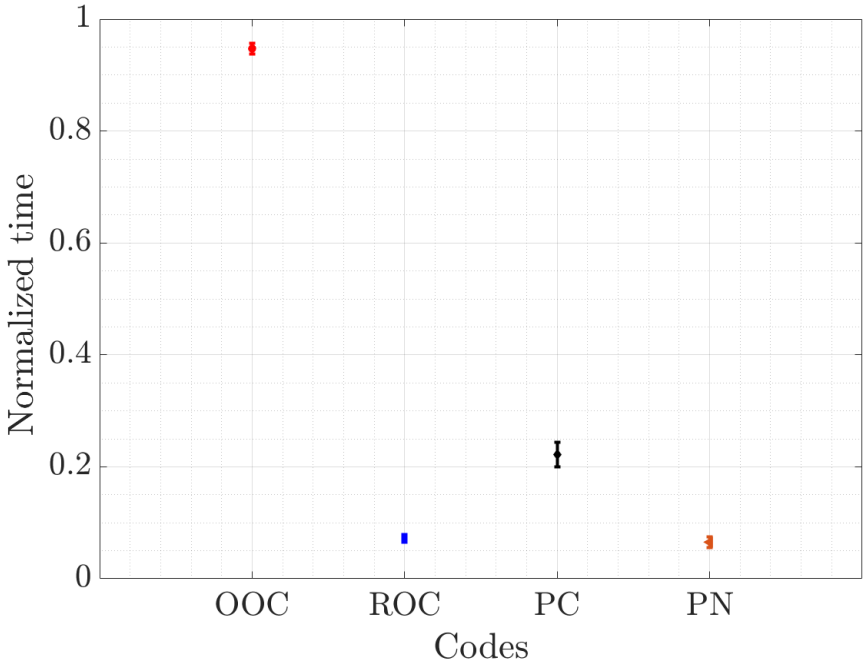

Figure 4.19 – Time of simulation to transmit 32 bytes of information with the different codes implemented - OOC, ROC, PC and PN.

4.5 . Conclusion

The findings reported in this chapter contribute from our perspectives to provide a basis for implementing VLC technology in the vehicular domain and offering a potential solution to MUI problems, especially for autonomous vehicles. From the description of the MAC protocol to its validation through simulation, the OCDMA solution promises to deliver excellent performance even for the most critical case when two transmitters send a message simultaneously to a single receiver over the visible light channel. Furthermore, the non-orthogonal codes present a desirable performance, similar to the OOC code, but with less processing time, that can be

interpolated like low latency. Table 4.6 displays a summary of the findings, highlighting the variations between the codes. In terms of average values, the OOC codes perform the best, with an average value of 99.2% and maximum and minimum PDR values of 100% and 97.6%, respectively. Non-orthogonal PC codes, on the other hand, exhibit a higher PDR performance against the other codes, with an average value of 97.9% and maximum and minimum PDR values of 100% and 94.8%, respectively.

5 - Conclusion and perspectives

The current study aimes to determine the impact of the interference vehicular VLC links that can perturb the communication between two intended vehicles. The study uses mathematical models, simulation, and experimentation. We propose also a solution based on an Optical CDMA MAC protocol and evaluate it through mathematical analysis and simulations to compare the PDR performance. The following sections present the conclusions of these studies and simulations, including the future perspectives related to vehicular VLC growth.

5.1 . Summary

Chapter 1 presents the main scenario and application of this research work. We introduce the C-ITS concept, the autonomous vehicle technology, platooning application, and communication constraints for this technology and application. We explain research motivations and objectives at the end of this chapter, summarizing the key characteristics of the proposed solution.

Chapter 2 introduces a brief resume of OWC systems and the most typical VLC-system configurations. Moreover, we present an overview of the state-of-the-art vehicular VLC systems in the last decades and some VLC research tools like the OpenVLC system and Veins simulator. Even when the study of VLC technology and its applications in vehicular environments has grown in the last decades, Figure 2.7 shows that it was not the case for MAC-protocol studies. The most relevant MAC-protocol-related works and the configuration implemented on them are presented in Figure 2.8. This figure shows that the domain research does not present a specific tendency for a preferred MAC protocol. Only a few authors focus on analyzing the outdoor application of this technology. Nonetheless, the most typical technology implemented in outdoor applications is the LED-PD link instead of the camera as a receiver. We present the well-studied channel model for VLC systems at the end of this chapter.

In Chapter 3, we establish an analytical methodology for identifying the MUI zone from which interference must be assessed to safeguard a continuing visible light V2V connection. Also, we estimate the maximum number of interference nodes regarding the FOV constraints and inter-vehicular distances, resulting in a maximum of 6 potential interference vehicles for a 3-lanes highway. In addition, we calculate the PDR performance of a VLC when the interfering nodes have a Poisson distribution. Then, we use a Simulink model to do simulation assessments. The model incorporates one or more interference vehicles and an intended transmitter, generating, encoding, and sending random messages to the target receiver over the

same VLC channel.

We evaluate the findings obtained by simulation in Veins and Matlab, comparing the analytical model described on section 3.1 against the channel model for VLC communications presented in section 2.4, incorporating a commonly used PD physical and electrical features. The simulation outcomes first confirm the analytical models accuracy on the MUI zone. The results further reveal that, even at low traffic densities and message production rates, vehicles in the MUI zone may considerably reduce the PDR performance of the target VLC communication, highlighting the inherent need for a MAC protocol for V2V communications. Finally, we presente our VLC platform and the experimental set-up used to measure the maximum communication distance and the impact of the environmental noise and interference transmitters. Here we must highlight that most of the objectives for the test platform presented in the section 1.3.1 are achieved. Nevertheless, some of there like the communication distance, should be improved.

While LOS and direct connections distinguish VLC V2V, multi-user interferences become a problem. Chapter 4 looks at current MAC protocols and suggests a CDMA-based MAC protocol. The suggested MAC protocol picks an OCDMA code based on their position and the current lane Id. We use Matlab simulator to develop the proposed MAC protocol and assess the PDR performance when OOC, ROC, PC, and PN codes are employed. Simulation findings demonstrate that the proposed approach, regardless of code type, may deliver PDR superior to 90%, with up to 40% performance gain over the no-MAC option. A resume of the results is presented on Table 4.6, showing the differences between the codes. In terms of average values, the best performance is presented by the OOC codes with an average value of 99.2% with maximum and minimum PDR values of 100% and 97.6%, respectively. On the other hand, the non-orthogonal PC codes present an upper PDR performance with a mean value of 97.9% and a maximum and minimum PDR values of 100% and 94.8%.

Furthermore, the simulation research on asynchronous communications demonstrates that both non-orthogonal and orthogonal codes exhibit similar behavior. Both codes offer sufficiently high PDR (above 90%) with fewer disturbances than when synchronized transmissions. Finally, a processing time study reveals that non-orthogonal codes are more appealing than orthogonal codes for automotive applications requiring low latency communication.

5.2 . Perspectives

In order to increase the communication range of the vehicular VLC platform to fit with the simulation results, it is imperative to update our system. Due to the nature of the application, it is impossible to increase the power of the transmitted signal or concentrate the pattern of the emitted light due to norms and

constraints that must be respected in the vehicular lighting system. Also, the implementation of an oversized lens to collect more light is inconvenient, as shown in section 3.3.1, due to the reduction experimented on the FOV. Consequently, a possible progression of this work is to update the AFE circuit, implementing a pre and post-equalization to improve the throughput as suggested by Merah in his work [113]. Also an improvement on the filtering stage, adding an Automatic Gain Controller as in the related work presented by Avătămăniței et al. [43]. Nonetheless, those improvements of the AFE are out of the scope of this thesis work. Those improvements should increase the quality of the received signal and, therefore, the communication distance and network throughput. Also, the implementation of optical filters can decrease the noise impact, especially in the outdoor environment, improving the quality of the link, hence, the communication range.

Afterward, different scenarios can be set to highlight the behavior of the vehicular VLC link under different conditions :

- a curved road, a crossroad intersection, a road roundabout,
- different weather conditions, to evaluate the attenuation generated by the atmosphere, the snow, rain, and fog at different densities,
- the evaluation of the vehicular VLC platform under dynamic situations, at different speeds and under different roads such as asphalt and dirt,
- also, it is essential to corroborate the MAC protocol performance on the vehicular VLC platform, implementing the different codes described in Chapter 4,
- therefore, this implementation of MAC protocol should generate a more precise data about PDT and latency,
- finally, the simulations developed in Matlab can be improved by considering the shadowing impact of vehicle bodywork or the reflections due the road characteristics as sugested by [114] and confirming the analysis of the section 3.1.3.

Those evaluations should generate a more realistic comprehension of the protocol against different scenarios and suggest new improvements or modifications for each implemented code.

We know that Matlab can simulate ray-tracing for RF communications [115]. Also, we can imagine a simulation as the developed by Combeau *et al.* for aircraft cockpits [116] but applied to the vehicular scenario. Likewise, Torres Zapata *et al.* [117] present a modified Monte Carlo ray-tracing simulation to obtain the impulse channel response of a vehicular VLC system proposed to be installed into a tunnel.

Nonetheless, the simulations carried with Matlab use a developed toolbox where antenna parameters are already defined, which is impossible to customize. Hence, developing a ray-tracing simulation capable of showing the VLC power attenuations and the interaction with physical objects of different materials can grow the comprehension of this technology in the automotive field.

5.3 . Publications

The following publications where drafted during the realization of this research work :

— E. Plascencia, O. Shagdar, H. Guan, and L. Chassagne, "Study on Multi-Users Interference in Vehicle to Vehicle Visible Light Communications," in International VEHICULAR 2020, Porto, Portugal : IARIA, Oct. 2020, pp. 1–7. [81]

— L. -M. Cosovanu, E. Zadobrischi, M. Dimian and E. Plascencia, "Unified Road Infrastructure Safety System using Visible Light Communication," 2020 28th Telecommunications Forum (TELFOR), 2020, pp. 1-4, doi : 10.1109 /TELFOR51502.2020.9306674. [40]

— Plascencia, E. ; Shagdar, O. ; Guan, H. ; Barrois, O. ; Chassagne, L. Optical CDMA MAC Evaluation in Vehicle-to-Vehicle Visible Light Communications. Electronics 2022, 11, 1454. https ://doi.org/10.3390/electronics1109 1454 [118]

6 - Annexe : Synthèse

La communication par lumière visible (VLC) est apparue comme une option viable pour aider les systèmes de transport intelligents coopératifs (C-ITS). Les connexions en visibilité directe (LOS) avec un champ de vision limité (FOV) sont utilisées dans VLC pour permettre des communications dirigées à courte portée. VLC est parfaitement adapté à diverses applications de communication V2V, notamment celles nécessitant des communications hautement sécurisées, fiables et à faible latence entre les véhicules, tels que les pelotons, en raison de ces qualités. De plus, la technologie peut coexister avec les technologies RF (WiFi, 4G/5G, etc.), permettant une expansion du spectre potentiellement illimitée avec un accès sans entrave. Une grande partie des recherches de VLC a porté sur le développement de la couche physique (PHY). PHY-I, PHY-II et PHY-III sont les trois couches physiques définies par les normes IEEE 802.15.7 [27] et 802.15.7r1 [28], PHY-I étant pour les applications extérieures. La modulation ON-OFF (OOK) et la modulation de position d'impulsion variable (VPPM) sont deux caractéristiques d'un système VLC avec PHY-I. Il a été conçu pour des vitesses de données de dizaines à centaines de kbps dans des applications extérieures. Plusieurs recherches ont montré que VLC peut être utilisé pour les communications V2V. Les auteurs ont prouvé le caractère pratique de VLC pour la communication V2V et V2I (Vehicle-to-Infrastructure) à des distances allant de 20 à 130 m et des débits de données allant de 11 à 500 kbps dans [43, 119, 120, 121]. VLC offre une variété d'options de couche physique. Cependant, l'absence de protocole MAC ne peut pas être utilisée pour les réseaux ad hoc véhiculaires dispersés (VANET). Les interférences multi-utilisateurs (MUI) peuvent réduire considérablement les performances de livraison des paquets dans des conditions de trafic moyennes à denses, comme le montre un article récent [81]. La recherche a prouvé l'importance du MAC dans VLC pour les applications automobiles. L'accès aléatoire sans fente, l'accès aléatoire à fente, l'accès multiple à détection de porteuse sans fente avec évitement de collision (CSMA/CA) et le CSMA/CA à fente sont les quatre techniques d'accès aléatoire définies dans les normes actuelles qui peuvent être utilisées comme MAC pour VLC [28, 82] . CSMA/CA n'est pas réalisable dans le VLC véhiculaire unidirectionnel, à notre avis, car il a besoin que l'émetteur connaisse l'état du canal du récepteur. Pour commencer, la détection de porteuse au niveau de l'émetteur VLC est inefficace car les conditions du support de transmission au niveau de l'émetteur ne reflètent pas avec précision les besoins d'un récepteur VLC en raison du FOV étroit du VLC. En conséquence, seule la détection de porteuse au niveau du récepteur VLC serait pratique. D'autre part, le récepteur doit donner les informations à l'émetteur VLC, ce qui ne peut pas être fait sur le même canal VLC car les liaisons bidirectionnelles dans une architecture de réseau dynamique comme VANET sont difficiles à établir.

Dans ce cas, une approche convaincante pour utiliser CSMA/CA pour VLC serait que le récepteur VLC transmette des informations sur les conditions du support de transmission via un autre canal, tel que la technologie RF. Nous proposons un protocole MAC basé sur l'accès multiple par répartition en code (CDMA) pour la communication VLC de véhicule à véhicule dans ce travail de thèse. Le protocole CDMA suggéré n'utilise pas la détection de porteuse, ce qui signifie que le récepteur n'a pas besoin d'informer l'émetteur des circonstances du support de transmission. Nous avons examiné les codes CDMA orthogonaux et non orthogonaux. Nous avons démontré que les codes PN, PC et ROC non orthogonaux pouvaient délivrer près de 100% de paquets et sont plus intéressants que les codes orthogonaux car ils ne nécessitent pas de synchronisation temporelle entre les nœuds.

Bibliographie

[1] A. G. Bell, "The photophone," *Science*, vol. 1, no. 11, pp. 130–134, 1880.

[2] B. Béchadergue, "Visible light range-finding and communication using the automotive led lighting," Ph.D. dissertation, 2017.

[3] M. Abualhoul, "Visible light and radio communication for cooperative autonomous driving : applied to vehicle convoy," Ph.D. dissertation, MINES ParisTech, 2016.

[4] J.-H. Yoo *et al.*, "Demonstration of vehicular visible light communication based on led headlamp," *International journal of automotive technology*, vol. 17, no. 2, pp. 347–352, 2016.

[5] H.-Y. Tseng *et al.*, "Characterizing link asymmetry in vehicle-to-vehicle visible light communications," in *2015 IEEE Vehicular Networking Conference (VNC)*. IEEE, 2015, pp. 88–95.

[6] M. D. Hina, H. Guan, A. Ramdane-Cherif, and N. Deng, "Secured data processing, notification and transmission in a human-vehicle interaction system," in *2016 IEEE 19th International Conference on Intelligent Transportation Systems (ITSC)*. IEEE, 2016, pp. 1277–1284.

[7] C. Bergenhem, S. Shladover, E. Coelingh, C. Englund, and S. Tsugawa, "Overview of platooning systems," in *Proceedings of the 19th ITS World Congress, Oct 22-26, Vienna, Austria (2012)*, 2012.

[8] P. Kavathekar and Y. Chen, "Vehicle platooning : A brief survey and categorization," in *International Design Engineering Technical Conferences and Computers and Information in Engineering Conference*, vol. 54808, 2011, pp. 829–845.

[9] A. Levedahl, F. Morales, and G. Mouzakitis, "Platooning dynamics and control on an intelligent vehicular transport system," *CSOIS, Utah State University*, pp. 1–7, 2010.

[10] S. E. Shladover, C. A. Desoer, J. K. Hedrick, M. Tomizuka, J. Walrand, W.-B. Zhang, D. H. McMahon, H. Peng, S. Sheikholeslam, and N. McKeown, "Automated vehicle control developments in the path program," *IEEE Transactions on vehicular technology*, vol. 40, no. 1, pp. 114–130, 1991.

[11] L. Li and F.-Y. Wang, *Advanced motion control and sensing for intelligent vehicles*. Springer Science & Business Media, 2007.

[12] C. Bergenhem, E. Hedin, and D. Skarin, "Vehicle-to-vehicle communication for a platooning system," *Procedia-Social and Behavioral Sciences*, vol. 48, pp. 1222–1233, 2012.

[13] E. Standard, "Intelligent transport systems (its) ; european profile standard for the physical and medium access control layer of intelligent transport systems operating in the 5 ghz frequency band," 2010.

[14] S. Ucar, S. C. Ergen, and O. Ozkasap, "Security vulnerabilities of ieee 802.11p and visible light communication based platoon," in *2016 IEEE Vehicular Networking Conference (VNC)*, 2016, pp. 1–4.

[15] Z. H. Khattak, B. L. Smith, and M. D. Fontaine, "Impact of cyberattacks on safety and stability of connected and automated vehicle platoons under lane changes," *Accident Analysis & Prevention*, vol. 150, p. 105861, 2021. [Online]. Available : https://www.sciencedirect.com/science/article/pii/S000145752031681X

[16] T. Yang, C. Murguia, D. Nešić, and C. Lv, "A robust cacc scheme against cyberattacks via multiple vehicle-to-vehicle networks," *arXiv preprint arXiv :2106.10448*, 2021.

[17] M. Y. Abualhoul, O. Shagdar, and F. Nashashibi, "Visible light inter-vehicle communication for platooning of autonomous vehicles," in *2016 IEEE Intelligent Vehicles Symposium (IV)*, 2016, pp. 508–513.

[18] S. Ucar, S. C. Ergen, and O. Ozkasap, "Ieee 802.11p and visible light hybrid communication based secure autonomous platoon," *IEEE Transactions on Vehicular Technology*, vol. 67, no. 9, pp. 8667–8681, 2018.

[19] M. Y. Abualhoul, E. T. Munoz, and F. Nashashibi, "The use of lane-centering to ensure the visible light communication connectivity for a platoon of autonomous vehicles," in *2018 IEEE International Conference on Vehicular Electronics and Safety (ICVES)*, 2018, pp. 1–6.

[20] F. Boukhalfa, M. Hadded, P. Muhlethaler, and O. Shagdar, "Evaluation of a new radio technology and visible light communication for a platooning application," in *2021 International Symposium on Networks, Computers and Communications (ISNCC)*, 2021, pp. 1–7.

[21] T. R. Gonçalves, V. S. Varma, and S. E. Elayoubi, "Performance and design of robust platoons under different communication technologies," in *2021 IEEE 93rd Vehicular Technology Conference (VTC2021-Spring)*, 2021, pp. 1–6.

[22] A. Paul, N. Chilamkurti, A. Daniel, and S. Rho, "Chapter 9 - future trends and challenges in its," in *Intelligent Vehicular Networks and Communications*, A. Paul, N. Chilamkurti, A. Daniel, and S. Rho, Eds. Elsevier, 2017, pp. 185–210. [Online]. Available : https://www.sciencedirect.com/science/article/pii/B9780128092668000090

[23] J. E. Siegel, D. C. Erb, and S. E. Sarma, "A survey of the connected vehicle landscape—architectures, enabling technologies, applications, and development areas," *IEEE Transactions on Intelligent Transportation Systems*, vol. 19, no. 8, pp. 2391–2406, 2017.

[24] T. ETSI, "Intelligent transport systems (its) ; vehicular communications ; geonetworking ; part 4 : Geographical addressing and forwarding for point-to-point and point-to-multipoint communications ; sub-part 2 : Media-dependent functionalities for its-g5," *ETSI TS*, vol. 102, pp. 636–4, 2013.

[25] "Ieee standard for wireless access in vehicular environments (wave)–identifiers," *IEEE Std 1609.12-2019 (Revision of IEEE Std 1609.12-2016)*, pp. 1–17, 2019.

[26] R. D. Dupuis and M. R. Krames, "History, development, and applications of high-brightness visible light-emitting diodes," *Journal of lightwave technology*, vol. 26, no. 9, pp. 1154–1171, 2008.

[27] *802.15.7-2011 - IEEE Standard for Local and Metropolitan Area Networks–Part 15.7 : Short-Range Wireless Optical Communication Using Visible Light*, IEEE Std., Sep. 2011, last accessed May 2020]. [Online]. Available : https://standards.ieee.org/standard/802_15_7-2011.html

[28] *802.15.7-2018 - IEEE Standard for Local and metropolitan area networks–Part 15.7 : Short-Range Optical Wireless Communications*, IEEE Std., Apr. 2019, last accessed May 2020]. [Online]. Available : https://standards.ieee.org/standard/802_15_7-2018.html

[29] *802.11 Light Communications Amendment - Task Group "bb"*, IEEE Std., last accessed May 2020]. [Online]. Available : http://www.ieee802.org/11/Reports/tgbb_update.htm

[30] M. Y. Abualhoul, M. Marouf, O. Shagdar, and F. Nashashibi, "Platooning control using visible light communications : A feasibility study," in *16th International IEEE Conference on Intelligent Transportation Systems (ITSC 2013)*. IEEE, 2013, pp. 1535–1540.

[31] B. Béchadergue, L. Chassagne, and H. Guan, "Visible light phase-shift rangefinder for platooning applications," in *2016 IEEE 19th International Conference on Intelligent Transportation Systems (ITSC)*. IEEE, 2016, pp. 2462–2468.

[32] J.-H. Lee, "Cross-layered ipv6 neighbor discovery scheme over wlan mesh networks," *IEEE Communications Letters*, vol. 13, no. 12, pp. 992–994, 2009.

[33] D. Caveney, "Cooperative vehicular safety applications," *IEEE Control Systems Magazine*, vol. 30, no. 4, pp. 38–53, 2010.

[34] *Road Users Code*, Hong Kong Transport Department - Stopping Distance, Jun 2020, last accessed November 2021]. [Online]. Available : https://www.td.gov.hk/en/road_safety/road_users_code/index/chapter_5_for_all_drivers/stopping_distance_/index.html

[35] *Stopping Distance + Braking Safely*, Ottawa Safety Council, Mar 2021, last accessed November 2021]. [Online]. Available : https://www.ottawasafetycouncil.ca/stopping-distances-and-distracted-driving/

[36] *Stopping distances on wet and dry roads*, The State of Queensland, Nov 2016, last accessed November 2021]. [Online]. Available : https://www.qld.gov.au/transport/safety/road-safety/driving-safely/stopping-distances/graph

[37] R. H. Patel., J. Härri., and C. Bonnet., "Braking strategy for an autonomous vehicle in a mixed traffic scenario," in *Proceedings of the 3rd International Conference on Vehicle Technology and Intelligent Transport Systems - VEHITS,*, INSTICC. SciTePress, 2017, pp. 268–275.

[38] "Laboratoire d'ingénierie des systemes de versailles," last accessed 12 January 2022. [Online]. Available : https://www.lisv.uvsq.fr/

[39] "Vedecom institute," last accessed 12 January 2022. [Online]. Available : http://www.vedecom.fr/

[40] L.-M. Cosovanu, E. Zadobrischi, M. Dimian, and E. Plascencia, "Unified road infrastructure safety system using visible light communication," in *2020 28th Telecommunications Forum (TELFOR)*. IEEE, 2020, pp. 1–4.

[41] M. Uysal, F. Miramirkhani, O. Narmanlioglu, T. Baykas, and E. Panayirci, "Ieee 802.15. 7r1 reference channel models for visible light communications," *IEEE Communications Magazine*, vol. 55, no. 1, pp. 212–217, 2017.

[42] A. Galisteo, D. Juara, and D. Giustiniano, "Research in visible light communication systems with openvlc1. 3," in *2019 IEEE 5th World Forum on Internet of Things (WF-IoT)*. IEEE, 2019, pp. 539–544.

[43] S.-A. Avătămăniței, A.-M. Căilean, E. Zadobrischi, A. Done, M. Dimian, and V. Popa, "Intensive testing of infrastructure-to-vehicle visible light communications in real outdoor scenario : Evaluation of a 50 meters link in direct sun exposure," in *2019 Global LIFI Congress (GLC)*. IEEE, 2019, pp. 1–5.

[44] V. Van Huynh, Y. M. Jang *et al.*, "Priority mac based on multi-parameter for ieee 802.15. 7 vlc," in *ICTC 2011*. IEEE, 2011, pp. 257–260.

[45] S. Ishihara, R. V. Rabsatt, and M. Gerla, "Improving reliability of platooning control messages using radio and visible light hybrid communication," in *2015 IEEE Vehicular Networking Conference (VNC)*. IEEE, 2015, pp. 96–103.

[46] P. Shams, M. Erol-Kantarci, and M. Uysal, "Mac layer performance of the ieee 802.15. 7 visible light communication standard," *Transactions on Emerging Telecommunications Technologies*, vol. 27, no. 5, pp. 662–674, 2016.

[47] Q. Mao, P. Yue, M. Xu, Y. Ji, and Z. Cui, "Octmac : A vlc based mac protocol combining optical cdma with tdma for vanets," in *2017 International Conference on Computer, Information and Telecommunication Systems (CITS)*. IEEE, 2017, pp. 234–238.

[48] Z. Ghassemlooy, W. Popoola, and S. Rajbhandari, *Optical wireless communications : system and channel modelling with Matlab®*. CRC press, 2019.

[49] J. M. Kahn and J. R. Barry, "Wireless infrared communications," *Proceedings of the IEEE*, vol. 85, no. 2, pp. 265–298, 1997.

[50] S. Selleri, "Claude chappe and the first telecommunication network (without electricity)," *URSI Radio Science Bulletin*, vol. 2017, no. 360, pp. 96–101, 2017.

[51] F. R. Gfeller and U. Bapst, "Wireless in-house data communication via diffuse infrared radiation," *Proceedings of the IEEE*, vol. 67, no. 11, pp. 1474–1486, 1979.

[52] A. Santamaría, J. Vento-Álvarez, J. Rabadán, and R. Pérez-Jiménez, "The irda standard," *Wireless LAN Standards and Applications*, p. 9, 2001.

[53] *Visible Light Communications Consortium*, VLCC Std., last accessed September 2021]. [Online]. Available : http://www.vlcc.net/

[54] D. M. Boroson, A. Biswas, and B. L. Edwards, "Mlcd : Overview of nasa's mars laser communications demonstration system," in *Free-Space Laser Communication Technologies XVI*, vol. 5338. International Society for Optics and Photonics, 2004, pp. 16–28.

[55] R. R. Craig, B. Li, and B. Chan, "Laser qualification for the semiconductor laser intersatellite link experiment (silex) program," in *Free-Space Laser Communication Technologies VI*, vol. 2123. International Society for Optics and Photonics, 1994, pp. 238–242.

[56] A. U. Chaudhry and H. Yanikomeroglu, "Free space optics for next-generation satellite networks," *IEEE Consumer Electronics Magazine*, 2020.

[57] C. Li, Y. Yi, K. Lee, and K. Lee, "Outdoor environment led-identification systems integrate stbc-ofdm," in *ICTC 2011*. IEEE, 2011, pp. 166–171.

[58] H. Elgala, R. Mesleh, and H. Haas, "Indoor broadcasting via white leds and ofdm," *IEEE Transactions on consumer electronics*, vol. 55, no. 3, pp. 1127–1134, 2009.

[59] C. Yeh, C. W. Chow, Y. Liu, and P. Huang, "Simple digital fir equalizer design for improving the phosphor led modulation bandwidth in visible light communication," *Optical and Quantum Electronics*, vol. 45, no. 8, pp. 901–905, 2013.

[60] H. Le Minh, D. O'Brien, G. Faulkner, L. Zeng, K. Lee, D. Jung, and Y. Oh, "High-speed visible light communications using multiple-resonant equalization," *IEEE photonics technology letters*, vol. 20, no. 14, pp. 1243–1245, 2008.

[61] H. Le Minh, D. O'Brien, G. Faulkner, L. Zeng, K. Lee, D. Jung, Y. Oh, and E. T. Won, "100-mb/s nrz visible light communications using a postequalized white led," *IEEE Photonics Technology Letters*, vol. 21, no. 15, pp. 1063–1065, 2009.

[62] J. Vučić, C. Kottke, S. Nerreter, K.-D. Langer, and J. W. Walewski, "513 mbit/s visible light communications link based on dmt-modulation of a white led," *Journal of lightwave technology*, vol. 28, no. 24, pp. 3512–3518, 2010.

[63] A. Street, P. Stavrinou, D. O'brien, and D. Edwards, "Indoor optical wireless systems–a review," *Optical and Quantum Electronics*, vol. 29, no. 3, pp. 349–378, 1997.

[64] O. Bouchet, H. Sizun, C. Boisrobert, and F. De Fornel, *Free-space optics : propagation and communication*. John Wiley & Sons, 2010, vol. 91.

[65] J. Guanetti, Y. Kim, and F. Borrelli, "Control of connected and automated vehicles : State of the art and future challenges," *Annual reviews in control*, vol. 45, pp. 18–40, 2018.

[66] J. Lavina and C. Bonelli, "V2v safety technology now standard on cadillac cts sedans," *Cadillac Pressroom.*, 2017. [Online]. Available : https://media.cadillac.com/media/us/en/cadillac/news.detail.html/content/Pages/news/us/en/2017/mar/0309-v2v.html

[67] N. Boovarahan, "Vehicle to everything an introduction," *Journal homepage : www. ijrpr. com ISSN*, vol. 2582, p. 7421.

[68] S. E. Shladover, D. Su, and X.-Y. Lu, "Impacts of cooperative adaptive cruise control on freeway traffic flow," *Transportation Research Record*, vol. 2324, no. 1, pp. 63–70, 2012.

[69] J. Lioris, R. Pedarsani, F. Y. Tascikaraoglu, and P. Varaiya, "Platoons of connected vehicles can double throughput in urban roads," *Transportation Research Part C : Emerging Technologies*, vol. 77, pp. 292–305, 2017.

[70] C. Bonnet and H. Fritz, "Fuel consumption reduction in a platoon : Experimental results with two electronically coupled trucks at close spacing," SAE technical paper, Tech. Rep., 2000.

[71] S. E. Shladover, "Path at 20—history and major milestones," *IEEE Transactions on intelligent transportation systems*, vol. 8, no. 4, pp. 584–592, 2007.

[72] A. Alam, B. Besselink, V. Turri, J. Mårtensson, and K. H. Johansson, "Heavy-duty vehicle platooning for sustainable freight transportation : A cooperative method to enhance safety and efficiency," *IEEE Control Systems Magazine*, vol. 35, no. 6, pp. 34–56, 2015.

[73] S. Darbha, "String stability of interconnected systems : An application to platooning in automated highway systems," *Ph. D. Dissertation, University of California*, 1994.

[74] A. Hsu, F. Eskafi, S. Sachs, and P. Varaiya, "Design of platoon maneuver protocols for ivhs," 1991.

[75] J. van de Sluis, L. Chen, and L. Garcia-Sol, "Del_i-game_d3. 2 proposal for extended message set for supervised automated driving," *European Commission, Seventh Framework Programme*, 2015.

[76] J. Ploeg, C. Englund, H. Nijmeijer, E. Semsar-Kazerooni, S. E. Shladover, A. Voronov, and N. Van de Wouw, "Guest editorial introduction to the special issue on the 2016 grand cooperative driving challenge," *IEEE Transactions on Intelligent Transportation Systems*, vol. 19, no. 4, pp. 1208–1212, 2018.

[77] A. Bellè, M. Falcitelli, M. Petracca, and P. Pagano, "Development of ieee802. 15.7 based its services using low cost embedded systems," in *2013 13th International Conference on ITS Telecommunications (ITST)*. IEEE, 2013, pp. 419–425.

[78] R. Corsini *et al.*, "Free space optical communication in the visible bandwidth for v2v safety critical protocols," in *2012 8th International Wireless Communications and Mobile Computing Conference (IWCMC)*. IEEE, 2012, pp. 1097–1102.

[79] *802.15.4-2015 - IEEE Standard for Low-Rate Wireless Networks*, IEEE Std., Apr. 2016, last accessed May 2020]. [Online]. Available : https://standards.ieee.org/standard/802_15_4-2015.html

[80] Q. Wang, D. Giustiniano, and O. Gnawali, "Low-cost, flexible and open platform for visible light communication networks," in *Proceedings of the 2nd International Workshop on Hot Topics in Wireless*, 2015, pp. 31–35.

[81] E. Plascencia, O. Shagdar, H. Guan, and L. Chassagne, "Study on multi-users interference in vehicle to vehicle visible light communications," in *VEHICULAR 2020 : The Ninth International Conference on Advances in Vehicular Systems, Technologies and Applications*. IARIA, 2020, pp. 1–7.

[82] K. A. Mehr, S. K. Nobar, and J. M. Niya, "Ieee 802.15. 7 mac under unsaturated traffic : Performance analysis and queue modeling," *Journal of Optical Communications and Networking*, vol. 7, no. 9, pp. 875–884, 2015.

[83] A. Memedi, H.-M. Tsai, and F. Dressler, "Impact of realistic light radiation pattern on vehicular visible light communication," in *GLOBECOM 2017-2017 IEEE Global Communications Conference*. IEEE, 2017, pp. 1–6.

[84] A. Memedi, C. Tebruegge, J. Jahneke, and F. Dressler, "Impact of vehicle type and headlight characteristics on vehicular vlc performance," in *2018 IEEE Vehicular Networking Conference (VNC)*. IEEE, 2018, pp. 1–8.

[85] M. Irfan, U. Habib, F. Muhammad, F. Ali, A. S. Alwadie, S. Ullah, A. Glowacz, and W. Glowacz, "Optical-interference mitigation in visible light communication for intelligent transport systems applications," *Energies*, vol. 13, no. 19, p. 5064, 2020.

[86] B. Soner and S. Coleri, "Visible light communication based vehicle localization for collision avoidance and platooning," *IEEE Transactions on Vehicular Technology*, vol. 70, no. 3, pp. 2167–2180, 2021.

[87] N. Chacko and S. Davies, "Free-space optical networking using the spectrum of visible light," *Int J Trends Eng Technol*, vol. 5, no. 2, pp. 217–224, 2015.

[88] K. Cui, G. Chen, Z. Xu, and R. D. Roberts, "Traffic light to vehicle visible light communication channel characterization," *Appl. Opt.*, vol. 51, no. 27, pp. 6594–6605, Sep 2012. [Online]. Available : http://opg.optica.org/ao/abstract.cfm?URI=ao-51-27-6594

[89] A. J. Moreira, R. T. Valadas, and A. de Oliveira Duarte, "Optical interference produced by artificial light," *Wireless Networks*, vol. 3, no. 2, pp. 131–140, 1997.

[90] M. Kavehrad and R. Aminikashani, *Visible Light Communication Based Indoor Localization*. CRC Press, 2019.

[91] J. Zhang, L. Cheng, and I. Marsic, "Models for non-intrusive estimation of wireless link bandwidth," in *IFIP International Conference on Personal Wireless Communications*. Springer, 2003, pp. 334–348.

[92] *Radial Sidelooker Silicon PIN Photodiode*, OSRAM, 01 2020, last accessed Mars 2021]. [Online]. Available : https://www.osram.com/ecat/Radial%20Sidelooker%20SFH%20206%20K/com/en/class_pim_web_catalog_103489/prd_pim_device_2219558/

[93] R. J. Salter, *Highway traffic analysis and design*. Macmillan International Higher Education, 1996.

[94] O. Shagdar, F. Nashashibi, and S. Tohme, "Performance study of cam over ieee 802.11 p for cooperative adaptive cruise control," in *2017 Wireless Days*. IEEE, 2017, pp. 70–76.

[95] S. Zhalehpour and M. Uysal, "Performance of multiuser scheduling in free space optical systems over atmospheric turbulence channels," *IET Optoelectronics*, vol. 9, no. 5, pp. 275–281, 2015.

[96] M. Elamassie, M. Karbalayghareh, F. Miramirkhani, R. C. Kizilirmak, and M. Uysal, "Effect of fog and rain on the performance of vehicular visible light communications," in *2018 IEEE 87th Vehicular Technology Conference (VTC Spring)*. IEEE, 2018, pp. 1–6.

[97] C. Sommer, R. German, and F. Dressler, "Bidirectionally Coupled Network and Road Traffic Simulation for Improved IVC Analysis," *IEEE Transactions on Mobile Computing (TMC)*, vol. 10, no. 1, pp. 3–15, January 2011.

[98] B. B. beagleboard.org, "Beaglebone black," 2021, last accessed 03 December 2021. [Online]. Available : https://beagleboard.org/black

[99] Last accessed 03 December 2021. [Online]. Available : http://www.openvlc.org/

[100] *AM335x Sitara™ Processors*, Texas Instruments, 03 2020, last accessed May 2022]. [Online]. Available :

https://www.ti.com/lit/ds/symlink/am3358.pdf?ts=1653992384191&ref_url=https%253A%252F%252Fwww.ti.com%252Fproduct%252FAM3358

[101] M. F. Guerra-Medina, B. Rojas-Guillama, O. González, J. A. Martín-González, E. Poves, and F. J. López-Hernández, "Experimental optical code-division multiple access system for visible light communications," in *2011 Wireless Telecommunications Symposium (WTS)*, 2011, pp. 1–6.

[102] H. Nakata, T. Inoue, M. Itami, and K. Itoh, "A study of inter vehicle communication scheme allocating pn codes to the location on the road," in *Proceedings of the 2003 IEEE International Conference on Intelligent Transportation Systems*, vol. 2. IEEE, 2003, pp. 1527–1532.

[103] A. Rizaldi and M. Althoff, "Formalising traffic rules for accountability of autonomous vehicles," in *2015 IEEE 18th international conference on intelligent transportation systems*. IEEE, 2015, pp. 1658–1665.

[104] J. Lioris, A. Bracquemond, G. Thiolon, and L. Bonic, "Real time level lane decision algorithm based on autonomous vehicle sensor data," in *2018 Annual American Control Conference (ACC)*. IEEE, 2018, pp. 6297–6302.

[105] M. F. Guerra-Medina, O. Gonzalez, B. Rojas-Guillama, J. Martin-Gonzalez, F. Delgado, and J. Rabadan, "Ethernet-ocdma system for multi-user visible light communications," *Electronics letters*, vol. 48, no. 4, pp. 227–228, 2012.

[106] T. K. Matsushima, S. Sasaki, M. Kakuyama, S. Yamasaki, Y. Murata, and Y. Teramachi, "A visible-light communication system using optical cdma with inverted mpsc," in *The Sixth International Workshop on Signal Design and Its Applications in Communications*, 2013, pp. 52–55.

[107] M. Pal and S. Chattopadhyay, "A novel orthogonal minimum cross-correlation spreading code in cdma system," in *INTERACT-2010*. IEEE, 2010, pp. 80–84.

[108] C. Nishanthi and R. S. Rajan, "Cross spectral density analysis for various codes suitable for spread spectrum under awgn conditions with error detecting code," *International Journal of Modern Engineering Research*, vol. 3, no. 4, pp. 2244–2249, 2013.

[109] B. K. Kim, S. Park, Y. Yeon, and B. W. Kim, "Radio-over-fiber system using fiber-grating-based optical cdma with modified pn codes," *IEEE Photonics Technology Letters*, vol. 15, no. 10, pp. 1485–1487, 2003.

[110] M. B. Mollah and M. R. Islam, "Comparative analysis of gold codes with pn codes using correlation property in cdma technology," in *2012 International Conference on Computer Communication and Informatics*. IEEE, 2012, pp. 1–6.

[111] F. R. Chung, J. A. Salehi, and V. K. Wei, "Optical orthogonal codes : design, analysis and applications," *IEEE Transactions on Information theory*, vol. 35, no. 3, pp. 595–604, 1989.

[112] J. A. Salehi, "Code division multiple-access techniques in optical fiber networks. i. fundamental principles," *IEEE transactions on communications*, vol. 37, no. 8, pp. 824–833, 1989.

[113] M. M. Merah, "Conception and realization of an indoor multi-user light-fidelity link," Ph.D. dissertation, Université Paris-Saclay, 2019.

[114] H. B. Eldeeb, E. Eso, E. A. Jarchlo, S. Zvanovec, M. Uysal, Z. Ghassemlooy, and J. Sathian, "Vehicular vlc : A ray tracing study based on measured radiation patterns of commercial taillights," *IEEE Photonics Technology Letters*, vol. 33, no. 16, pp. 904–907, 2021.

[115] M. . Simulink, "Propagation model," 2022, last accessed 25 February 2022. [Online]. Available : https://www.mathworks.com/help//antenna/ug/urban-channel-link-analysis-and-visualization-using-ray-tracing.html

[116] P. Combeau, S. Joumessi-Demeffo, A. Julien-Vergonjanne, L. Aveneau, S. Sahuguède, H. Boeglen, and D. Sauveron, "Optical wireless channel simulation for communications inside aircraft cockpits," *Journal of Lightwave Technology*, vol. 38, no. 20, pp. 5635–5648, 2020.

[117] E. Torres-Zapata, V. Guerra, J. Rabadan, R. Perez-Jimenez, and J. M. Luna-Rivera, "Vehicular communications in tunnels using vlc," in *2019 15th International Conference on Telecommunications (ConTEL)*, 2019, pp. 1–6.

[118] E. Plascencia, O. Shagdar, H. Guan, O. Barrois, and L. Chassagne, "Optical cdma mac evaluation in vehicle-to-vehicle visible light communications," *Electronics*, vol. 11, no. 9, p. 1454, 2022.

[119] A.-M. Cailean, M. Dimian, and A. Done, "Enhanced design of visible light communication sensor for automotive applications : Experimental demonstration of a 130 meters link," in *2018 Global LIFI Congress (GLC)*. IEEE, 2018, pp. 1–4.

[120] K. Siddiqi, A. Raza, and S. S. Muhammad, "Visible light communication for v2v intelligent transport system," in *2016 International Conference on Broadband Communications for Next Generation Networks and Multimedia Applications (CoBCom)*. IEEE, 2016, pp. 1–4.

[121] T. Nawaz, M. Seminara, S. Caputo, L. Mucchi, and J. Catani, "Low-latency vlc system with fresnel receiver for i2v its applications," *Journal of Sensor and Actuator Networks*, vol. 9, no. 3, p. 35, 2020.